Biophysical model for measurement of brain tissue conductivity and diagnostic applications

Andrés Nicolás Carvallo Pecci

THESE DE DOCTORAT DE

L'UNIVERSITE DE RENNES 1
COMUE UNIVERSITE BRETAGNE LOIRE

ECOLE DOCTORALE N° 601
Mathématiques et Sciences et Technologies de l'Information et de la Communication
Spécialité : AST – Signal, image et vision

Par

Andrés Nicolás CARVALLO PECCI

Modèle biophysique pour la mesure de la conductivité électrique cérébrale et apport diagnostique.

Thèse présentée et soutenue à Rennes, le 7 Décembre 2018
Unité de recherche : LTSI – INSERM UMR-S 1099
Université de Rennes 1 – Laboratoire Traitement du Signal et de l'image

Rapporteurs avant soutenance :

Sylvie RENAUD	Professeur des universités, Université de Bordeaux
Olivier FRANÇAIS	Directeur de recherches, ESIEE-Paris

Composition du Jury :

Président :	Guy CARRAULT	Professeur des universités, Université Rennes 1
Rapporteur :	Sylvie RENAUD	Professeur des universités, Université de Bordeaux
Rapporteur :	Olivier FRANÇAIS	Directeur de recherches, ESIEE-Paris
Examinateur :	Fabrice BARTOLOMEI	Professeur des universités – Praticien hospitalier, Université Aix-Marseille
Dir. de thèse :	Fabrice WENDLING	Directeur de recherches, Université Rennes 1
Co-dir. de thèse :	Julien MODOLO	Chargé de recherches, Université Rennes 1

Remerciements

Je remercie tout d'abord mon directeur Fabrice Wendling, ainsi qu'à mon co-directeur Julien Modolo, pour toute l'aide et la confiance qu'ils m'ont apporté au cours de mes trois années de thèse.

J'aimerais remercier tous ceux qui ont participé, directement ou indirectement, à la réalisation de ce travail de recherche. Notamment à Fabrice Bartolomei et Stanislas Lagarde pour leurs apports au cours des tests qui ont été réalisés chez l'homme et également Pascal Benquet pour son aide au cours des tests in-silico et chez le rat.

Bien sûr, j'aimerais remercier mes rapporteurs, Sylvie Renaud et Olivier Français, ainsi que tous les membres du jury, d'avoir accepté d'assister à mon exposé oral.

Je voudrais remercier M. le directeur Lotfi Senhadji de m'avoir accueilli au sein du LTSI. Enfin, je voudrais remercier tous mes collègues pour leur soutien et leur compagnie au cours de ces dernières années, et à mes collègues de bureau d'avoir supporté mes humeurs lunatiques. Un merci spécial à Gustavo Guerrero pour son soutien moral.

A Mama, Gabri, Fran y Santi

A Cata

A mi Padre, el mundo se expresa de maneras absurdas…

Résumé en français

Le contexte de ce travail de thèse en génie biomédical est l'identification de nouveaux biomarqueurs pour le diagnostic de l'épilepsie pharmaco-résistante. Puisque les patients épileptiques candidats à la chirurgie sont systématiquement implantés avec des électrodes intracrâniennes et que ces patients sont stimulés électriquement pour faciliter l'identification de la zone épileptogène, nous avons souhaité utiliser cette possibilité unique d'analyser les propriétés électriques des tissus cérébraux directement au niveau de tissu cérébral. Plus spécifiquement, les objectifs de ce travail sont: 1) Développer une nouvelle méthode pour estimer la conductivité électrique des tissus cérébraux en utilisant des électrodes intracrâniennes, et 2) Quantifier la corrélation potentielle entre l'épileptogénicité des régions cérébrales et leur conductivité à des fins diagnostiques.

Généralités sur l'épilepsie

L'épilepsie est un trouble neurologique chronique (Ngugi et al., 2010), caractérisé par des crises récurrentes spontanées qui interfèrent avec le comportement, telles que le langage ou la motricité. Environ 65 millions de personnes souffrent d'épilepsie dans le monde, ce qui représente en Europe plus de 6 millions de patients. Le coût correspondant pour le système de santé est supérieur à 20 milliards d'euros par an (Pugliatti et al., 2007). L'épilepsie est la conséquence d'un déséquilibre entre les processus d'excitation et inhibition dans les circuits cérébraux, entraînant une hyperexcitabilité pathologique qui se manifeste par des symptômes tels que des crises ou des absences par exemple. Les

caractéristiques des crises varient selon leur origine et leur répartition, et sont divisées en deux classes; les *crises focales*, qui proviennent d'une petite région cérébrale bien identifiée; et des *crises généralisées*, où l'activité épileptiforme se propage et implique une grande partie du cerveau. Les personnes atteintes d'épilepsie répondent au traitement environ 70% du temps, laissant environ 30% des patients réfractaires aux médicaments. Les patients réfractaires aux médicaments peuvent être candidats pour une chirurgie de la zone épileptogène si le foyer résécable n'affecte pas les fonctions cognitives trop sévèrement, et si la probabilité d'amélioration de la qualité de vie est élevée.

Pour opérer la zone épileptogène, il est crucial de la localiser précisément pour éviter de retirer des tissus sains. Dans ce contexte, la planification pré-chirurgicale implique fréquemment des enregistrements invasifs tels que l'électroencéphalographie stéréotaxique (SEEG). La SEEG consiste en l'implantation intracrânienne de plusieurs électrodes enregistrant des signaux électrophysiologiques dans un grand nombre de régions cérébrales, généralement entre 150 et 250 contacts. Cette méthode a une bonne résolution spatiale (ordre de 2 mm sur l'axe des électrodes) et une excellente résolution temporelle (de l'ordre de la milliseconde). Les signaux électrophysiologiques obtenus avec SEEG visent à détecter l'activité épileptiforme pour identifier la zone épileptogène (Cossu et al., 2005; Engel, 1993; Mercier et al., 2012). Dans ce contexte, la stimulation électrique est appliquée dans les régions implantées en utilisant des impulsions biphasiques à courant constant, dans le but d'induire une activité épileptiforme qui pourrait aider à identifier la zone épileptogène. Cependant, une telle identification peut être difficile, car cela prend du temps (les patients sont normalement implantés pendant deux semaines) et il n'est pas toujours possible d'évoquer une activité épileptiforme chez les patients. Certains biomarqueurs ont été rapportés comme l'indice d'épileptogénicité (Bartolomei et al., 2008). Néanmoins, le diagnostic clinique pourrait être grandement facilité par de nouveaux biomarqueurs fournissant une indication quantitative de l'épileptogénicité des tissus cérébraux.

Applications diagnostiques de la conductivité

L'estimation de la conductivité tissulaire a suscité un intérêt dans d'autres domaines médicaux tels que l'oncologie à des fins de diagnostic. Les cellules saines maintiennent une concentration élevée de potassium et une faible concentration de sodium. Lorsque les cellules sont endommagées ou cancéreuses, le sodium et l'eau s'écoulent dans la cellule, diminuant la concentration de potassium et d'autres ions dans le milieu intracellulaire, entraînant ainsi une diminution de l'impédance (Cone, 1970). Dans le même ordre d'idées, des études récentes ont montré des différences dans les propriétés diélectriques des cellules saines et cancéreuses, et ont conclu que les cellules saines ont une conductivité supérieure à celle des cellules tumorales (Cone, 1974; Qiao et al., 2010). Le fait que les processus pathophysiologiques puissent altérer les propriétés électriques motive le développement de nouvelles applications pour les maladies neurologiques. En effet, il est établi que l'équilibre entre l'inhibition/excitation est modifié dans l'épilepsie, ce qui pourrait également modifier la concentration en ions dans le milieu extracellulaire. Comme la stimulation intracrânienne s'est largement développée

au cours des dernières décennies pour devenir un outil important pour le diagnostic et le traitement des troubles neurologiques (épilepsie, Parkinson, etc.), nous avons cherché à mesurer directement la conductivité cérébrale chez les patients épileptiques.

Etat de l'art

L'étude des propriétés électriques des tissus biologiques en général (et des tissus cérébraux en particulier), est un domaine d'intérêt significatif dans le domaine du génie biomédical. Il est désormais admis que les propriétés électriques des tissus peuvent être indicatives des processus physiopathologiques, ce qui a un potentiel significatif pour des applications diagnostiques. Cependant, il peut être difficile de mesurer les caractéristiques électriques des tissus biologiques.

L'étude des propriétés électriques des tissus biologiques a débuté il y a près d'un siècle, l'une des premières bases de données remontant au début du XXe siècle (Crile et al., 1922). Cette étude a analysé principalement des lapins, en examinant la conductivité de différents tissus et liquides corporels. Les techniques de mesure et d'analyse des propriétés électriques ont continué à se développer, jusqu'à ce qu'une étude (Schwan and Kay, 1957) qui fut l'une des premières à analyser la résistance spécifique en fonction de la fréquence des tissus canins vivants *in situ*, et à observer les différentes dispersions. À la fin des années 1990, il était publié une étude documentaire et une vaste base de données de mesures à différentes fréquences (C. Gabriel et al., 1996; S. Gabriel et al., 1996), qui comprenait tous les principaux tissus pour lesquels il y avait au moins trois études documentées. Pour la plupart des tissus, les données étaient limitées ou inexistantes. La base de données a étudié la permittivité et de la conductivité de différents tissus humains et animaux à la température corporelle, pour une gamme de fréquence comprise entre 10 Hz et 20 GHz. Les auteurs ont conclu que pour les mesures en basse fréquence, les erreurs causées par la polarisation des électrodes affectaient les résultats en dessous de 1 kHz. C'est pourquoi, de nos jours, la mesure à basse fréquence des propriétés électriques des tissus restent encore une question ouverte.

Méthodologie

Cette thèse a pour objectif d'appliquer des techniques théoriques fondamentales pour estimer la conductivité des tissus cérébraux locaux à l'aide d'électrodes intracrâniennes. Premièrement, les protocoles de stimulation sont conçus pour éviter d'endommager les tissus cérébraux. Les stimulateurs cliniques utilisent généralement des formes d'onde à courant constant et équilibrées en charge pour minimiser les dommages tissulaires. Par conséquent, une des principales contraintes est que notre modèle sera basé sur des formes d'onde à courant constant pour estimer la conductivité cérébrale locale. En se basant sur l'utilisation de stimulations d'impulsions biphasiques à courant constant, nous proposons d'estimer le potentiel électrique et le champ électrique résultants. Le potentiel/champ électrique est estimé à l'aide d'une approche analytique et d'un logiciel permettant de trouver une solution numérique. Deuxièmement, les électrodes utilisées en clinique sont des électrodes

cylindriques qui ont une constante de cellule (constante qui lie l'impédance à la conductivité) qui dépend de cette géométrie spécifique. À partir de l'estimation du champ électrique, une relation entre la conductivité moyenne et la résistance du milieu est obtenue en utilisant la géométrie spécifique de l'électrode utilisée pendant les stimulations cliniques. Troisièmement, les formes d'onde utilisées pour la stimulation pulsée ont un spectre basse fréquence (<1 kHz). L'un des problèmes de l'estimation de conductivité à basse fréquence est la polarisation des électrodes, ce qui doit être pris en compte dans la solution pour obtenir des estimations fiables. L'interface électrode/électrolyte est modélisée avec une capacité à double couche et une résistance de transfert de charge. La réponse du système à une impulsion biphasique à courant constant est modélisée, et utilisée pour estimer la résistance moyenne et l'interface électrode/électrolyte. Cela permet d'obtenir de meilleures estimations de la conductivité.

Expérimentation

Afin de valider la conductivité estimée à partir du modèle électrode/électrolyte, une solution saline calibrée a été utilisée comme vérité terrain. Le modèle à double couche électrode-milieu a permis de reproduire l'évolution temporelle de l'artefact de stimulation enregistré, et nous a permis d'estimer la résistance et donc la conductivité des solutions étalonnées. Même si les solutions salines sont beaucoup plus simples que les tissus (par exemple, aucune anisotropie), il s'agissait d'une première étape d'analyse des signaux qui a permis une validation de la méthode développée. De plus, les mesures de conductivité pourraient être calibrées et fournir un lien avec la théorie et l'expérience.

Des mesures de conductivité post-mortem ont été effectuées dans le cerveau de $N = 2$ adultes Sprague-Dawley. La stimulation a été effectuée quelques minutes après la mort dans l'hémisphère droit/gauche et était une première évaluation de la forme d'onde de la stimulation dans le tissu réel. Même si cette expérience était réalisée post-mortem, impliquant qu'aucune activité électrophysiologique n'était présente, cela fournissait des informations cruciales sur les propriétés des tissus.

Une fois la validation des solutions salines et des mesures post-mortem ont été effectuées, nous avons réalisé des études sur les patients (total N=7). Avant d'acquérir les données du patient, il fallait d'abord résoudre les limitations matérielles. Au cours des stimulations cliniques, le système SEEG enregistre les signaux pour analyser les marqueurs épileptiques. Les signaux électrophysiologiques sont normalement de l'ordre de 100 µV, ce qui implique que le système SEEG n'a pas besoin d'une large plage de quantification (valeurs typiques de ±1 mV). Cette plage de quantification est significativement inférieure à celle requise pour échantillonner correctement l'artefact de stimulation, ce qui induira une saturation en amplitude. En outre, la fréquence d'échantillonnage est généralement nettement inférieure (valeurs typiques de f_s = 2048 Hz) à celle requise pour capturer avec suffisamment de détails l'artefact de stimulation. Pour effectuer des enregistrements humains, un système d'acquisition a été mis en parallèle avec le système de stimulation. Le système d'enregistrement utilisé comportait une plage d'entrée élevée (±1 V) pour capturer l'intégralité de

l'artefact de stimulation sans saturation d'entrée et une fréquence d'échantillonnage élevée (100 kHz) pour capturer les détails de la forme d'onde afin d'estimer les paramètres biophysiques.

Résultats

Des solutions salines ont été préparées pour tester la forme d'onde de stimulation. La conductivité a été calibrée en utilisant un volume d'eau précis ainsi que la quantité précise de sel mesurée avec une échelle de haute précision (précision de 100 µg). L'évolution temporelle du potentiel électrique pendant une impulsion de stimulation pour une solution (0.1 S/m) et le modèle est montrée dans la Figure 1.

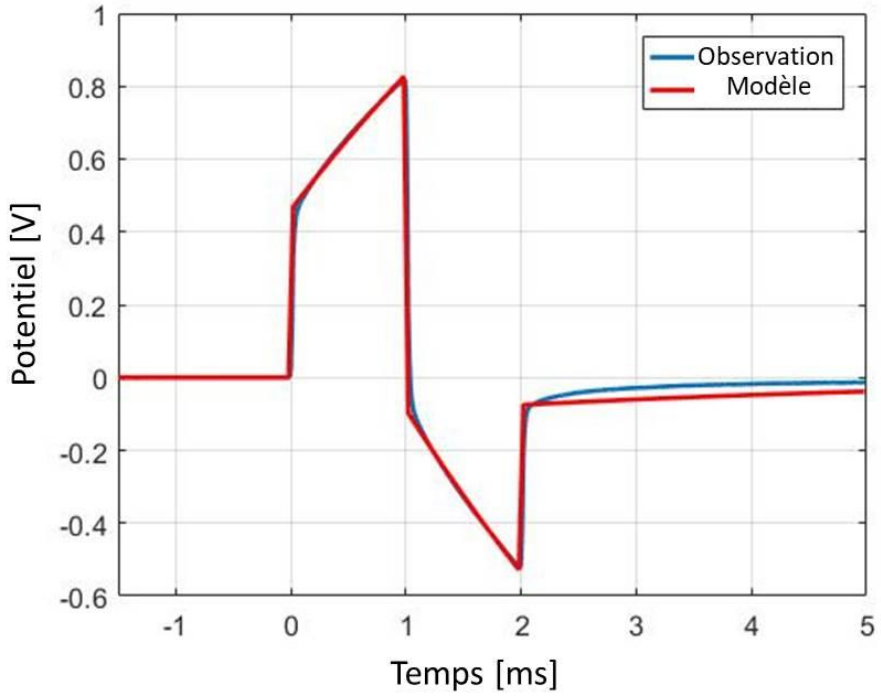

Figure 1. Accord du modèle avec les signaux enregistrés dans des solutions salines. Superposition des décours temporels entre les signaux simulés et enregistrés.

Le modèle reproduit fidèlement le décours temporel du potentiel enregistré pour les phases positives et négatives. Nous avons donc estimé des paramètres inconnus pour l'interface électrode/électrolyte ainsi que la résistance du milieu, en se basant sur les enregistrements expérimentaux. Notamment, la conductivité électrique a été calculée à partir de la valeur estimée de la résistance du milieu. L'estimation de la conductivité restait en moyenne avec une sous-estimation inférieure à 10% de la valeur de la solution calibrée.

Epileptique versus non épileptique

Les estimations de conductivité dans de multiples régions cérébrales chez les patients ont été comparées à des données électrophysiologiques, afin de déterminer si une région est saine ou zone

épileptogène. Pour montrer un exemple, nous avons estimé la conductivité de tous les contacts d'une électrode pour un patient (Figure 2). Cette électrode était située dans une région avec une activité pathologique et une région avec une activité saine. Les électrodes intérieures étaient situées dans le gyrus parahippocampique (électrodes OT1-4), suivies d'une jonction et de la substance blanche (électrodes OT4-7), puis on trouve le sillon occipito-temporal (électrodes OT7-10), une autre jonction (électrodes OT10-12) et enfin le gyrus temporal inférieur (électrode OT12-13).

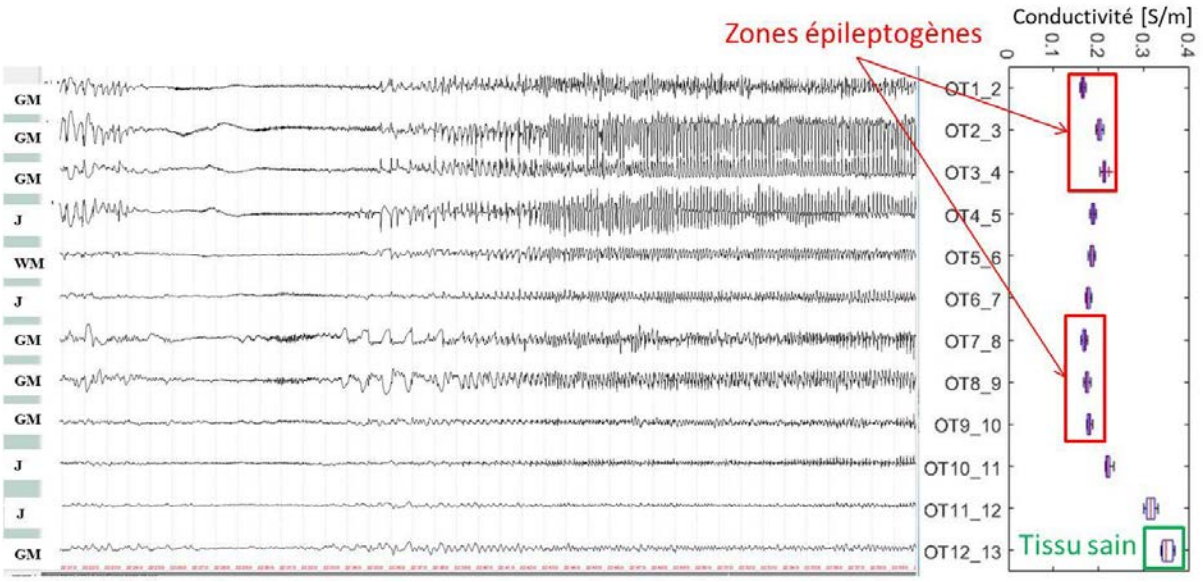

Figure 2. Crise d'épilepsie enregistrée pour chaque contact d'une électrode entière et valeurs de conductivité estimées (substance grise (GM), substance blanche (WM) et jonction (J)).

Les électrodes localisées dans le gyrus parahippocampique (électrodes OT1-4), et dans le sillon occipito-temporal (électrodes OT7-10) étaient classées comme des zones epileptogènes. Il est intéressant de noter ces électrodes ont une conductivité inférieure à celle de gyrus temporal inférieur (électrode OT12-13), classé comme région sain.

Discussion

La conductivité des tissus cérébraux pour des applications biomédicales a été principalement étudiée en utilisant des EEG de scalp *in vivo* (Baysal and Haueisen, 2004; Gonalves et al., 2003), des échantillons *ex vivo* fraîchement excisés (Akhtari et al., 2006; S. Gabriel et al., 1996), et des études intracrâniennes animales *in vivo* (Logothetis et al., 2007). Il y a eu peu d'études intracrâniennes *in vivo* chez l'homme (Koessler et al., 2017; J. A. Latikka et al., 2001). Les résultats ne sont pas cohérents entre ces études, probablement en raison des différences liées aux changements post-mortem des tissus, aux erreurs liées aux problèmes inverses, aux changements de température, à la polarisation des électrodes ou à la fréquence de stimulation. Notre méthode fournit des estimations de conductivité dans la gamme de 0.1 S/m à 0.3 S/m pour les expériences *in vivo* (matière grise) et post-mortem, respectivement, qui sont proches de celles rapportées dans la littérature (Akhtari et al., 2006; Koessler et al., 2017; J. A. Latikka et al., 2001). Une des principales limites des mesures invasives existantes de

la conductivité des tissus cérébraux est le manque de prise en compte des processus physiques intervenant à l'interface électrode/tissu. Comme l'ont souligné nos résultats, notamment en ce qui concerne l'impact de l'interface électrode/électrolyte sur la réponse simulée, de tels mécanismes doivent être pris en compte pour fournir des estimations précises de la conductivité à basse fréquence.

Les propriétés diélectriques ont de plus en plus retenu l'attention pour l'analyse des caractéristiques des tissus et elle a été étudiée dans différents domaines médicaux tels que l'oncologie et les maladies musculaires. Peu d'études ont été réalisées sur les propriétés électriques des tissus épileptiques. La classification des tissus épileptiques est encore aujourd'hui une tâche difficile. Dans un cadre clinique typique, la conductivité électrique n'est pas mesurée pendant les enregistrements SEEG, car le premier objectif des séances de stimulation fonctionnelle est d'identifier la zone épileptogène basée sur l'analyse des décharges provoquées par la stimulation, telles que les potentiels évoqués cortico-corticaux. Un avantage de notre approche est l'utilisation de paramètres de stimulation compatibles avec les stimulations cliniques. Nous démontrons que les caractéristiques de l'artefact de stimulation peuvent être utilisées pour mieux connaître les propriétés biophysiques du tissu cérébral, fournissant éventuellement des informations diagnostiques. Cette direction de recherche prometteuse nécessitera une confirmation dans une taille d'échantillon plus grande dans une étude clinique dédiée.

Une autre direction intéressante serait de relier plus spécifiquement les modifications de la conductivité du tissu cérébral aux mécanismes physiopathologiques. Par exemple, la conductivité électrique étant proportionnelle à la mobilité des ions dans les tissus, nous pourrions établir des liens entre les modifications de la régulation de la concentration ionique, la conductivité électrique et les processus physiopathologiques (Cone, 1970; Emin et al., 2015).

Conclusion

Nous avons proposé une nouvelle méthode pour étudier les propriétés biophysiques du tissu cérébral. Dans cette approche basée sur l'utilisation d'un modèle biophysique, nous tenons compte du potentiel électrique et du champ induits par l'électrode de stimulation, ainsi que des caractéristiques d'interface électrode-électrolyte, pour décrire avec précision la réponse du tissu cérébral à la stimulation par des pulses biphasiques. À partir de l'utilisation du modèle pour interpréter la réponse enregistrée, le modèle donne accès à des paramètres biophysiques pertinents, notamment la conductivité électrique.

La méthode proposée a été validée en utilisant des paramètres *in vitro* et *ex vivo*. Nous obtenons d'excellents résultats d'appariement pour les solutions salines et de bons résultats pour les données *ex-vivo*. De plus, des résultats pertinents sur le plan clinique ont été obtenus à partir de données intracérébrales enregistrées chez des patients épileptiques. Les principaux avantages de cette méthode basée sur un modèle sont sa précision, son faible coût de calcul et sa compatibilité avec les paramètres de stimulation couramment utilisés en clinique. L'estimation de la conductivité électrique pourrait

conduire au développement de nouveaux marqueurs d'épilepsie pouvant compléter l'analyse des enregistrements intracérébraux SEEG effectués classiquement avant la chirurgie.

L'influence de l'hétérogénéité des tissus est un aspect intéressant qui n'a pas été étudié dans cette thèse, car nous avons utilisé l'hypothèse de l'isotropie afin de développer un cadre analytique. Il a en effet été rapporté que des tissus hétérogènes pourraient altérer la distribution spatiale du champ électrique jusqu'à 10% en fonction de la région anatomique où l'électrode était placée (Aström et al., 2012). De telles erreurs sont particulièrement importantes dans les régions entourées de multiples fibres comme la région sous-thalamique. Une autre extension possible de ce travail serait de considérer le tissu comme un milieu hétérogène, notamment à la frontière entre la substance grise et la substance blanche. Dans ce cas, la limite entre la substance blanche et la substance grise serait considérée comme un milieu ayant deux conductivités différentes (milieu bi-conductivité).

Un autre développement intéressant consisterait à étudier l'évolution des paramètres d'interface électrode-tissu au cours des jours suivant l'implantation d'électrodes SEEG (Grill and Mortimer, 1994; Polikov et al., 2005; Riistama and Lekkala, 2006), reflétant peut-être une infiltration du LCR après une intervention chirurgicale, mais aussi une gliose se formant autour de l'électrode (Lempka et al., 2009; Yousif et al., 2008). Nous avons présenté dans cette thèse un modèle de tissu d'encapsulation, qui pourrait être utilisé pour mesurer l'impédance du tissu d'encapsulation et améliorer l'estimation de la conductivité même de la présence de ce tissu. Il serait possible d'étudier l'évolution de l'interface électrode-électrolyte sur plusieurs jours chez les mêmes patients, ce qui impliquerait un suivi un peu plus long, mais permettrait de mieux comprendre l'évolution de l'interaction électrode-tissu.

Contents

1 Introduction 1

2 State of the art 5

2.1 Conductivity in living tissues 5

2.1.1 Tissues basics components and dielectric properties 5

2.2 Electrophysiological activity 9

2.2.1 Neuron 9

2.2.2 Brain rhythms 10

2.2.3 Electrophysiological markers of epilepsy 11

2.3 Electrical stimulation 13

2.3.1 Stereotaxic EEG procedure 16

2.3.2 Intracranial electrodes 17

2.3.3 Charge delivery by current control 23

2.4 Conductivity measurement techniques 25

2.4.1 Impedance-based techniques 27

2.4.2 Imaging 29

2.5 Conductivity in medicine 30
2.5.1 Oncology 30
2.5.2 Muscle diseases 31
2.5.3 Neurology and epilepsy 31

3 Problem Statement 35

3.1 Local brain conductivity 35
3.1.1 Limitations of clinical stimulation 35
3.1.2 Limitations of materials and protocol 36
3.2 Proposed solution 36
3.2.1 Ground truth 37
3.3 Patient studies 37
3.3.1 Epileptic versus non-epileptic tissue 37

4 Materials and Methods 39

4.1 Electric field model 39
4.1.1 Macroscopic fields in biological tissue 40
4.1.2 Laplace Equation 41
4.1.3 Assumptions of the electric potential model 44
4.1.4 Finite-element method 46
4.2 Electrode-electrolyte interface: an electric circuit model 48
4.2.1 Electric circuit model solutions 50
4.1.1 Derivation of the model for other waveforms 53
4.2.2 Limitations of the model 56
4.2.3 Bioimpedance calculation 58
4.3 Model validation methodology: in vitro, in vivo and in clinico 60
4.3.1 Methodological choices for experimental validation 60
4.3.2 Parameter estimation 61
4.3.3 Saline solutions calibration 64
4.3.4 Ex vivo rat brain 66
4.3.5 In clinico experiment in drug-refractory epileptic patients 66

5 Results 73

5.1 Electric potential analytical model and Comsol 73

5.2 Saline solution experimentation 75
5.3 Ex-vivo rat brain 79
5.4 In-clinico acquisitions in drug-refractory epileptic patients 81
5.4.1 Detailed analysis 81
5.4.2 Post-implantation encapsulation tissue 85
5.5 Statistical analysis 89
5.5.1 Single patient-level analysis 90
5.5.2 Group analysis 92
5.5.3 Parameters sensitivity analysis 93
5.6 Conductivity estimation variability 95
5.7 Electrolyte electric potential offset 96

6 Discussion 99

6.1 Conductivity estimation 100
6.2 Relationship between electrical conductivity and pathophysiological processes 101
6.3 Future prospects and extensions of this work 102

7 Conclusion 105

Glossaries 107

List of Figures 109

List of Tables 113

List of Publications 115

References 117

1 Introduction

The context of this biomedical engineering thesis work is the identification of novel biomarkers for the diagnosis of epilepsy. More specifically, the objectives of this work are: 1) developing a novel model-based method for estimating brain tissue electrical conductivity using intracranial electrodes, and 2) quantifying the potential correlation between the epileptogenicity of brain regions and their conductivity.

Generalities about epilepsy

Epilepsy is a common (Ngugi et al., 2010), chronic neurological disorder characterized by spontaneously recurring seizures interfering with behavior, such as language or motor skills. It is the consequence of an altered balance between excitatory and inhibitory processes in brain circuits, resulting in an abnormal electrophysiological activity that manifests by symptoms such as seizures or absences. These symptoms or clinical signs vary from patient to patient and depend on brain structures that are involved at the onset of seizure and during the propagation Approximately 65 million people suffer from epilepsy worldwide, and in Europe specifically over 6 million patients involve a cost over € 20 billion per year (Pugliatti et al., 2007). Epilepsy is the consequence of an altered balance between excitatory and inhibitory processes in brain circuits, resulting in a pathological hyperexcitability that

manifests by symptoms such as seizures or absences for example. The characteristics of seizures vary according to their origin and spreading, and are divided in two classes; focal seizures, which originate in a small, well-identified brain region; and generalized seizures, where epileptiform activity propagates and involves a large portion of the brain. People with epilepsy respond to treatment approximately 70% of the time, leaving about 30% of drug-refractory patients. Drug-refractory patients can be considered for surgery of the epileptogenic zone (EZ) if the resectable focus does not impact severely cognitive or motor functions, and when the benefit is higher than the deficit that can potentially be induced by the resection of the EZ. Thus, surgery is performed in about 20% of candidate patients. The success of resective surgery depending on the anatomical location of the EZ is presented in Tab. 1.1, from a systematic review and meta-analysis (Téllez-Zenteno et al., 2005).

LONG-TERM SEIZURE SUPPRESSION

Type of surgery	Number of patients	Seizure free (%)
Temporal	3895	**66**
Hemispherectomy	169	**61**
Temporal and extratemporal	2334	**59**
Parietal	82	**46**
Occipital	35	**46**
Callosotomy	99	**35**
Extratemporal	169	**34**
Frontal	486	**27**

Tab. 1.1. Percentage of seizure-free patients on the long-term: overall proportion by type of surgery (adapted from Téllez-Zenteno et al., 2005)

In order to remove the EZ, it is crucial to locate it precisely to avoid removing healthy tissue. In this context, pre-surgical planning frequently involves invasive recordings such as stereotactic electroencephalography (SEEG). SEEG consists in the intracranial implantation of several (8-15) electrodes with multiple (10-15) contacts recording electrophysiological signals in a large number of brain regions. This method, detailed in Section 2, Chapter 2.3.1, has a good spatial resolution (order of 2 mm along the electrode axis) and an excellent time resolution (millisecond), which comes with the disadvantage of being invasive. The electrophysiological signals obtained with SEEG aim to detect epileptiform activity to identify the EZ and the subsequent surgical approach (Cossu et al., 2005; Engel, 1993; Mercier et al., 2012). In this context, electric stimulation is applied in EZ candidate regions using biphasic constant current pulses, with the objective of inducing epileptiform activity that could help identifying the EZ. However, such identification can be challenging, considering that it takes time (patients are typically implanted for two weeks) and it is not always possible to evoke epileptiform activity in the patients. Some biomarkers have been proposed, such as the epileptogenicity index (Bartolomei et al., 2008). Nevertheless, clinical diagnosis could be greatly

facilitated by new biomarkers providing quantitative indication of brain tissue epileptogenicity. In this thesis, a novel biomarker based on tissue electrical conductivity has been proposed and tested in patients during SEEG exploration.

Diagnostic applications of conductivity

The estimation of tissue conductivity has sparked interest in other medical fields such as oncology for diagnostic purposes. Healthy cells maintain a high concentration of potassium and a low concentration of sodium. When cells are injured or cancerous, sodium and water flows into the cell, decreasing potassium and other ions concentration in the intracellular medium, thus resulting in decreased impedance (Cone, 1970). Along the same line, recent studies have shown differences in the dielectric properties of healthy and cancer cells. Interestingly, the studies concluded that healthy cells have higher conductivity than tumor cells, given that cancer cells have different electrical and metabolic properties due to abnormalities in structures (Cone, 1974; Qiao et al., 2010). The fact that pathological tissue could have altered electric properties motivates the development of novel applications for neurological diseases. Indeed, since the balance between inhibition and exhibition is modified in epilepsy, it could be hypothesized that the concentration of ions in the extracellular medium is modified and subsequently alters normal conductivity values. Intracerebral stimulation has largely developed over the last few decades to become an important tool for the diagnosis and treatment of neurological disorders (epilepsy, Parkinson, etc.), It is a method routinely used in clinics to map epileptogenic networks. In this work, we make use of this kind of stimulation to directly measure brain conductivity in cerebral structures explored by SEEG. .

Summary and manuscript plan

Dielectric properties of tissue have been investigated in the literature for over a century (Crile et al., 1922; C. Gabriel et al., 1996; Schwan and Kay, 1957). Several *in vitro* and *in vivo* studies are documented; however human studies are rare, given that suitable data for such estimations is scarce. Since epileptic patients candidate to surgery are routinely implanted with intracranial electrodes, and that these patients are electrically stimulated to identify the EZ, we thought that this provides a unique possibility to analyze the bio-electric properties of brain tissue. On that basis, in this PhD thesis, the whole stimulation process (intracranial electrodes, volume conductor and electrode-tissue interface) was mathematically modelled to estimate of local brain conductivity. To validate the model, various experimental studies were performed, including calibrated saline solutions, *post-mortem* rat brain and *in*-vivo test performed in epileptic patients candidate to surgery. The conductivity results in patients were compared with electrophysiological data to classify if a region is healthy or epileptogenic. Statistical analysis of the correlation between conductivity and EZ was performed to investigate the diagnostic potential of conductivity measurements.

This thesis is organized as follows:

- *Chapter 2:* Provides a state of the art of biological tissue conductivity, methods of measuring conductivity with their advantages and challenges, an introduction to intracranial EEG and stimulation, and finally how conductivity is used nowadays in medicine for diagnosis and treatment.

- *Chapter 3:* The problem statement is presented. The main research topic is introduced in the context of the state of the art. Next, specific areas of the research conducted during this thesis are discussed. An outline of the proposed approach and solutions is provided.

- *Chapter 4:* Introduces the mathematical models used for the estimation of brain conductivity. These models include the electric field induced by the electrodes during stimulation, and a model for electrode polarization. The methodological choices for experimentation and the different tests that were performed to validate the model are presented: *in silico* (conductivity calibrated solutions)*, ex vivo* rat and *in clinico* studies.

- *Chapter 5:* Presents the results of the proposed approach to estimate the conductivity for the different experimental tests that were done (i.e.: *in vitro, in vivo* and *in clinico)*. The comparison between the analytical/numerical electric field models is also presented along. A detailed analysis of the *in-clinico* results is presented to evaluate a possible correlation between the epileptogenicity of brain tissue and conductivity measurements. This chapter also presents the parameter sensitivity analysis performed to assess the impact of model parameters on the model output and determine the key parameters.

- *Chapter 6:* The impact and current limitations of the results are discussed in the context of the existing literature, along with their relevance and future prospects of conductivity measurements as a tool to assist further in the identification of the epileptogenic zone (EZ). Finally, a general conclusion is presented.

2 State of the art

2.1 Conductivity in living tissues

The electrical properties of biological tissues in general (and of brain tissue in particular), is an area of significant interest in the field of biomedical engineering. It is now indeed accepted that tissue electrical properties can be indicative of pathophysiological processes, which has the potential for diagnostic applications. However, measuring the electrical characteristics of biological tissue can be challenging. In this Chapter, we first present the theory underlying the electric properties of biological tissue. Then, we introduce the frequency dependency, anisotropy and temperature dependency of electrical parameters. Finally, the main models that have been developed in order to evaluate tissue impedance, along with their advantages and limitations are reviewed.

2.1.1 Tissues basics components and dielectric properties

Life on Earth is carbon-based, i.e. carbon atoms are bonded to other elements. More specifically, the human body is indeed mostly composed of hydrogen (63%), oxygen (25%), carbon (9%) and nitrogen (1.4%). Virtually all cells are composed of water, proteins, carbohydrates and lipids (Grimnes, 2014). The electrical properties of organic compounds are diverse. Firstly, carbohydrates

are the main energy source, and are not believed to contribute with the electrical properties of biological tissues. Secondly, lipids are found in most of the passive cell membranes, and are at the origin of the capacitive nature of cells and tissue. Cell membranes consist of a bilayer lipid membrane of very low electric conductivity. Ions can flow through the membrane only through specialized membrane channels (Grimnes, 2014).

Most cells are primarily composed of proteins. Proteins, in electrical terms, can be approximated as a simple polar molecule, with zero net charge, possessing a dipole moment (Pethig and Kell, 1987). The environment of cells also plays a role in the electrical properties of tissue. Notably, living cells are surrounded by aqueous electrolytes, with the most important cations being H^+, Na^+, K^+, Ca^{2+} and Mg^{2+}, and most important anions being ${HCO_3}^-$, Cl^-, ${HPO_4}^-$, ${SO_4}^{2-}$. For aqueous biological materials, the conductivity results primarily from the mobility of hydrated ions. Overall, the total conductivity includes the steady state conductivity related with ions mobility, and dielectric losses associated with polarization processes. Since biological tissue is a highly heterogeneous material, (e.g., different cell membranes, channels, cell orientation, extracellular ions concentration, cell size...), this variability explains the observed large range of dielectric properties associated with various body tissues (Plonsey and Barr, 2007).

Regarding brain tissue in particular, neurons are composed of 70-80% water, while the dry material is about 80% protein and 20% lipid (Grimnes, 2014; Plonsey and Barr, 2007). Neurons are organized mainly according to three parts: cell body (soma), dendrites, and axon. Dendrites receive impulses (excitatory or inhibitory) from other neurons, and conduct them to the soma. The axon transfers action potentials from the soma to other neurons. Importantly, the membrane of neurons has different voltage-dependent ionic channels that are macromolecular pores through which sodium, potassium and chloride ions flow (Malmivuo and Plonsey, 1995), with a flow depending on neuron membrane polarization.

Frequency dependency and tissue impedance

In general, for all materials, dielectric permeability decreases and conductance increases as frequency increases, which mean that tissue impedance is frequency dependent. The complex electrical permittivity (inversely proportional to the impedance) can be expressed as:

$$\boldsymbol{\varepsilon^*(\omega) = \varepsilon'(\omega) - j\varepsilon''(\omega)}$$

where $\boldsymbol{\varepsilon'}$ is the dielectric permeability, $\boldsymbol{\varepsilon''}$ the dielectric loss factor and $\boldsymbol{\omega}$ the angular frequency. The dielectric loss factor is a function of conductivity and the angular frequency (i.e. $\boldsymbol{\varepsilon^*(\omega) = \varepsilon'(\omega) - j\frac{\sigma(\omega)}{\omega}}$). Biological tissues have ionic conductivities that depend mostly of the nature and quantity of their ionic content and mobility (C. Gabriel et al., 1996; Malmivuo and Plonsey, 1995; Plonsey and Barr, 2007). When an electric field is applied, a current will form due to the movement of

ions in the aqueous medium, and is expressed as a function of tissue conductivity. At higher frequencies, the membrane lets alternating currents go through, as shown in Fig. 2-1.

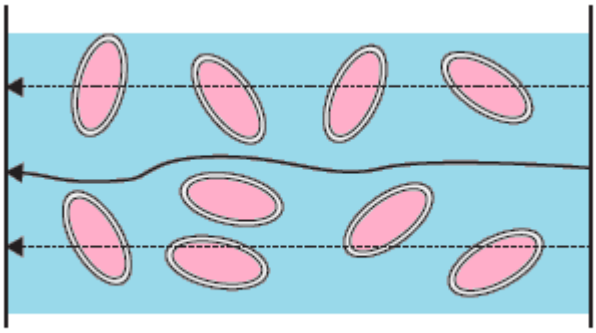

Fig. 2-1. Current flow in tissue at low and high frequencies. High frequency is presented with a dotted line, and low frequency with a solid line (adapted from Grimnes, 2014, no permission requested)

For biological materials, the frequency dependence of conductivity is rather complex, and depends on several factors. Three different dispersions are generally identified: *alpha*, *beta*, and *gamma*, which are defined for well-known physical properties. *Alpha dispersions* are found in the Hz-kHz range and are associated with ionic diffusion processes at the cellular membrane level. *Beta dispersions* start occurring in the kHz-MHz range (C. Gabriel et al., 1996; S. Gabriel et al., 1996), and is caused by the polarization of cell membranes which act as barriers to ionic flow and protein polarization. *Gamma polarizations* are in the GHz range, and are associated with water polarization (C. Gabriel et al., 1996; Grant, 1981).

In conclusion, biological tissues feature two electrically conducting compartments: the *extracellular* and *intracellular* spaces, separated by the membrane. The conduction of electric currents through tissue is strongly dependent on frequency. Furthermore, the relationship between impedance, conductivity and permittivity depends on electrode geometry. As an example, a parallel plate electrode of area A and distance between plates of d, has a capacitance $C = \varepsilon'(\omega)A/d$ and a conductance $G = \sigma(\omega)A/d$, leading to the expression of the complex impedance (Grimnes, 2014):

$$Z(\omega) = \left(\frac{d}{A}\right)\frac{1}{\sigma(\omega) + j\omega\varepsilon'(\omega)}$$

In this example, it is observed that impedance is inversely proportional to the complex electrical permittivity and proportional to a constant that depends on electrode geometry (i.e.: cell constant). For experimental measurements of the frequency dependency of a material, impedance spectroscopy is commonly used, consisting in applying a weak oscillatory voltage and measuring the current. Impedance can be fitted against analytical formulas derived from circuit models (e.g. intracellular and extracellular resistance and membrane capacitance). Impedance spectroscopy is an accepted and

validated technique in different medical fields for diagnosis and monitoring purposes, as reviewed below.

The investigation of the electrical properties of biological tissue has been initiated almost a century ago, with one of the first databases dating back to the early 20th century (Crile et al., 1922). This study analyzed mostly rabbits, examining the conductivity of different tissues and body liquids. Techniques to measure and analyze electrical properties have continued to develop, until a study (Schwan and Kay, 1957) which was one of the first to analyze the frequency-dependent specific resistance of *in situ* living dog tissues, and observing the different dispersions. By the end of the 1990's, a literature survey (C. Gabriel et al., 1996) and an extensive database of measurements at different frequencies (S. Gabriel et al., 1996) were published by Gabriel *et al*. The literature survey included all the main tissues for which there were three of more literature reports. For most tissues, data was limited or non-existent. The database, investigated the dielectric properties of permittivity and conductivity for different human and animal tissues at body temperature, for a frequency range between 10 Hz and 20 GHz, using automatic swept-frequency and impedance analyzers. The tissues analyzed were: brain (grey and white matter), heart muscle, kidney, liver, lung, spleen, muscle (paravertebral cut across and along the fibers), uterus, skin, thyroid, testis, ovary and bladder. Measured tissues were from bovine origin, human post-mortem and human *in-vivo*. Gabriel *et al*. concluded that the measurements fell well within the values in the literature, and that for measurements on the low-frequency experimental set-up, electrode polarization errors affected the results below 1 kHz. Therefore, nowadays low-frequency measurements still remain an open question.

Isotropic and anisotropic tissues

Isotropy (resp. anisotropy) is the property of being independent (resp. dependent) of the spatial direction when measuring a physical magnitude. Electrical properties such as permittivity and conductivity are usually dependent of the cell orientation in tissue. The fact that tissues are highly heterogeneous, with different sizes and functions, lead to significant differences in electrical conductivity (Grimnes, 2014). Considering tissue as an anisotropic medium implies that it must be considered as a volume conductor (i.e. 3-dimension conductivity tensor). Electrical anisotropy is related to the physiology of tissue, an example being bones and skeletal muscle, which support longitudinal tension, explaining why muscles are composed of fibers that are large longitudinal cells aligned in the same direction. This results in higher electrical conductivity along the length of the fiber (Miklavcic et al., 2006). In (Epstein and Foster, 1983), freshly excised dog skeletal muscle was measured for different frequencies. Over the entire frequency range, the dielectric properties of muscle were found to be significantly anisotropic, with the kHz band anisotropy ratios (perpendicular/parallel to the fiber axis) found to be ten times higher, and less so in the MHz band.

Temperature dependence of conductivity

The ions mobility in an electrolyte solution depends on temperature. In general, conductivity increases with temperature as shown in (Kuyucak and Chung, 1994). Therefore, this must be taken into account if there are large variations in temperature between measurements as emphasized in (Baumann et al., 1997), where cerebrospinal fluid (CSF) conductivity was measured in seven patients and was found to be 23% higher at body temperature (37°C) than at room temperature (25°C).

2.2 Electrophysiological activity

This chapter provides a short primer to electrophysiology. Furthermore, the specific markers investigated in stereoelectroencephalography (SEEG, intracranial EEG) recordings to identify an epileptic zone are also described. General information about neurons is first presented, followed by the physiological electrophysiological patterns, and finally the pathological activity patterns found in epilepsy which are used to identify the epileptogenic zone (EZ) from recordings, either by visual inspect or using signal processing.

2.2.1 Neuron

From an anatomical perspective, a neuron is composed of four parts: the dendrites, the cell body (soma), the axons and the synapses, as shown in Fig. 2-2.

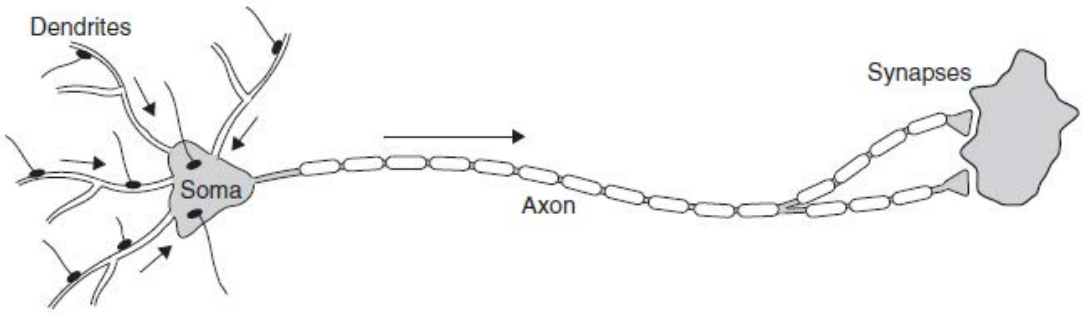

Fig. 2-2. Anatomical structure of a neuron. The main components of a neuron are dendrites, the cell body (soma), the axon and synapses (adapted from (Grimnes, 2014), no permission requested).

Neurons communicate with each other through action potentials, which are a transient phenomenon characterized by a drastic local depolarization of the membrane. When the total incoming post-synaptic potential exceeds the firing threshold, an action potential is triggered. Membranes channels enable the regulation of extra/intracellular ionic concentrations (calcium, potassium and chloride), and their differential dynamics and properties underlie action potential dynamics (depolarization, repolarization and hyperpolarization) as shown in Fig. 2-3.

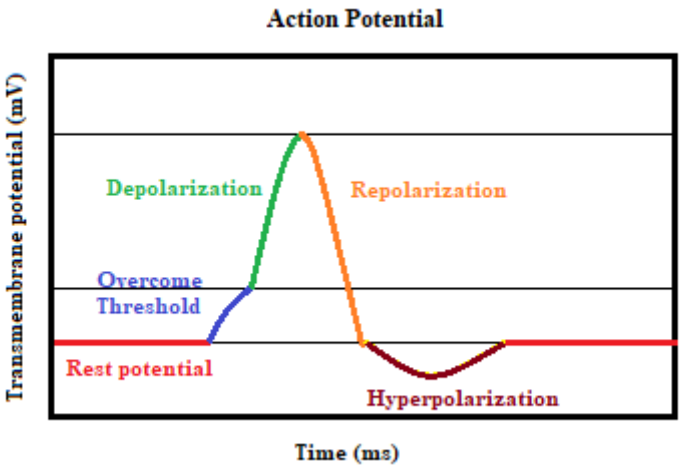

Fig. 2-3. Action potential time course. When the firing threshold is exceeded, a rapid depolarization occurs, followed by a repolarization and hyperpolarization phase of the transmembrane potential (Adapted from Plonsey and Barr, 2007).

The firing threshold depends on the type of neuron. During the depolarization and repolarization phases, neurons cannot trigger other action potentials. The action potential propagates through the axon until the synapse, and the synapse transmits the signal from one neuron to another using a neurotransmitter that is emitted by the afferent neuron, diffuses into the synaptic cleft, and binds to postsynaptic receptors to create a postsynaptic potential.

When considering macroelectrodes (as is the case in this thesis), the action potentials are not directly measured. It is admitted that the electric fields produced by an action potential can only be detected at proximity of ~10 µm from the source (Bédard et al., 2006). In fact, due to the large size of the electrodes, the measured signal represents mostly the contributions of post-synaptic potentials (Destexhe and Bedard, 2013).

2.2.2 Brain rhythms

Brain rhythms reflect the activity of large assemblies of neurons, i.e. a complex spatial summation of numerous post-synaptic potentials. One common non-invasive modality of recording brain rhythms is electroencephalography (EEG), which consists in recording neuronal activity from cortical sources using scalp electrodes. The EEG signals are generated from several neuron populations (synaptic activity of pyramidal cells), which are groups of neurons organized both in time and space. The sums of several populations of neurons generate different brain rhythms, that are signals transmitted between brain structures. Nevertheless, given the distance between cortical sources of neuronal activity and scalp electrodes, the EEG does not measure the action potentials but instead the synchronized oscillations of a large number of neurons (Nunez and Srinivasan, 2006). These oscillations are classified according to their dominant frequency. The principal rhythms are the following (Nunez, 1995; Silva et al., 2012):

- *Delta* (< 3 Hz): these oscillations are strongest in amplitude, are typically attributed to the thalamus, and are involved in different sleep states.
- *Theta* (4-7 Hz): These waves are observed principally in the hippocampus and in the frontal cortex. They participate in the process of short-term storage of information also known as working memory, and in the regulation of emotions.
- *Alpha* (8-13 Hz): They are historically the first waves to be observed by Hans Berger in 1929, given their significant amplitude. These oscillations are related to awareness, visual attention, and inhibition of task-irrelevant networks.
- *Beta* (15-30 Hz): These oscillations are associated with normal waking consciousness, and can be linked to anxiety or active focus. In the motor cortex, this rhythm is related with muscle contractions.
- *Gamma* (> 30 Hz): This rhythm is common in the cortex, and is associated with cognitive processes such as perception.

Intense research efforts are ongoing to understand how functional brain communication between cortical regions depends on these oscillations. One hypothesis is that cross-frequency couplings between different regions and rhythms could be a way of multiplexing and encoding information. Readers may refer to (Bonnefond et al., 2017) for additional information on this topic.

2.2.3 Electrophysiological markers of epilepsy

The investigation of EEG has played an essential role in the study of neurological diseases such as epilepsy. Some neurological disorders are associated with specific electrophysiological signatures (Schnitzler and Gross, 2005). These electrophysiological markers recorded by EEG/SEEG are used to detect neuronal dysfunction to ends of diagnosis. In epilepsy, beside ictal activity, some typical signatures that can be distinguished are spikes-wave events, high frequency oscillations (HFO) and after-seizure slow waves (Worrell et al., 2008). Several methods exist to define epileptic networks from the aforementioned electrophysiological markers (Bartolomei et al., 2008). Differences could be made between the regions that are lesional, those that are epileptogenic zones, the regions where the seizures starts (often referred to as the seizure onset zone, SOZ) and regions that are not considered to generate discharges but rather receive epileptiform activity (i.e. belonging to the propagation zone PZ). Another zone that could be classified is the irritating zone (IZ), a zone which is source of interictal epileptiform discharges (IED) (de Curtis et al., 2012; Marsh et al., 2010). It is important to determine cautiously the different structures with imaging and EEG investigations and for the definition of the surgery zones for resection. This is not always easy to determine, motivating the development of novel techniques.

Inter-ictal epileptiform discharges

Inter-ictal epileptiform discharges (IED) are often observed in the EEG, and are believed to be associated with cognitive deficiencies (Ung et al., 2017). IED originate from abnormal neuronal synchronization and are characterized by spikes, poly-spikes and spike-waves as shown in Fig. 2-4. (de Curtis et al., 2012; Schulze-Bonhage et al., 2011). When such activity is sparse, it does not result in clinical symptoms. Nevertheless, IED spikes are not benign, and a higher IED occurrence correlates with longer epilepsy duration (Selvitelli et al., 2010). Furthermore, IED can disrupt cognitive processes such as visual word recognition and memory (Ung et al., 2017).

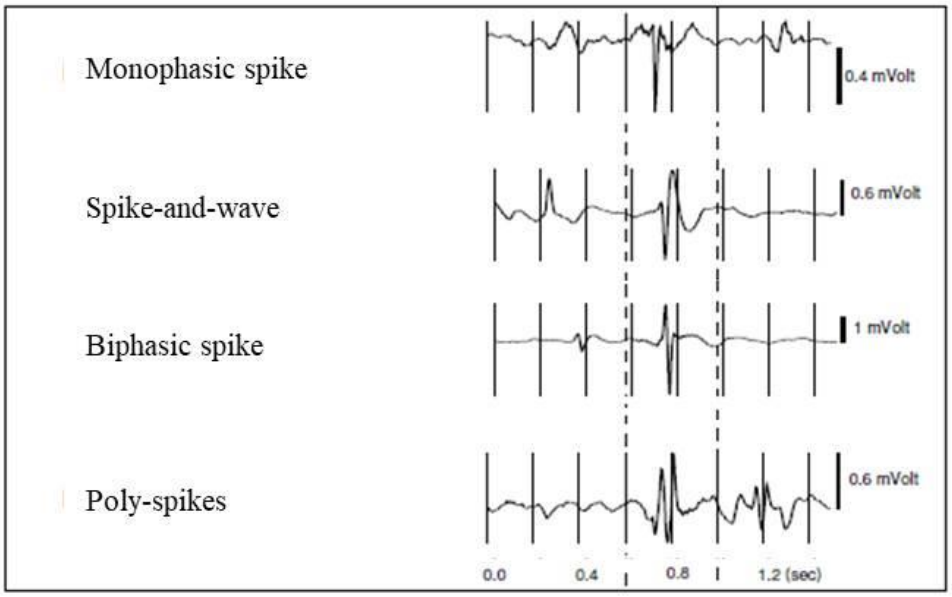

Fig. 2-4. EEG inter-ictal epileptiform discharges. Monophasic spike, spike-wave, biphasic spike and poly-spike (Adapted from Bourien, 2003)

An electrophysiological pattern associated with the EZ consists in rapid discharges called inter-ictal high frequency oscillations (inter-ictal HFO or fast ripples), with frequencies between 250 and 500 Hz. A number of studies have shown that favorable surgical outcome is associated with the resection of regions that generated fast ripples (Fujiwara et al., 2012).

Ictal activity

The proposed definition of seizure by the international league against epilepsy (ILAE) is a *transient occurrence of signs and/or symptoms due to abnormal excessive synchronous neuronal activity*. This seizure activity can be observed in the EEG and provides valuable information about the tissue. Important information about tissue can be gained by recording the regions generating seizures and their propagation pattern. During the interictal to ictal transition, it is sometimes observed a different kind of HFO, known as ictal HFO or fingerprint. This fingerprint is recognized as a biomarker representative of the seizure onset zone (SOZ) in focal seizures (Grinenko et al., 2018; Jirsch et al.,

2006). Following the ictal HFO, another typical pattern of epileptic zones are rhythmic large amplitude spikes often observed in SEEG (Fisher et al., 2014).

Post-ictal activity

After the end of a seizure, there can be a post-ictal period during which patients may be confused, have problems remembering, or be disoriented. Post-ictal state denotes brain recovery from seizure, and is characterized by a polymorphic delta activity (slow waves), regional signal attenuation and activation of focal spikes. An elevation of cortical slow waves after seizures has been associated with anatomical and functional abnormalities, and when clearly present is highly correlated with the side of the SOZ (Jan et al., 2001; Yang et al., 2012). So far, there is only little literature regarding the seizure termination process, the mechanisms of which remaining largely unknown.

2.3 Electrical stimulation

Brain stimulation has been thoroughly investigated for diagnosis (e.g., pre-surgical functional stimulation for drug-refractory patients) and therapy (e.g., deep brain stimulation in Parkinson's disease) for the last decades. Since neurons are excitable cells, their activity can be modulated by the application of extracellular fields. Therefore, when stimulating a nerve cell, the transmembrane voltage changes, which can result in an excitatory (increase of the membrane potential, facilitating action potentials generation) or inhibitory (decrease of the membrane potential, preventing the onset of action potentials) effects on neuronal activity (Malmivuo and Plonsey, 1995). The main two types of brain stimulation are *electric* and *magnetic* stimulation. Electric stimulation can be delivered non-invasively or invasively through the use of intracranial electrodes, while magnetic stimulation is typically delivered through coils in which flows a high-intensity current.

Chronaxie and Rheobase

The relation between the current I required to initiate an action potential and the duration T of the pulse have been first derived experimentally by Lapique at the beginning of the 20th century. For clinical electrical stimulation applications, the analysis of the minimal couple ($I - T$) required to trigger action potentials in the targeted region is essential to evaluate the effects of stimulation. Importantly, the amount of charge induced in tissue depends on the current intensity and pulse duration ($Q = I \times T$). An example of a current-time curve is shown in Fig. 2-5:

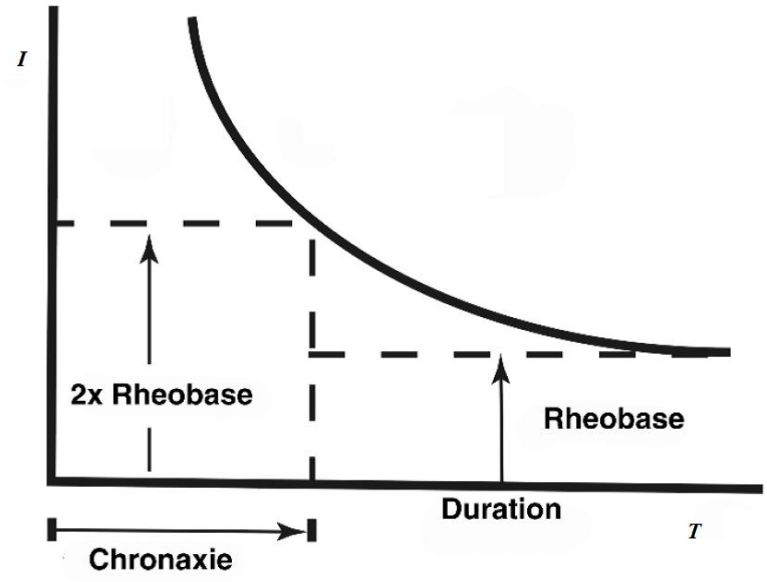

Fig. 2-5. Current-time curve, combination of stimulating current *I* and the stimulus duration, that are just sufficient to reach the threshold level (adapted from Plonsey and Barr, 2007, no permission requested).

The minimal value of current I_{rh} that still produces a threshold value of transmembrane voltage, as the pulse duration tends to infinity, is called the rheobase. The rheobase depends upon factors such as the distance between the neuronal population of interest and the electrode. The chronaxie is defined as the minimal pulse duration T which triggers action potentials with a current twice the I_{rh}. Chronaxie is used for choosing the stimulus strength in a stimulation protocol (the minimum time required to reach transmembrane potential threshold). These concepts provide a guide for understanding why greater stimulus current can create an action potential despite being shorter in time, or why no action potential are observed when stimulating at low currents (Plonsey and Barr, 2007).

Excitable tissues

Excitable tissues are tissues sensitive to electrical stimulation. The goal of stimulation is often to trigger action potentials in axons, due to the depolarization of some portion of the axon membrane. The resulting induced activity depends on many factors, including, but not limited to, the electrical properties of local cell membranes and the transmembrane potential (difference between the extracellular and intracellular potential), orientation of the electric field with respect to the somatodendritic axis of cells, neuronal morphology (Grimnes, 2014). The most common excitable cells are muscular and neuronal cells. In the case of muscle tissue, the stimulating electric field in a cell induces a contraction that propagates over muscular tissue when the transmembrane threshold is reached. Similarly, in the case of neurons, if the membrane stimulus is not sufficient to bring the transmembrane potential to threshold, no action potentials are induced. If the excitatory stimulus is strong enough, the extracellular region is driven to more negative potentials (charge is transferred across the membrane through passive and active ion channels), which is equivalent to driving the

intracellular compartment of a cell to more positive potentials, which induces a spike that propagates over the axon and reaches other neurons (Malmivuo and Plonsey, 1995).

Subsequently, the objective of stimulation is to induce an electric potential in the surrounding tissue to achieve a tissue response. In this thesis, bipolar stimulation is used. When stimulating with bipolar stimulation, current flows from the working electrode to the extracellular fluid surrounding the tissue, and finally to the counter electrode. Constant current stimulation induces a constant electric potential and electric field in the tissue during the duration pulse. The generated electric field induces depolarizing/hyperpolarizing (depending on the current sign and if considering the working/counter electrode, and of the relative orientation between the somatodendritic axis and electric field) of the surrounding axon membrane (Merrill et al., 2005; Plonsey and Barr, 2007).

Subthreshold stimulation is sometimes used for producing the phenomenon of accommodation. A stimulus that produces subthreshold depolarization will reduce the number of axons that can be recruited and so increasing the threshold for action potentials. It is often desirable to activate one population of neurons without activating a neighboring population. This is sometimes achieved with subthreshold stimulation, provided that different populations may have different thresholds (Bikson et al., 2012; Nitsche and Paulus, 2009).

Electrical stimulations used clinically are typically performed at intensities higher than 1 mA (inducing electric fields near the electrode ~100V/m). This level of stimulation can evoke pyramidal cells activity (Esser et al., 2005; Radman et al., 2009). Interestingly, it is has also been shown that interneuron activity can be induced at lower intensities (< 1 mA) (Wendling et al., 2016).

Transcranial stimulation

In terms of non-invasive electrical brain stimulation, transcranial direct current stimulation (tDCS) and transcranial alternating current stimulation (tACS) are increasingly used for research purposes, and are developing in terms of therapy. It is worth mentioning that tDCS and tACS use low-level electric fields, as compared to invasive electrical brain stimulation (e.g., ~1 V/m versus 50-200 V/m): it is therefore suspected that the principal mechanism of tDCS is the subthreshold modulation of the membrane potential or neurotransmitter release probability, which alters cortical excitability (Woods et al., 2016). tDCS has become an interesting tool to modulate cortical excitability and activity in epilepsy (Lafon et al., 2017; Nitsche and Paulus, 2009; Tecchio et al., 2018).

Regarding magnetic stimulation, the most common stimulation modality is TMS, consisting in a short (~100 μs), strong (~ 1 T) magnetic stimulus, inducing an electric current in cortical tissue that triggers action potentials in cortical neurons. Depending on the stimulation frequency, TMS can induce increases/decreases in cortical excitability (Nitsche and Paulus, 2009). In this thesis work, we will focus on intracranial, electric stimulation of brain tissue.

2.3.1 Stereotaxic EEG procedure

In order to perform intracranial electrical stimulation, electrodes have to be carefully implanted in multiple brain regions. This is achieved through a stereotaxic procedure, a neurosurgical intervention using a three-dimensional coordinate and an atlas to precisely implant the electrodes (Mercier et al., 2012; Olivier et al., 2012; Talairach and Bancaud, 1973). The surgical procedure for implantation consists in three main parts: trajectory planning, implantation surgery and post-implantation phase.

Trajectory planning

Pre-surgical evaluation is conducted for defining the subsequent therapeutic approach, typically surgery. During this planning, when SEEG exploration is decided, the location and the trajectory of the electrodes are defined. During this assessment, the acquisition of preoperative signal/images is performed to evaluate possible epileptic zones and determine possible trajectories for the electrodes. Scalp video EEG is used to record seizures and detect possible implantation regions, followed by MRI scan with particular attention to the regions identified using EEG. This process leads to the generation of hypotheses about the localization of the EZ. Then, the planning of the electrode trajectories is defined by the target and the skull entry point. The major complication in electrode implantation is intracranial hemorrhage (Zuluaga et al., 2014), therefore extreme caution is required in the definition of the electrode trajectory to avoid any major vessel.

Electrode implantation

The surgical technique for electrodes implantation is performed under general anesthesia. The patient's head is in a stereotactic frame, which is used as a three-dimensional coordinate system, as shown in Fig. 2-6.(a). The trajectories are defined as to reach the selected cortical targets and avoid the vessels.

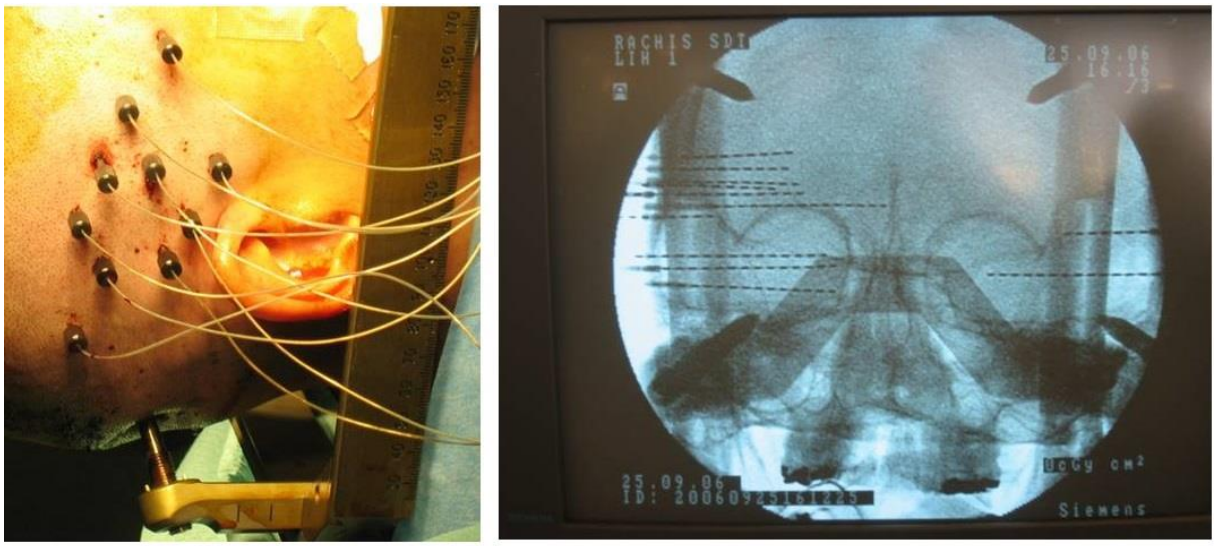

(a) (b)

Fig. 2-6. (a) Implanted stereotactic EEG electrodes and (b) postoperative CT of a patient with stereotactic EEG electrodes (courtesy of Dr. A. Biraben).

For the implantation of each electrode, the removal of a circular piece of cranium is performed with a twist drill. Titanium hollow pegs, for the insertion and the fixation of the electrodes are then attached to the cranium. Finally, the electrode is inserted and advanced to the target, and is fixed to the peg by a plastic cap (Cossu et al., 2005; Munari et al., 1994).

Postoperative phase

A MRI/CT scan is done after electrodes implantation to define the actual position of each contact as shown in Fig. 2-6.(b). After that, the video SEEG recording begins with the purpose to record patient's seizures. Finally, the patient undergoes a series of electrical stimulations with the purpose of inducing ictal activity and assist further in identifying the EZ.

2.3.2 Intracranial electrodes

The primary objective of SEEG exploration is to record seizures in order to accurately define the organization of the EZ and thus the best resection aimed at suppressing seizures. In addition, intracranial electrodes offer the unique opportunity to perform electrical stimulation of explored brain region. Therefore, a crucial prerequisite to exploit fully the information provided by the recorded signals is to understand the biophysical phenomenon involved when intracranial electrodes are placed in brain tissue. In the following, I provide details about the models found in the literature to approximate the biophysical properties stimulation using intracranial electrodes.

Dipole approximation of the electric potential

The simplest case for approximating the electric field/potential is considering the electrode with two active contacts as a dipole. Let us consider the bipolar electrodes as a point source, as shown in Fig. 2-7.(a).

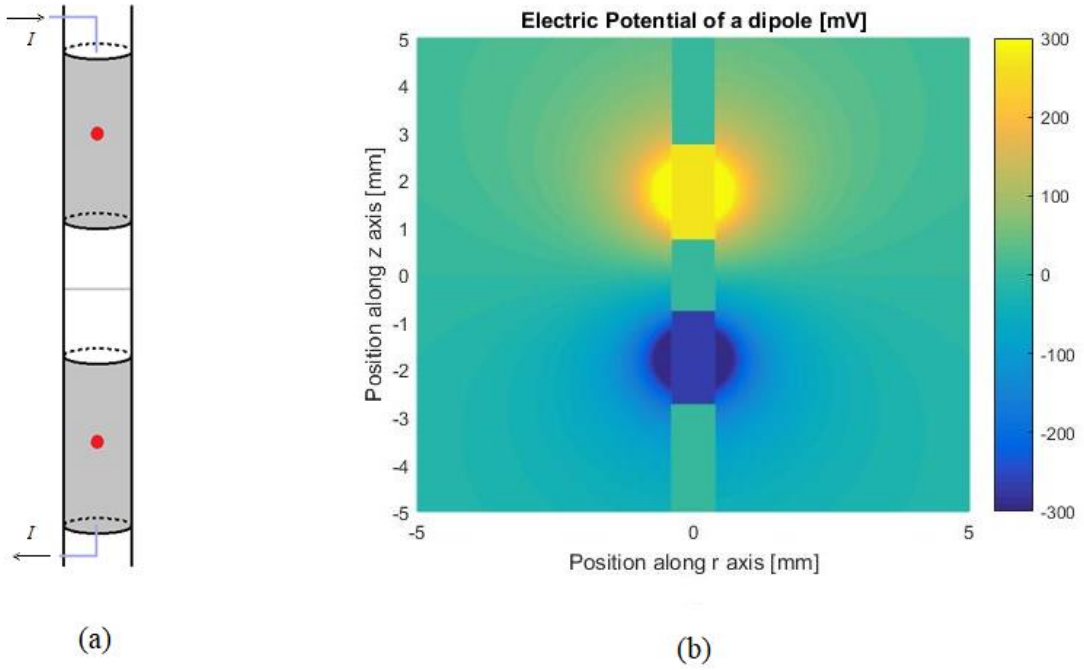

Fig. 2-7. Two-contacts seen as a dipole (a) The two dipole source with a constant current *I* and (b) Electric potential generated by a two bipolar electrode modeled by a dipole source.

Assuming that the two electrodes can be considered as a dipole, using spherical coordinates and considering an arbitrary point in space, the total current is induced is (Bossetti et al., 2008):

$$I = \oint \vec{J} dA = 4\pi r^2 J(d) \Rightarrow J(d) = \frac{I}{4\pi d^2}$$

Using Ohm's law, the linear relationship between the current density and the electric field is $\boldsymbol{J} = \sigma \boldsymbol{E}$, therefore the radial electric field and electric potential are respectively:

$$E_r = \frac{I}{4\pi\sigma d^2}$$

$$V(d) = \frac{I}{4\pi\sigma d}$$

$V(d)$ is the electric potential for a point source, in the case of a dipole the total electric potential is:

$$V = \frac{I}{4\pi\sigma d_1} - \frac{I}{4\pi\sigma d_2}$$

where d_1 and d_2 are the distance from each source to an arbitrary point in space. Considering this distance in Cartesian coordinates, and for $r > R$:

$$V(r,z) = \frac{I}{4\pi\sigma}\left(\frac{1}{\sqrt{r^2 + \left(z - \frac{l+h}{2}\right)^2}} - \frac{1}{\sqrt{r^2 + \left(z + \frac{l+h}{2}\right)^2}}\right)$$

This simple model is useful to visualize the approximate behavior of the electric potential in the space surrounding the electrode as shown in Fig. 2-7.(b).

Electrode-electrolyte interface

When a metal is placed inside a physiological medium, an interface forms between them. In metal electrodes, charge is carried by electrons while ions (present in the extracellular medium) carry charge in brain tissue. At the level of the electrode-electrolyte interface, the fundamental physical process is the transduction of charge carriers from electrons in the metal electrode to ions in the electrolyte. There are basically charge transfer mechanism in the electrode-electrolyte interface, non-faradaic (capacitive) charge transfer and faradaic reactions (Merrill et al., 2005). The non-faradaic charge transfer consists in several physical phenomena, the most important being that, when a metal electrode is placed in an electrolyte; charge redistribution occurs resulting in a plane of charge at the surface of the metal electrode. Another reason is that polar molecules, such as water, may have a preferred orientation at the interface so that the net orientation separates charges. When a current source is applied at the level of a pair of electrodes, an excess of negative charges is driven at one of the interfaces, which will attract cations in the solution toward the electrode and repel anions. At the other electrode, the opposite occurs. If the total amount of charge delivered is sufficiently small, only charge redistribution occurs, and there is no transfer of electrons as shown in Fig. 2-8.

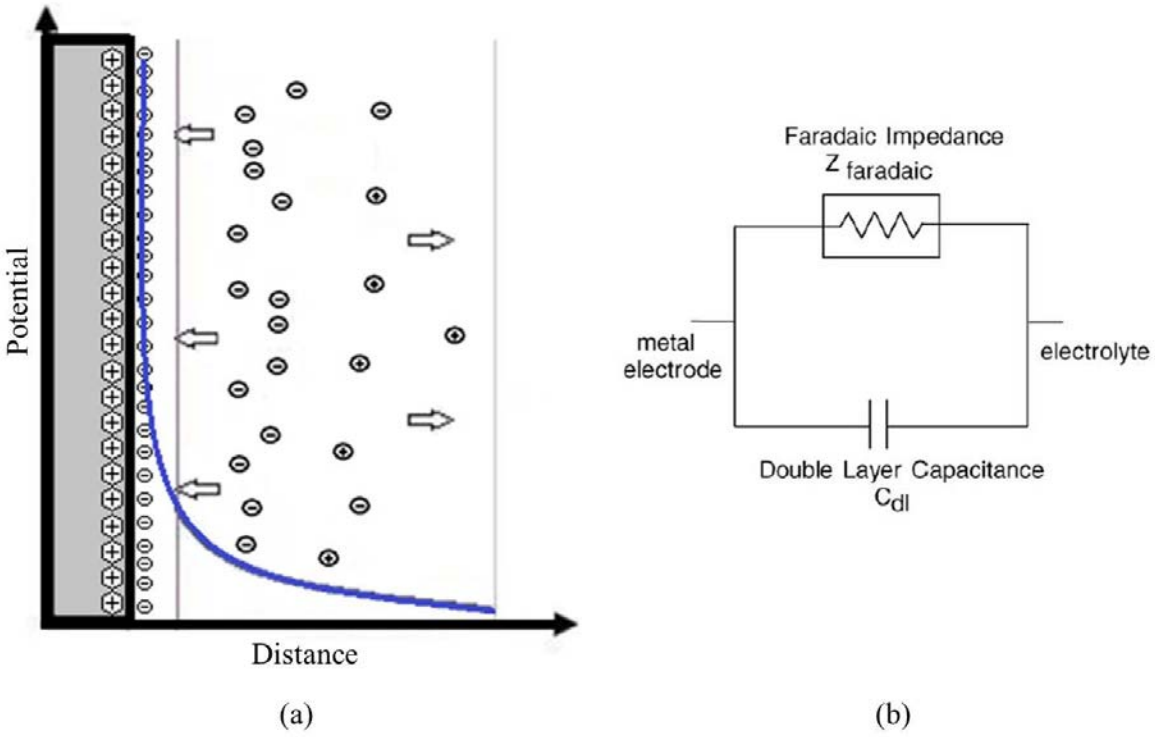

Fig. 2-8. (a) Ionic distribution at the electrode interface, showing a ion redistribution inducing a double layer. (b)Two-element electrical circuit mode for mechanism of ion redistribution and charge transfer at the electrode interface.

In this case, the interface can be approximated as a capacitor. Charge may be transferred from the electrode to the electrolyte by faradaic processes of reduction and oxidation. In this case, electrons are transferred from the metal electrode to the electrolyte. Reduction occurs at the negative electrode (an electron is added during the reaction), and oxidation occurs at the positive electrode (an electron is removed during the reaction). Frequently, these reactions form products when charge cannot be recovered by reversing the current direction. A simple electric circuit model of the processes involved at the electrode-electrolyte interface is shown in Fig. 2-8 (b). The double layer capacitance C_{dl} represents non-faradaic physical phenomena, and the faradaic impedance Z_f models the electron charge transfer in the interface.

Pseudo-capacitive behavior of electrodes

The term *pseudo-capacitance* is used to define certain electrodes materials. In electrochemistry, it is used to describe the behavior of some capacitive electrodes which there charge storage originates from different chemical reactions. While regular double layer capacitance arises from the potential-dependence of the surface density of charges stored non-faradaically at the interfaces, pseudo-capacitance is of faradaic origin (Brousse et al., 2015), and occurs when a fraction of the electrode surface (depending on the voltage) is covered by adsorbed material (Dymond, 1976). Other sources

are surface roughness, distribution of reaction rates, varying electrode thickness and non-uniform current distribution.

To understand pseudo-capacitive behavior, we need to present briefly the concept of fractional calculus, which involves a class of differential operators with any real or complex order. The differential operator is generally defined as (Riemann-Liouville type) (Demirci, 2012):

$$D^{\alpha}f(t) = \frac{d^n}{dt^n}\frac{1}{\Gamma(n-\alpha)}\int_0^t (t-\tau)^{n-\alpha-1}f(\tau)d\tau$$

where α is the order of the differential operator, generally between $0 \leq \alpha \leq 1$, and $\Gamma(*)$ the gamma function. Fractional calculus has today several fields of application in mathematics including electrical networks, control theory, and chemical physics (Kilbas et al., 2006). In our case, we are interested in its application in electrochemistry of corrosion, which is closely tight to electrodes/electrolyte behavior.

A pseudo-capacitance, or constant phase element (CPE), is not physically achievable with ordinary electric components, but it rather usually described as a frequency-dependent capacitance. The constant phase element is directly expressed in the Laplace domain as:

$$Z_{CPE} = 1/As^{\alpha}$$

which contains two independent parameters A and the exponent α (fractional order of the differential equation). The equivalent circuit consists in modeling the electrode-electrolyte interface using a CPE. In this thesis, both the double layer model and the constant phase element are used to model the electrode/electrolyte effects.

Redox reactions and platinum electrodes

The electrochemically significant components of tissue fluids are water, $NaCl$, HCO^{3-}, CO_2 and organic material such as glucose and proteins. The following are some redox reactions that occur when a electrode is inside a tissue (Brummer and Turner, 1975; Llopis et al., 1959; Onaral and Schwan, 1982):

$$2H_2O \rightarrow O_2(g) + 4H^+ + 4e^- \ (oxidation)$$

$$Cl^- + H_2O \rightarrow ClO^- + 2H^+ + 2e^- \ (saline\ oxidation)$$

Oxidation at the anode is hazardous, since it produces gas and induces a change in local pH near the electrode. Saline oxidation (there are other possible reactions) would probably be harmful too, since ClO^- is a strong oxidizing agent and is possibly physiologically toxic.

In this thesis, platinum/iridium (90/10) electrodes are used to stimulate brain tissue, so analyzing the reactions proper to platinum is important. The metal oxidation and dissolution of Pt under anodic condition in Cl^- are dangerous, since the dissolution products are powerful oxidizing agents.

$$Pt + 4Cl^- \rightarrow PtCl_4{}^{2-} + 2e^- (metal\ corrosion)$$

Therefore, this emphasizes the precautions that have to be taken for the design of safe stimulation protocols that do not damage brain tissue (Merrill et al., 2005).

Gliosis and impedance variation after implantation

When a foreign body is introduced into the brain (or any other living tissue), reactions occur in the tissue, consisting in the attachment of proteins and cells directly to the electrode. This explains why, during the days after surgical implantation, electrode impedance increases (Grill and Mortimer, 1994), and stabilizes several weeks after implantation. Different tissue encapsulation models have been analyzed and tested in *in-vivo* in non-human primates, and the model presented below captures the most accurately the encapsulation tissue forming after implantation (Lempka et al., 2009):

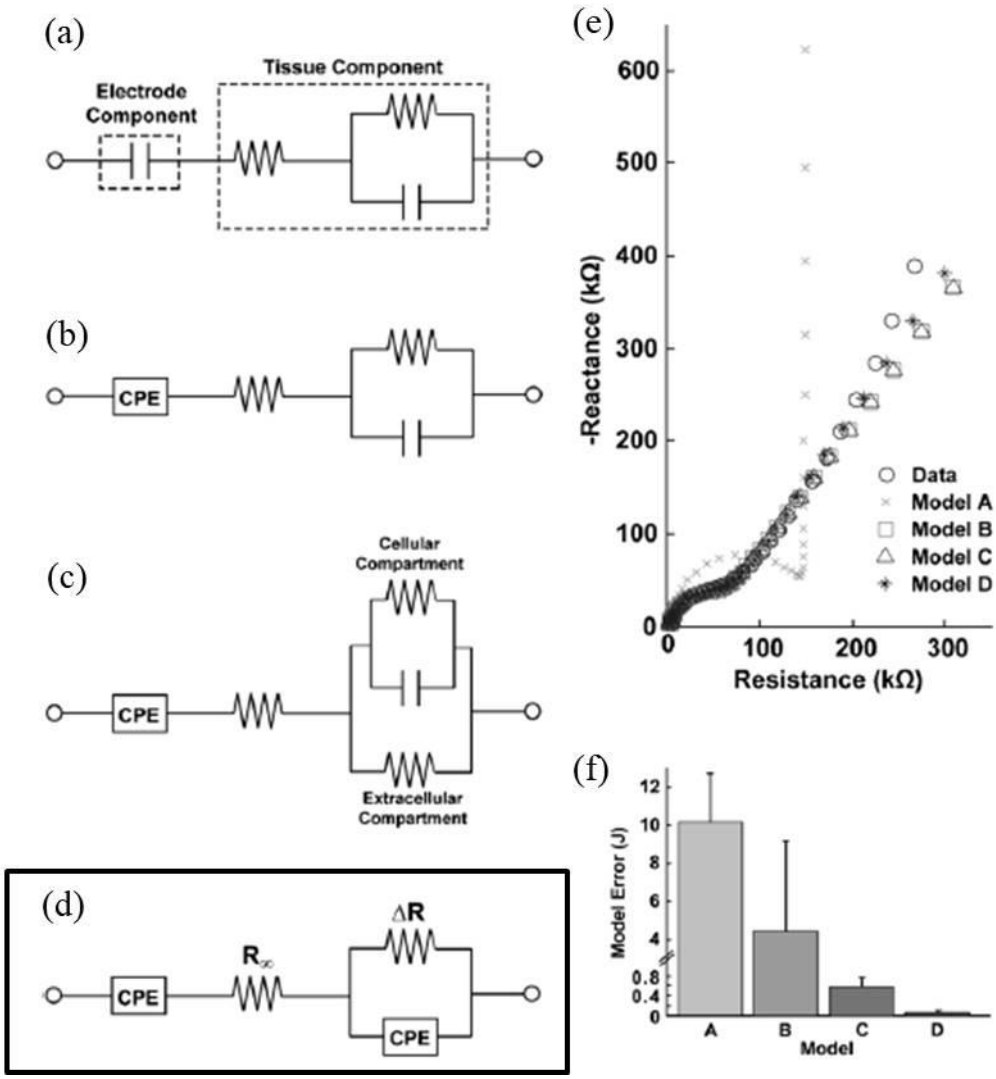

Fig. 2-9. The electrode-electrolyte interface and tissue layer impedance equivalent circuit models (adapted from Lempka et al., 2009, no permission requested).

Fig. 2-9. (a)–(d) presents four models for the encapsulation tissue. These models follow a pattern of electrode component and tissue component as shown in Fig. 2-9. (a). The electrode component in Fig. 2-9.(a) is modeled as a simple capacitance taking into account only ions redistribution. In other models, the electrode component is taken as a constant phase element, which takes into account some of the charge transfer effects on the electrode-electrolyte interface. The tissue components in all models are a combination of resistances and capacitances (or CPE). It is considered that the electric model in Fig. 2-9. (d). is the one with the smallest error. This model will be further developed in this thesis as an attempt to capture the properties of the encapsulation tissue.

2.3.3 Charge delivery by current control

Constant current stimulation is commonly used for the stimulation of brain tissue. This method is preferred over constant voltage, since the current injected by voltage-controlled methods is dependent

on the electrode's impedance. As aforementioned, this impedance is dependent on the electrode-electrolyte interface and on the encapsulation tissue forming within the days after implantation. On the other hand, the electric potential generated in the tissue during constant current stimulation is independent of intracranial electrodes impedance. Constant current stimulation is what will be used in this thesis.

Tissue damage and electrode corrosion

If the electrical stimulation intensity is too high, it has the potential harm the tissue or damage the electrode itself. Indeed, an electrode that suffers significant oxidation driven by electrode potentials that exceeds standard limits could be irreversibly damaged. Such corrosion can be reached with platinum/iridium electrodes (as is the case during clinical stimulation, 90% platinum and 10% iridium electrode are used) in an extracellular medium containing chloride. It must be noted that corrosion is an irreversible faradaic process.

The mechanisms of tissue damage induced by stimulation are not completely understood, even if some hypotheses have been proposed (Merrill et al., 2005):

1) Damage induced by a hyperactivity of neurons for an extended period of time.
2) Creation of toxic electrochemical reaction products at the electrode surface.

There is empirical data that support both theories, which means that they are not mutually exclusive. It is believed that the charge per phase and charge density are important factors for neuronal damage (McCreery et al., 1990). Charge per phase and charge density are related to the hyperactivity of neurons, provided that they determine the total change in the extracellular medium. Thus, when considering a stimulation protocol, the geometry of the electrode must be taken into account for charge density (i.e. typical microelectrode stimulations have less charge per phase with larger charge densities), as shown in Fig. 2-10. which provides the maximum threshold for safe stimulations.

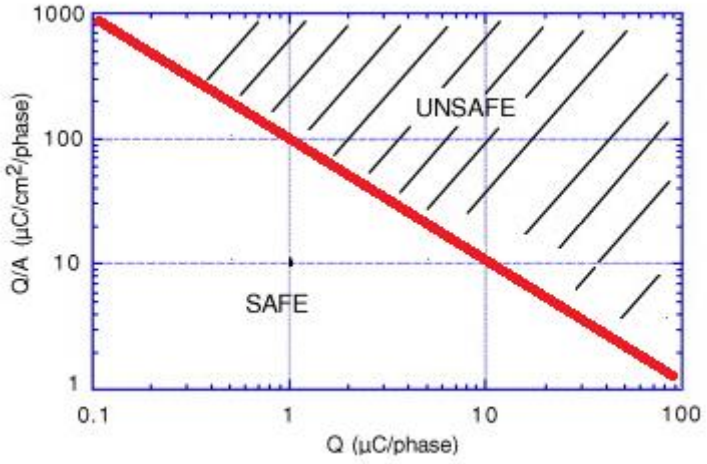

Fig. 2-10. Charge per phase and charge density for safe stimulation (adapted from (Merrill et al., 2005), no permission requested).

Charge-balanced waveforms

Monophasic stimulation causes greater tissue damage at comparable levels of charge per phase than biphasic stimulation (Lilly et al., 1955; Mortimer et al., 1980, 1970). These studies showed that monophasic stimulation causes significantly greater tissue damage at 1μC/mm^2 per phase than biphasic stimulation at levels up to 2μC/mm^2 per phase. Nevertheless, biphasic stimulation is less efficient in terms of ability to evoke a physiological response.

A stimulation protocol must be safe and efficient. Electrochemical reactions produced during stimulation damage the tissue, and there is evidence that a perfect symmetry of electrochemical reactions results in significantly decreased tissue damage. This symmetry of electrochemical reactions can be obtained using biphasic charge-balanced waveforms. Additionally, charge should be injected via non-faradaic process, to avoid injecting toxic materials into the tissue (Brummer and Turner, 1975).

Nowadays, typical clinical stimulation waveforms are biphasic, pulsed stimulation, with values of charge per phase of 1 μC/phase and charge density of 10 μC/mm^2 per phase (in the safety limits as shown in Fig. 2-10), to achieve efficient initiation of action potentials. The advantage of this stimulation mode is to control the total charge delivered to the tissue, and that the form of the waveform transmitted to the tissue is not dependent on the electrode/electrolyte interface.

2.4 Conductivity measurement techniques

Several methods have been developed to estimate electrical conductivity. In the electrochemical industry, conductivity instrumentation is used for quality control purposes, such as surveillance of water quality and purity, or estimation of the total number of ions in a solution (Gray, 2005; Huggins, 2002). The conductivity of ionic solutions depends on the concentration of the solution, the frequency

of the source, the mobility of the ions and the temperature. Measurements are performed with an alternating electric current *I*, using two electrodes cells immerged in a solution measure the voltage *V* as shown in Fig. 2-11 (Radiometer analytical, 2008).

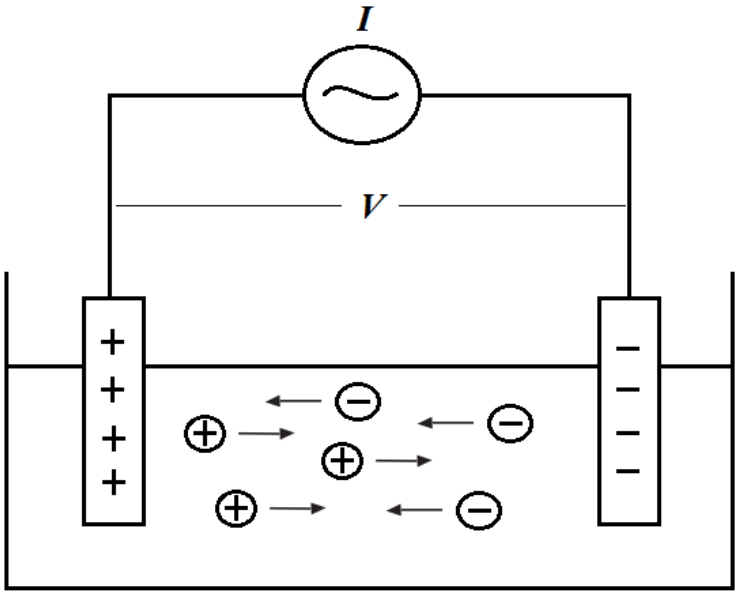

Fig. 2-11. Migration of ions in an electrolyte solution

The medium resistance is given by:

$$R = V / I$$

The constant of a K cell is a factor that depends on electrodes geometry. It corresponds to the relationship between the conductivity σ and the resistance of the solution R.

$$\sigma = K / R$$

The cell constant is given by the ratio between the distance between electrodes d and the electrode area:

$$K = d/A$$

There are some mechanisms that influence measurements such as electrode polarization, contamination of electrode surface, geometry errors related to field border effects, frequencies variation, and cable capacitance/resistance. Several techniques can prevent some of these effects, depending on the type of current/tension applied, and of the properties of the material being measured. Two types of cells are commonly used to measure conductivity: 2-electrode cell and 4-electrode cells.

2-electrode cell

This is the most simple and sufficient form for general industrial measurements, consisting in two electrodes: one applies an alternating current and one measures the tension. This measurement is altered by the impedance related to electrode/electrolyte interface phenomena.

In this thesis, given that two electrode stimulating electrodes are used, it will be considered as a 2-electode cell configuration.

4-electrode cell

These cells have two pairs of electrodes. One measures the current flowing through the solution; the other measures the voltage in the solution. The potential is measured in the presence of a weak current, so the effects related to the interface are negligible. This configuration is ideal for high conductivity measurements (Gray, 2005). In the area of medical applications, conductivity probes are not used, so other model-based methods are considered.

Two main approaches to measure impedance are used in biomedical applications: impedance-based and imaging-based techniques.

2.4.1 Impedance-based techniques

These techniques use electrodes (non-invasive or invasive) to calculate impedance, and then use a model to identify the relationship between impedance and conductivity. Some approaches consider the use of non-invasive measurements (Ferree et al., 2000; Gutierrez et al., 2004; Khalil et al., 2014). However, they involve inverse problems in their model to account for the layers between the electrode contact and the targeted tissue. Invasive measurements provide a more accurate estimate of local conductivity; however they involve surgery for electrode implantation. In the following, we do not present an exhaustive review of all the techniques of impedance spectroscopy measurement with their advantages and drawbacks, but instead focus instead on the two most common methods to measure impedance.

Current-Voltage method

This method is based on Ohm's law: a resistance is placed in series with the Z_x impedance that is to be measured as shown in Fig. 2-12. It is assumed that the same current that passes through R passes through Z_x.

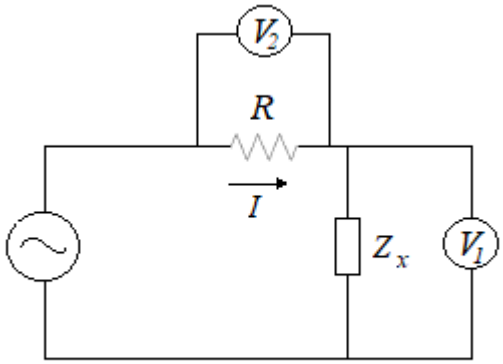

Fig. 2-12. Basic current-voltage impedance measurement setup.

The electric potential in R is measured to calculate the current that passes through the impedance Z_x. Measuring the electric potential in Z_x, it results in:

$$Z_x = \frac{V_1}{V_2} R$$

In practice, a low-loss transformer is used instead of the resistance R to prevent the effects caused by placing a low value resistor in the circuit, so a disadvantage of this setup is that the operating frequency range is limited by the transformer used in the probe (Dumbrava and Svilainis, 2008).

Bridge method

The bridge method uses a Wheatstone bridge, as shown in Fig. 2-13, and is based on Kirchhoff's first and second laws to identify relationships between currents, voltages and impedances.

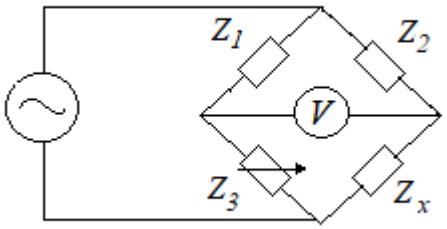

Fig. 2-13. Wheatstone bridge setup

When no current flows through the voltmeter V, the value of the unknown impedance is:

$$Z_x = \frac{Z_1}{Z_2} Z_3$$

The advantages of this method are its high accuracy, wide frequency range coverage by using different types of bridges and low cost, however this method requires a manual balance and has a narrow frequency coverage if used with a single bridge (Kaatze, 2013).

2.4.2 Imaging

Imaging techniques appear especially appealing, since they are non-invasive approaches that could measure the dielectric properties of tissue. However, the accuracy of imaging-based techniques for the measurement of dielectric properties of living tissue is still under investigation.

Diffusion tensor imaging

Diffusion tensor imaging (DTI) is a technique based in magnetic resonance imaging (MRI), which measures the diffusion of water molecules for each direction of space. Interestingly, it has been shown that the electrical conductivity tensor of tissue can be computed form the water self-diffusion tensor, with a strong linear relationship between conductivity and diffusion tensor imaging eigenvalues (Tuch et al., 2001). Nonetheless, this relationship has not been thoroughly evaluated, and has not been evaluated for different frequencies. Therefore, its potential use for diagnostic remains unconclusive. DTI has also been used in a study measuring the electrical conductivities of freshly excised cortex in 21 epilepsy surgery patients. Conductivity varied from patient to patient between 0.066 and 0.156 S/m. Of particular interest was the finding that focal cortical dysplasia tissue had increased conductivity (Akhtari et al., 2006). This study concluded that understanding how pathophysiological processes impact cortical conductivity on the one hand, and measuring it non-invasively on the other hand, could provide supplementary information in epileptic patients candidates to resective surgery.

Magnetic resonance electrical impedance tomography

A new imaging technique, combining electrical impedance tomography (EIT) and MRI, termed MREIT, has also emerged. Indeed, for conductivity imaging, MREIT has been proposed to overcome the inverse problem limitations of EIT. The physical principle is the following: an electrical current is injected in a conducting subject, which produces an electromagnetic field that can be measured by an MRI scanner. Using voltage measurements and magnetic field measurements, it has been shown that a conductivity tensor can be obtained non-invasively (Katscher et al., 2009; Seo et al., 2005). MREIT remains a technique under evaluation for non-invasive conductivity measurements. Applications of MREIT include the search brain abscess (Kim et al., 2015; Oh et al., 2013). In these studies, brain abscess was induced in healthy dogs, four electrodes were attached to the head and a 5 mA current was injected. Dogs were placed inside the MRI and relative conductivity ratios (before and after lesion) were computed. The study concluded that the increased conductivity of inflammation may provide evidence of injured tissues. However, these methods are not yet tested in humans given that

the required current level to achieve a good resolution is excessively high for being safely used in the head (Abascal et al., 2008). Thus, to our knowledge, MREIT is not yet been used for epilepsy.

2.5 Conductivity in medicine

Due to its possible application in diagnosis, the estimation of tissue conductivity has sparked interest in other areas of medicine such as oncology, muscles diseases and neurology, which we briefly review below.

2.5.1 Oncology

One feature of cancerous cells is indeed their lower cell membrane potential as compared to healthy adult cells, as shown in ovary cells immersed in culture media (Cone, 1974, 1970). As reported, healthy cells maintain a high concentration of potassium and a low concentration of sodium. In contrast, when cells are injured or cancerous, sodium and water flows into the cell, decreasing potassium and other ions concentration in the intracellular medium, resulting in decreased impedance (Muftuler et al., 2006, 2004). Along the same line, recent studies have shown differences in the dielectric properties of healthy and cancer tissue (Qiao et al., 2010; Sree et al., 2011) as measured with needle electrodes. Interestingly, both studies concluded that healthy tissue has higher conductivity than tumor tissue, given that cancer tissue has different electrical and metabolic properties due to abnormalities in structures.

Other studies for breast cancer detection with conductivity made use of *in-vivo* imaging techniques. In a study using electrical impedance scanning in 181 breast cancer patients, potential differences in conductivity were investigated to ends of diagnosis (Daglar et al., 2016). Twelve true positive out of fourteen were malignant tumors, while seven out of eleven true negatives benign lesions, leading to the conclusion that breast electrical impedance measures could be useful to reduce the number of unnecessary follow-up and biopsy rates. Another study (Shin et al., 2015) used MRI in 50 previously biopsy-confirmed breast tumor and 40 normal subjects (90 subjects total). The conductivity estimation for malignant tissue was 0.89 S/m, while it was lower (0.56 S/m) for benign tissue. Taken together, these results suggest that conductivity mapping of breast cancers is feasible non-invasively using MRI, and that this method may provide a tool in improving diagnosis of breast cancer.

Ex vivo electrical conductivity of healthy liver and metastatic tumor tissue has also been measured using the four-electrode method (Haemmerich et al., 2009; Laufer et al., 2010) and the coaxial contact probe technique (Peyman et al., 2015). All three studies found that tumor tissue conductivity was significantly higher over the entire frequency range measured, and concluded that the knowledge of dielectric properties of liver tissue may be useful for 1) tumor detection, and 2) optimization of the electroporation process for treatment planning procedures.

A study of particular interest measured resistivity on nine patients during brain tumor surgery (J. Latikka et al., 2001). Measurements were made along the same path planned for the surgery of deep brain tumors, using a monopolar needle electrode, and a 2 μA and 50 kHz sinusoidal current. Tumor conductivity values depended on the tumor type, varying between 0.10 and 0.43 S/m. The values of conductivity for grey matter where between 0.18 and 0.51 S/m and of white matter 0.20 and 0.31 S/m. All measurements were made near the tumor; therefore it is possible that not all measurements were made from healthy tissues.

2.5.2 Muscle diseases

In addition to oncology, electrical conductivity measures have been performed in the field of muscular diseases to attempt differentiating healthy and diseased tissue based on conductivity. A study used the four-electrode setup attached around the knee along with MREIT to measure conductivity in five healthy volunteers to differentiate bone and muscle (Jeong et al., 2014). Although MREIT still suffers from estimation errors inherent to inverse/forward problems, authors found conductivity values of 0.097 S/m for spongy bone, 0.029 S/m for cortical bone, 0.055 S/m for adipose tissues, and 0.125 S/m for muscle, showing conductivity differences between two types of bones, muscle tissues and body fluids (Kim et al., 2008; Woo et al., 2007). Another study attempted to detect neuromuscular disorders based on passive electrical material properties in *ex vivo* mice muscles, using electrodes plates to inject a 50 kHz current while recording voltage with needle electrodes (Li et al., 2015). Inherent passive electrical properties of muscle differed by disease type, providing evidence that such conductivity measurements could be relevant in muscular disease diagnosis. A few studies measured the bioelectrical impedance of muscular tissue for the diagnosis of sarcopenia (an age-related skeletal muscle loss), and were inconclusive (Rubbieri et al., 2014; Yamada et al., 2017).

2.5.3 Neurology and epilepsy

The measure of brain tissue conductivity for biomedical applications has been initiated in the 60s, especially for electrodes localization inverse problems (Laitinen and Johansson, 1967; Robinson, 1962). These initial efforts aimed at characterizing brain tissue by measuring its impedance, which pointed at greater impedance values in white matter (WM), least in cerebrospinal fluid (CSF) and intermediate in grey matter (GM). A measure of the dielectric properties of bovine grey matter is shown in Fig. 2-14. for frequencies between 10 Hz to 20 GHz. It is interesting to note that conductivity is relatively constant between 0.1-100 kHz, while permittivity is highly frequency dependent.

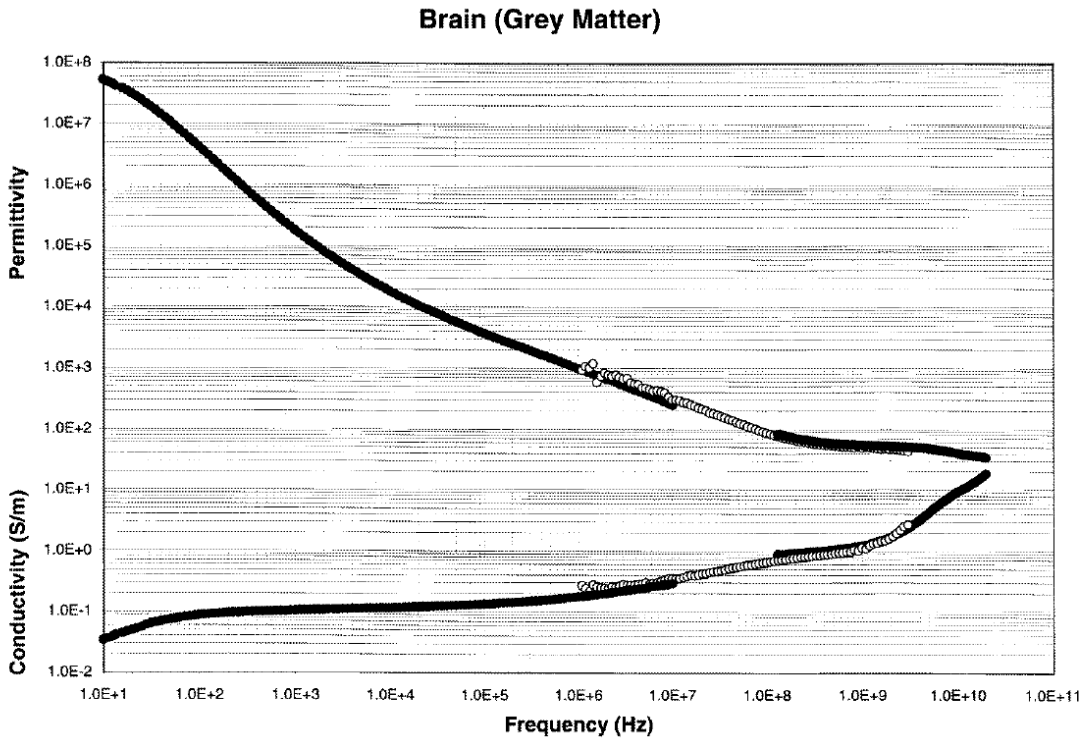

Fig. 2-14. Permittivity and conductivity of brain tissue (gray matter). Three different experimental arrangements with overlapping frequency coverage are shown from bovine origin (Adapted from (S. Gabriel et al., 1996), no permission requested).

As aforementioned, anisotropy depends mainly on fibers orientations. Brain tissue is composed of two different types of tissue: grey matter, consisting mostly in cell bodies such as neuronal cell bodies, glial cells and capillaries; and white matter, referring mainly to myelinated axons. White matter has a different conductivity whether it is considered in the longitudinal (along the axons) or transversal (perpendicular to the axons) direction, therefore it is considered to be significantly more anisotropic than grey matter. Anisotropic water diffusion in neural fiber is used for example in DTI (Beaulieu, 2002) for the estimation of white matter anisotropy, and its influence on EEG/MEG forward/inverse problems (Güllmar et al., 2010) and estimating the effects of transcranial magnetic stimulation (De Lucia et al., 2007). Interestingly, results have shown that anisotropy has minor effects both on the position of the main locus of activation and its intensity.

EEG and Bioimpedance

Estimation of brain conductivity from scalp measurements presents challenges. The head is considered as a volume conductor, consisting of the skin, skull, CSF and brain tissues. Skull resistivity remains a complicated issue, since the skull consists three layers: two compact layers and the cancellous bone in between the compact layers. Further deep, there is the CSF, and finally the cortex (Nunez and Srinivasan, 2006), all these tissues having different conductivities. Furthermore, such estimations require source localization techniques, which are based on EEG and using the electrical

potential recorded at the scalp level to identify the location of brain neural activity. One issue is that the EEG inverse problem is ill-posed, and knowledge of conductivity is required for solving the so-called EEG direct problem. Furthermore, it is plausible that brain lesions could have different conductivity values than healthy tissue, potentially leading to source reconstruction errors.

The use of bioimpedance as a non-invasive technique to measure biophysical properties of tissue has been studied recently. Some studies consider bioimpedance spectroscopy as a possible technique for the diagnosis of brain damage caused by a cerebrovascular accident. For example, it has been demonstrated that, using scalp potential differences between left-right asymmetries between healthy and damaged tissues, intracranial hemorrhage could be diagnosed (Atefi et al., 2016; Cohen et al., 2015; Seoane et al., 2015). In the specific case of epilepsy, it has been suggested that EIT could improve the accuracy of the localization of epileptic foci (Fabrizi et al., 2006).

Ex-vivo, in-vivo and human studies

A study has determined bidirectional conductivity (perpendicular and parallel to the surface of the neocortex and white matter) in freshly excised brain tissues obtained from *n=15* pediatric epilepsy surgery patients (Akhtari et al., 2010). Conductivities were lower in patients with cortical dysplasia as compared to non-dysplasia etiologies. The study concluded that conductivity values differ significantly from patient to patient, with variable anisotropic and isotropic shapes depending on the type and proximity of the lesion observed with MRI. Even if *ex-vivo* measurements could be enlightening, electric fields in the brain during electric stimulation differ considerably between *in-vivo* and *ex-vivo* due to postmortem time and body temperature (Opitz et al., 2017).

Deep brain stimulation (DBS) is an example of invasive method consisting in surgically implanting electrodes to stimulate specific brain nuclei. DBS is an established therapy for the treatment of Parkinson's disease and other neuropsychological disorders. The spatial and temporal characteristics of the voltage distribution of intracranial electrodes have been characterized in an experimental study (Miocinovic et al., 2009) in the non-human primate brain. Stimulation parameters were constant voltage (0.3 V), and constant current (30 μA) pulses (500 μs cathodic pulse, 500 μs inter-pulse delay and 500 μs anodic pulse delay) delivered at 20 Hz. Microelectrodes positioned at various positions were used to spatially map the voltage induced by the intracranial electrodes. By varying the vertical and horizontal position of the microelectrode, multiple recordings were obtained and voltage distribution maps were constructed. Three features of the electrode and tissue medium had a substantial impact on the results: 1) electrode impedance, dictated by a voltage drop at the electrode-electrolyte interface and the conductivity of the medium; 2) capacitive effects in stimulus waveform due to tissue capacitance; and 3) anisotropic tissue properties.

In vivo measurements of human brain tissue conductivity at body temperature have also been conducted using focal current stimulation to measure the bioelectrical impedance and conductivity as a possible indicator of brain tissue epileptogenicity (Koessler et al., 2017). Conductivity measurements

were done in 15 epileptic patients using multicontact electrodes and a radiofrequency generator that injected an electric current at a 50 kHz frequency. Estimated conductivity values were 0.26 S/m for gray matter and 0.17 S/m for white matter. The study concluded that *in vivo* conductivity values could contribute to improve the accuracy of volume conduction models and refine the identification of intracerebral contacts, especially when located within the epileptogenic zone of an MRI-invisible lesion. Overall, there is conflicting data in the literature about the relevance of using electrical conductivity in diagnostic applications, motivating further efforts in that direction.

3 Problem Statement

In the previous section, we provided an overview regarding the conductivity of living tissue, the challenges of measuring conductivity, as well as the strong interest of studying biophysical properties of tissue in medicine. Thus, the main problem that will be addressed in this thesis is the measurement of **local brain conductivity** using invasive electrodes and **its possible diagnostic application**.

3.1 Local brain conductivity

As it was analyzed in the state of the art (Section 2), designing stimulation based protocol for estimation of tissue impedance is a timely and important objective. This thesis has the objective of applying fundamental theoretical techniques for estimating local brain tissue conductivity using intracranial electrodes.

3.1.1 Limitations of clinical stimulation

First, stimulation protocols need a careful design avoid the damage of brain tissue. Clinical stimulators typically use charged-balanced constant current waveforms to minimize tissue damage, and do not permit other waveforms. Therefore, one major constraint is that our model will be based on

charged-balanced constant current waveforms to estimate local brain conductivity. Second, the electrodes used during stimulation are not the same electrodes than those used to estimate conductivity in measuring systems. Typical probe electrodes used to measure conductivity consist of two parallel plates, which have a cell constant (relating conductivity to the medium resistance) that is directly proportional to the distance separating the two plates and inversely proportional to their surface area. Electrodes used during stimulation are cylindrical electrodes which have a cell constant that depends on this specific geometry. This must be taken into account when estimating conductivity. Third, the waveforms used for pulsed stimulation have a low frequency spectra (< 1 kHz), implying that the estimated conductivity will be low-frequency conductivity. One issue is that low-frequency conductivity estimation can suffer from electrode polarization (S. Gabriel et al., 1996), which has to be taken into account in the solution to achieve reliable estimations.

3.1.2 Limitations of materials and protocol

The stimulation waveform must be sampled to observe the tissue response and estimate tissue conductivity. During clinical stimulations, the SEEG sampling system is in parallel with the stimulator. The SEEG system records the signals for analyzing epileptic markers. Electrophysiological signals are normally in the order of 100 µV, involving that the system does not need a large sampling range (typical values of sampling range of $\pm 1\ mV$). This sampling range is significant lower than required for properly sampling the stimulation artifact, which will induce amplitude saturation. Furthermore, the sampling frequency is usually significantly lower (typical values of sampling frequencies of f_s=2048 Hz) than needed to capture with enough details the stimulation artifact.

Patient typically stays in the hospital during two weeks: they are admitted on Sunday night, and surgery is performed the following Monday. The patient is stimulated on the following days, and SEEG are analyzed to identify the EZ, which leaves only a few days to record tissue responses to stimulation.

3.2 Proposed solution

Based on the use of constant current biphasic pulse stimulations, we propose to estimate the resulting electric potential and electric field. The electric potential/field is estimated using an analytical approach, and also with a software for finding a numerical solution. From the electric field estimation, a relationship between the medium conductivity and resistance is derived using the specific geometry of the cylindrical electrode used during clinical stimulations (cell constant). Moreover, a model of electrode polarization is proposed. The electrode/electrolyte interface is modeled with a double layer capacitance and a charge transfer resistance. The system response to a constant current biphasic pulse is modelled and used to estimate the medium resistance and electrode/electrolyte interface. This provides an improvement of medium resistance estimation, and hence conductivity.

3.2.1 Ground truth

In order to validate the electrode-medium model conductivity, calibrated saline solution were used as a ground truth. The electrode-medium double layer model reproduced the time course of the recorded stimulation artifact, and enabled us to estimate the resistance, and the conductivity of the calibrated solutions. Even if saline solutions are less complex than tissue (e.g., no anisotropies), it was used as a first validation of the developed method. Also, conductivity measurements could be calibrated and provided a link to bridge theory and experiment. Moreover, post-mortem conductivity measurements were performed in the brain of *N=2* adults Sprague-Dawley rats. Stimulation was performed within a few minutes post-mortem within the right/left hemisphere, and was a first assessment of the stimulation waveform in actual tissue. Even if this experiment was performed post-mortem (involving that no electrophysiological activity was present), this provided crucial insights into tissue properties.

3.3 Patient studies

Once that ground truth validation was completed, we moved on to the patient studies. Prior to acquiring patient data, hardware limitations had first to be resolved. To perform human recordings, an acquisition system was put in parallel of the stimulating system. Importantly, the recording system used had a high input range to capture the entire stimulation artifact without input saturation, and a high sampling rate to capture waveform details to estimate the biophysical parameters.

3.3.1 Epileptic versus non-epileptic tissue

Few studies have been performed regarding the electrical properties of epileptic tissue. Classification of epileptic tissue is still today a challenging task. Neurophysiological data must be analyzed in detail, and no obvious electrophysiological markers are recorded, stimulation must be performed to induce and analyze post-discharges. Our results demonstrate that clinically-relevant results are possible from intracerebral data recorded in epileptic patients.

4 Materials and Methods

In this chapter, we introduce the modeling and experimenting methods used during the study. An electric potential model is presented and coupled with an electrode-electrolyte interface model, as an attempt to improve existing methods based on bioimpedance. A model-based method linking the characteristics of the stimulation current, physical properties of the electrode, with biophysical parameters (conductivity, double layer capacitance and faradaic resistance of the electrode-electrolyte interface) is presented. The proposed method is based on an analytical model of the resulting electric field, which enables an explicit calculation of conductivity from experimentally recorded signals.

4.1 *Electric field model*

There are two versions of Maxwell's equations, namely microscopic and macroscopic formulations. The microscopic equations provide a good description for few charges and isolated currents. However, in a medium such as biological tissue, they are practically of no use since it is virtually impossible to know the position of all charges. In this case, the macroscopic version must be used.

4.1.1 Macroscopic fields in biological tissue

All materials have conductive and capacitive properties, characterized by the electrical conductivity σ and electrical permittivity ε. Depending on the measurement scale, these values are space averaged over the tissue volume. In order to provide a perspective, a typical SEEG electrode contact is neighbor to approximately 10^6 cells (neurons and glia) (von Bartheld et al., 2016), therefore the dielectric properties and conductivity must refer to the average properties of tissue at this scale. Relative permeability of human tissues is very close to that of free-space, and magnetic properties can slightly vary depending on the tissue types and water content. An exception is blood containing hemoglobin, and when hemoglobin loses oxygen the magnetic properties changes (Buxton, 2013). This property is used in fMRI for measuring the information of magnetic susceptibility. Since permeability and magnetic susceptibility are not in the scope of our study, these magnetic properties of tissues will not be further discussed.

Resistive and capacitive tissue

The electric behavior of tissue is governed by the extracellular liquid ions conductivity and cell membranes dielectric properties. Since conductivity and permittivity differ considerably depending on frequency, the associated impedance that is measured varies as well. For the 1 kHz frequency band, conductivity is considered as quasi-static (low frequency conductivity), and it is therefore assumed constant in this frequency band (Ranta et al., 2017). The dielectric property of tissue is also an important issue. Indeed, at the cellular scale, the membrane capacity needs to be taken into account. A patch of brain tissue containing many conductively membranes with substantial capacitive properties can be described as a linear conductor with negligible capacitive properties, and can be modeled as a resistor in parallel with a capacitor (Nunez and Srinivasan, 2006). At low frequencies (< 1 kHz), most of the current is expected to bypass cells, i.e. tissue can be approximated as a simple conductor with negligible capacitive properties (quasi-static approximations) and follows simplified versions of Maxwell's macroscopic equations (Bossetti et al., 2008; Nunez and Srinivasan, 2006; Plonsey and Heppner, 1967).

Electrodes Geometry

A typical SEEG electrode for human use is shown in Fig. 4-1. (DIXI medical, D08-15AM, Besancon, France).

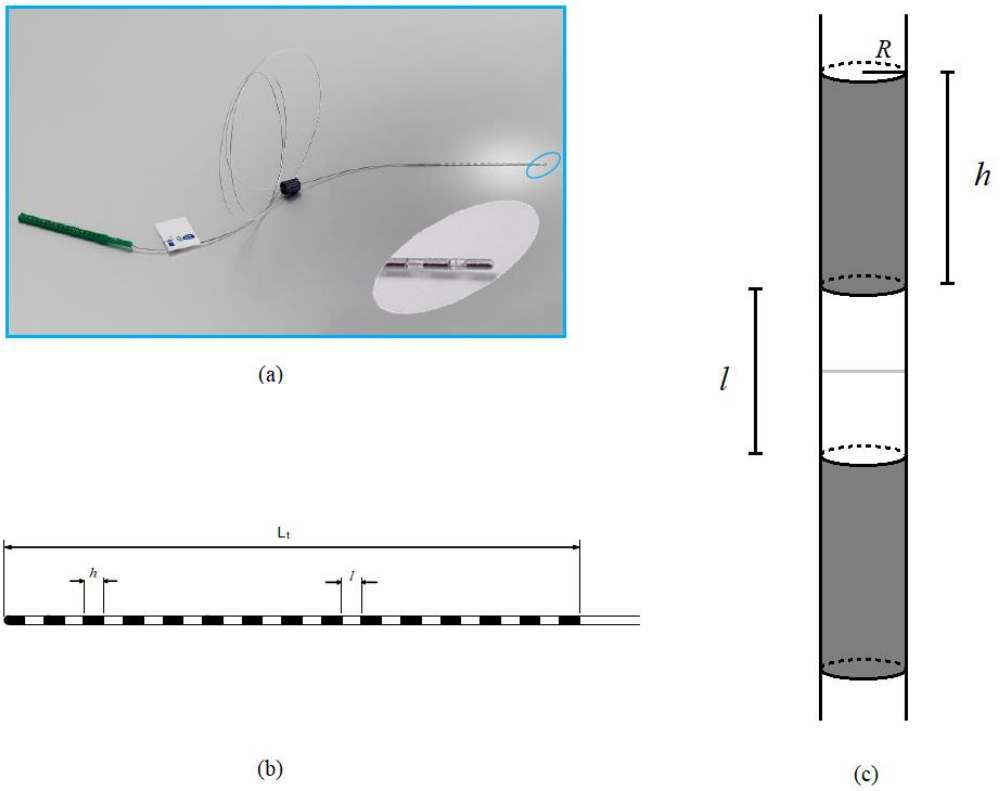

Fig. 4-1. Illustration of a cylindrical electrode used clinically. (a) Image of a DIXI medical SEEG electrode, (b) diagram of a 15-contact electrode and (c) electrode geometry with radius *R*, isolation separation l and height *h*. (Adapted from DIXI electrodes datasheet, no permission requested)

Implanted SEEG electrodes have between 10-15 contacts. The metal used for the electrodes is usually platinum/iridium, with an isolation material between contacts. The contact electrode in the case of the specific model shown in Fig. 4-1 has a height $h = 2\ mm$, isolation separation $l = 1.5\ mm$ and a radius $R = 0.4\ mm$. It is a sterile material and disposable after use. Such electrodes have CE marking certified by the European regulations for medical devices (LNE/G-MED 0459).

4.1.2 Laplace Equation

After this brief introduction on the model's assumptions, we detail below the electric potential and electric field model. Our objective is to establish the equations governing the potential and electric field distribution induced by electrical stimulation when clinical intracerebral electrodes (fig. 4-1) are being used. First, we consider the differential version of Ampere's law:

$$\nabla \times \boldsymbol{B} = \mu_0 \boldsymbol{J} + \mu_0 \varepsilon_0 \frac{\partial \boldsymbol{E}}{\partial t}$$

where $\boldsymbol{E}$ and $\boldsymbol{B}$ are the electric and magnetic fields, respectively; $\boldsymbol{J}$ the current density; μ_0 and ε_0 the electric permeability and permittivity of vacuum, respectively. Considering a steady state situation,

(meaning that there is no time dependence, i.e. $\frac{\partial \boldsymbol{E}}{\partial t} = 0$) and given that the divergence of the curl for any vector field is null, (i.e. $\nabla \cdot (\nabla \times \boldsymbol{B}) = 0$), we obtain that the divergence of the current density vector is zero:

$$\nabla \cdot \boldsymbol{J} = 0$$

Following the general form of Ohm's law, providing a linear relationship between the current density and the electric field $\boldsymbol{J} = \sigma . \boldsymbol{E}$, and assuming that grey matter is locally isotropic, we obtain:

$$\nabla \cdot E = 0$$

The scalar potential equation $\boldsymbol{E} = -\nabla \cdot V$ is valid whenever magnetic induction is negligible, which is the case for electrophysiological applications (Nunez and Srinivasan, 2006). This leads to Laplace's equation:

$$\vec{\nabla}^2 V = \Delta V = 0$$

where V is the electric potential induced in brain tissue. Considering the geometry of SEEG electrodes, cylindrical coordinates (r, θ, z) is an appropriate choice to solve the partial differential equations (PDE). Given the rotational symmetry of the electrodes $V(r, z)$, the electric potential will be the same for all θ values in the $[0, 2\pi[$ interval, simplifying further calculations. Hence, the Laplace equation in cylindrical coordinates writes as:

$$\vec{\nabla}^2 V = \frac{1}{r}\frac{\partial}{\partial r}\left(r\frac{\partial V(r,z)}{\partial r}\right) + \frac{\partial^2 V(r,z)}{\partial z^2} = 0$$

One of the most common methods for solving PDE is the variable separation method. Separation of variables requires appropriate boundary conditions, initial conditions, and a region where the PDE is defined. Bearing this in mind, the general solution of the Laplace equation is first analyzed, followed by the boundary conditions.

Method of separation of variables

Considering the region where the PDE is defined as $\Re = \{ |r| > R, z \in \mathbb{R}\}$. Using the method of variables separation, the general solution to the Laplace equation takes the form:

$$V(r, z) = f(r)g(z)$$

$$\frac{1}{f(r)}\left(\frac{\partial^2 f(r)}{\partial r^2}+\frac{1}{r}\frac{\partial f(r)}{\partial r}\right)+\frac{1}{g(z)}\frac{\partial^2 g(z)}{\partial z^2}=0$$

This equation reduces to two ordinary differential equations of the form:

$$\begin{cases} g''(z)-k^2 g(z)=0 \\ f''(r)+\frac{1}{r}f'(r)+k^2 f(r)=0 \end{cases}$$

The general solution for the z axis is:

$$g(z)=a_1 e^{kz}+a_2 e^{-kz}$$

where a_1 and a_2 are constants. Such a solution, when considering a specific boundary condition, causes $g(z)$ to vanish for $z \to \infty$, which makes physical sense (meaning $k^2 > 0$, for avoiding trigonometric solutions that do not converge towards to zero). For the r axis, the ordinary differential equation is a Bessel equation of order zero and the general solution is:

$$f(r)=b_1 J_0(kr)+b_2 Y_0(kr)$$

where J_0 and Y_0 are the so-called order zero Bessel's function of the first and second kind. Therefore, the general solution writes under the form:

$$V(r,z)=\left(a_1 e^{kz}+a_2 e^{-kz}\right)\left(b_1 J_0(kr)+b_2 Y_0(kr)\right)$$

Constant values could be in principle computed from the boundary and initial conditions. However, the analytical knowledge of the boundary conditions is typically (if at all) difficult to obtain.

Boundary conditions

As stated before, we aim to identify the solution to the Laplace equation in the region $\Re = \{|r| > R, z \in \mathbb{R}\}$. In this case, the boundary of this region is the border of the electrode, i.e. $r = R$. The Dirichlet problem consists of finding a solution to the Laplace equation in the region $\Re$ such that the solution is equal to a given function in the boundary of this region. Taking into account the cylindrical geometry of the electrodes used in intracranial stimulations, the boundary function is not given. In the case where the boundary function is not known, there is still one possibility for solving the Laplace equation when the normal derivative of the boundary function is known (Neumann boundary condition). In our case, this corresponds to identifying the potential of a field in the boundary. However, the normal derivative of this boundary function is also unknown. As a consequence, the

finite-element method is often used to solve such PDEs to compute the electric field distribution with complex boundaries conditions.

4.1.3 Assumptions of the electric potential model

Hereafter, we present a novel electric potential model taking into account electrodes geometry. We first consider a differential ring, assumed as a point source so that a differential current dI induces an electric potential $dV(\rho) = dI/4\pi\sigma\rho$, where ρ is the distance from the differential ring as shown in Fig. 4-2.

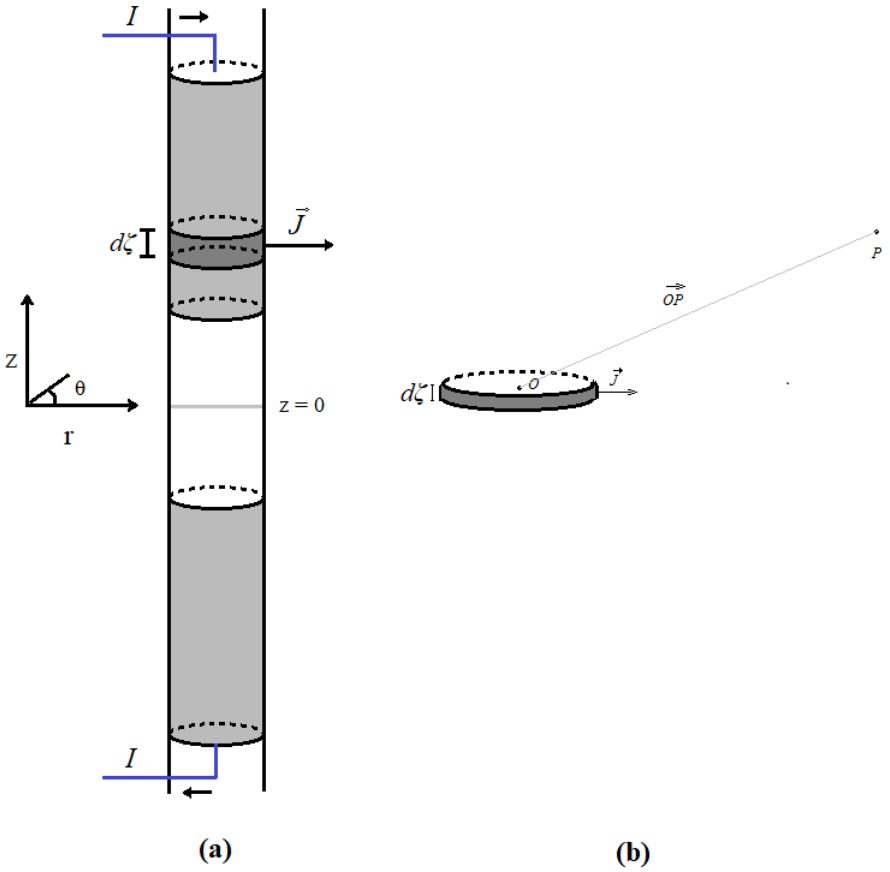

Fig. 4-2.(a) Cylindrical electrode with differential ring, accounting for the electrode geometry and (b) differential ring electric potential contribution, measured in a point *P*, induced by a normal current density *J*.

Assuming the differential ring at a distance $\|\overrightarrow{OP}\|$ from point $P = (r, z)$, and expressing the differential current as:

$$dI = J\, 2\pi R d\xi$$

We can then integrate the contribution of each differential ring along the electrode length:

$$V_1 = \int_{\frac{l}{2}}^{\frac{l}{2}+h} \frac{J\,2\pi R}{4\pi\sigma\sqrt{r^2+(z-\xi)^2}}d\xi = \frac{I}{4\pi\sigma h}\left[sinh^{-1}\left(\frac{z-\frac{l}{2}}{r}\right) - sinh^{-1}\left(\frac{z-\frac{l}{2}-h}{r}\right)\right]$$

Considering the same expression for the second contact, and using the superposition principle, the total electric potential induced by both contacts is:

$$V(r,z) = \frac{I}{4\pi\sigma h}\left[sinh^{-1}\left(\frac{z-\frac{l}{2}}{r}\right) - sinh^{-1}\left(\frac{z-\frac{l}{2}-h}{r}\right) + sinh^{-1}\left(\frac{z+\frac{l}{2}}{r}\right) - sinh^{-1}\left(\frac{z+\frac{l}{2}+h}{r}\right)\right]$$

where h is the height of the electrode. Applying the gradient operator on the electric potential leads to the electric field components in cylindrical coordinates:

$$E_r(r,z) = \frac{I}{4\pi\sigma hr}\left[\frac{z-\frac{l}{2}}{\sqrt{r^2+(z-\frac{l}{2})^2}} - \frac{z-\frac{l}{2}-h}{\sqrt{r^2+(z-\frac{l}{2}-h)^2}} + \frac{z+\frac{l}{2}}{\sqrt{r^2+(z+\frac{l}{2})^2}} - \frac{z+\frac{l}{2}+h}{\sqrt{r^2+(z+\frac{l}{2}+h)^2}}\right]$$

$$E_z(r,z) = \frac{I}{4\pi\sigma h}\left[\frac{1}{\sqrt{r^2+\left(z-\frac{l}{2}-h\right)^2}} - \frac{1}{\sqrt{r^2+\left(z-\frac{l}{2}\right)^2}} + \frac{1}{\sqrt{r^2+\left(z+\frac{l}{2}+h\right)^2}} - \frac{1}{\sqrt{r^2+(z+\frac{l}{2})^2}}\right]$$

This approximation provides an analytical expression of the electric field and potential, while taking into account the electrode geometry.

Electrical resistance and conductivity

As a reminder, conductivity is an electrical property that characterizes materials, including biological tissues. We are interested in estimating brain tissue electrical conductivity during stimulation. A relationship between conductivity and the medium resistance is needed in order to estimate conductivity. For an arbitrary geometry, the medium resistance can be expressed as a function of the electric field as:

$$R_m = \frac{V}{I} = \frac{\int \boldsymbol{E}\cdot dl}{\oint \boldsymbol{J}\cdot dS} = \frac{\int \boldsymbol{E}\cdot dl}{\oint \sigma\boldsymbol{E}\cdot dS}$$

From this expression, the solution's resistance only depends on medium geometry and conductivity σ. In the general case, it is however challenging to derive an analytical expression for the resistance given that the surface and line integrals must be solved. Using the aforementioned

cylindrical electric potential $V(r,z)$, we can derive an approximation of the medium electrical resistance. Assuming that the electric potential difference measured is approximately equal to the difference between the potential at the border of the first electrode (at $r = R$) and the potential in the border of the second electrode, the cylindrical model leads to:

$$V(z) = \frac{I}{4\pi\sigma h}\left[sinh^{-1}\left(\frac{z-\frac{l}{2}}{R}\right) - sinh^{-1}\left(\frac{z-\frac{l}{2}-h}{R}\right) + sinh^{-1}\left(\frac{z+\frac{l}{2}}{R}\right) - sinh^{-1}\left(\frac{z+\frac{l}{2}+h}{R}\right)\right]$$

We used the mid-point of the electrode $z = \pm\frac{1}{2}(l+h)$, in order to estimate the medium resistance. Deriving an analytical expression would involve solving an integral along the z-axis, to obtain a mean electrical potential value. Therefore, this simplification was made (i.e. taking the electrode's mid-point electric potential) since solving this integral analytically was not possible.

$$\Delta V = V\left(\tfrac{1}{2}(l+h)\right) - V\left(-\tfrac{1}{2}(l+h)\right)$$

$$\Delta V = \frac{I}{2\pi\sigma h}\left[2sinh^{-1}\left(\frac{h}{2R}\right) + sinh^{-1}\left(\frac{l+\frac{h}{2}}{R}\right) - sinh^{-1}\left(\frac{l+\frac{3h}{2}}{R}\right)\right]$$

From this expression, the medium resistance is:

$$R_m = \frac{1}{2\pi\sigma h}\left[2sinh^{-1}\left(\frac{h}{2R}\right) + sinh^{-1}\left(\frac{l+\frac{h}{2}}{R}\right) - sinh^{-1}\left(\frac{l+\frac{3h}{2}}{R}\right)\right]$$

This expression provides the relationship between the resistance of the medium, the electrode geometry and the volume conductor property. It can be noted that the resistance will decrease when the radius or the height of the electrode increases. Moreover, the resistance R_m will increase if the separation between the contacts is increased. Similarly, it will increase when the medium conductivity sigma decreases.

4.1.4 Finite-element method

Another method for solving PDEs is the finite-element method (FEM). An approximation of the equations can be constructed using different types of discretization. These are numerical versions of the original PDEs:

$$\vec{\nabla}^2 V = \frac{1}{r}\frac{\partial}{\partial r}\left(r\frac{\partial V(r,z)}{\partial r}\right) + \frac{\partial^2 V(r,z)}{\partial z^2} = 0$$

The numerical solution is an approximation of the original solution. This method is commonly known as the finite element method (FEM). The electric potential V can be approximated by approximated using linear combinations of basis function:

$$V \approx \sum_i v_i \psi_i$$

where ψ_i are the basis functions and v_i the coefficients of the function that approximate the electric potential. By translating continuous equations into discrete functions, the system integral will be approximated with discrete sums, and derivatives will be approximated by differences. The boundary condition is also an important factor when using FEM: the continuous boundary region must be turned into a discrete mesh, and the choice of the mesh has to be carefully considered. The FEM was solved using Comsol Multiphysics AC/DC module (Comsol, Stockholm, Sweden), that is a finite-element solver software for multi-physics problems, as shown in Fig. 4-3.

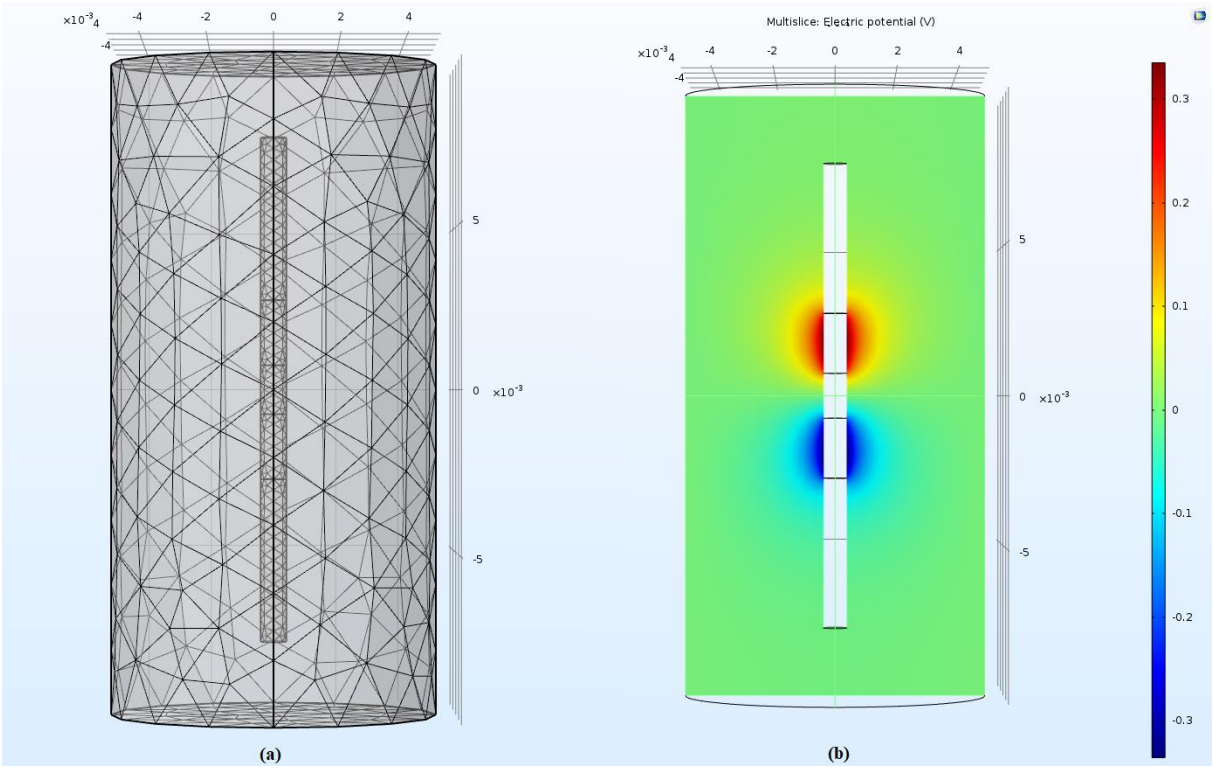

Fig. 4-3. Comsol Multiphysics FEM solver (a) mesh (b) Electric potential.

The system's topology was discretized as shown in Fig. 4-3.(a), considering a small mesh around the electrode surface and larger mesh in the outside border. The outside border is "far away" from the electrode, so the boundary condition for the potential is considered to be equal to zero. The boundary conditions for the electrode contacts are considered to be of constant normal current density with a value of:

$$J_n = \frac{\pm I}{2\pi hR}$$

The normal current density depends if it is inward or outward to the electrode surface (positive/negative). Outside the electrode contacts, the normal current density of the insulating part of the electrodes is considered to be zero. Finally the system is considered to be homogenous and isotropic with conductivity equal to $\sigma = 0.35\ S/m$. Once the system was discretized and the boundary conditions were imposed, the electric potential was solved as shown in Fig. 4-3.(b). Comsol was used as a benchmark to validate the analytical model presented in this chapter (see also Section 5. Results).

4.2 *Electrode-electrolyte interface: an electric circuit model*

When a metal is placed into a physiological medium (electrolyte), charge is carried by ions in the electrolyte (Merrill et al., 2005). In order to understand how the waveform of the delivered electric stimulus is altered by the biophysical properties of brain tissue, we introduce a model of the complex processes taking place during electrical stimulation of excitable tissue. This model enables the estimation of electrical conductivity from the recorded brain tissue response, while accounting for the contribution of the electrode-electrolyte interface to this response.

Double Layer (DL) model

The first model studied here considers the electrode/electrolyte interface as the contribution of a double layer capacitance and faradaic impedance. The configuration with two electrode contacts is presented in Fig. 4-4 (a).

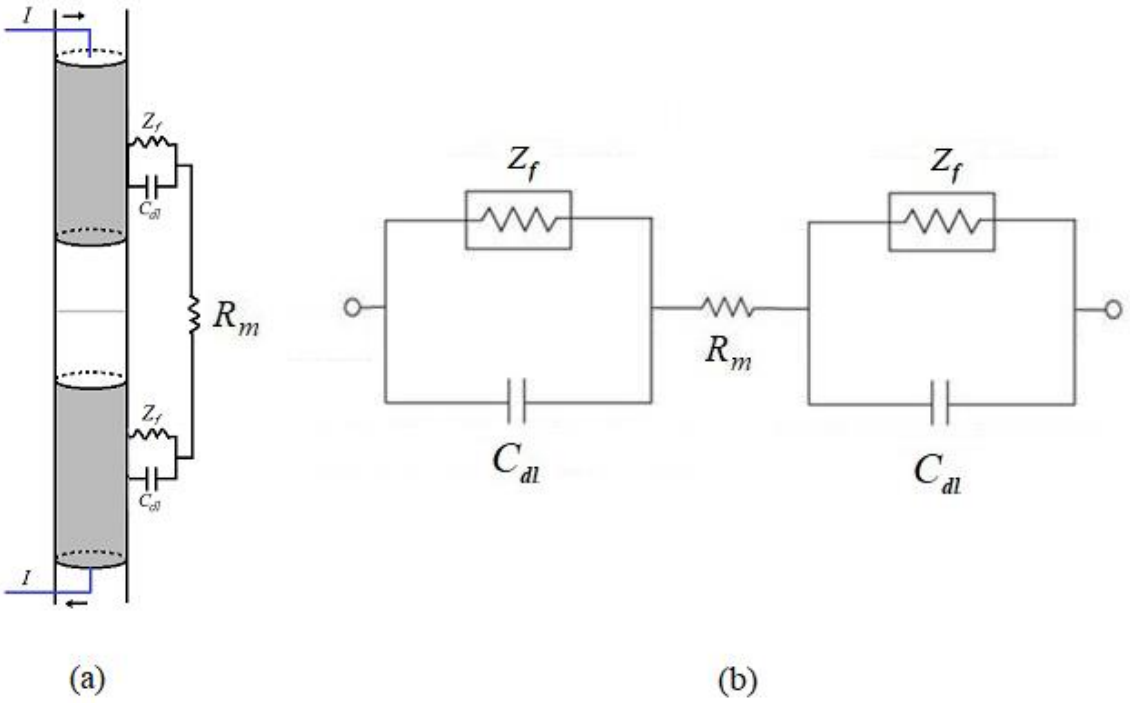

Fig. 4-4. (a) Graphic representation of the equivalent electric circuit (b) Two-electrode double layer circuit model, where R_m models the medium resistance.

This model includes two electrode/electrolyte interfaces, assuming that charge is redistributed parallel to the electrode surface (double layer capacitance), and that charge is injected from the electrode to the medium through Faradaic processes of reduction/oxidation. The tissue is modeled as a resistive medium. Using this model, we find the circuit model as shown in Fig. 4-4 (b).

Constant phase element (CPE) model

The behavior of metal electrodes when immerged into an electrolyte is better described by a pseudo-capacitance (Dymond, 1976), adding both the phenomena of redox reaction and double layer electrostatic storage within a single element. The electrode electrolyte circuit model is shown in Fig. 4-5.

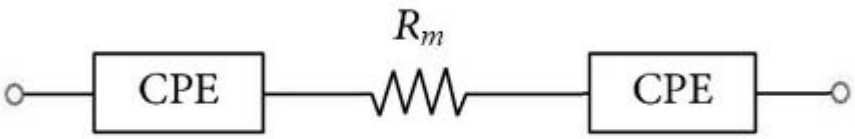

Fig. 4-5. Working and counter electrode modelled as a CPE, and the medium modelled as a resistance.

We remind that the constant phase element in the Laplace domain takes the form $Z_{CPE} = 1/As^{\alpha}$, with the exponent $0 \leq \alpha \leq 1$, and A the pseudo-capacitance parameter (equal to the capacitance when $\alpha = 1$).

4.2.1 Electric circuit model solutions

To solve the corresponding differential equation, we used the Laplace transform. Considering the double layer model, the potential between the working and counter electrodes in the Laplace domain is:

$$V_{DL}(s) = \left[R_m + \frac{2Z_f}{\left(1 + C_{dl}Z_f s\right)}\right] I(s)$$

where $I(s) = L\{i(t)\}$, $i(t)$ being the stimulating current waveform. Considering next the CPE model, the Laplace transform of the voltage between the working and counter electrodes is:

$$V_{CPE}(s) = [R_m + \frac{2}{As^{\alpha}}]I(s)$$

The time domain expression of the electric potential depends on the chosen stimulating waveform.

Biphasic constant current pulse

As depicted in the State-of-the-Art section, biphasic current stimulation (as illustrated in Fig. 4-6) is typically used in clinical stimulation to avoid charge accumulation that may subsequently lead to tissue damage. The biphasic constant current stimulation pulse is shown in Fig. 4-6.

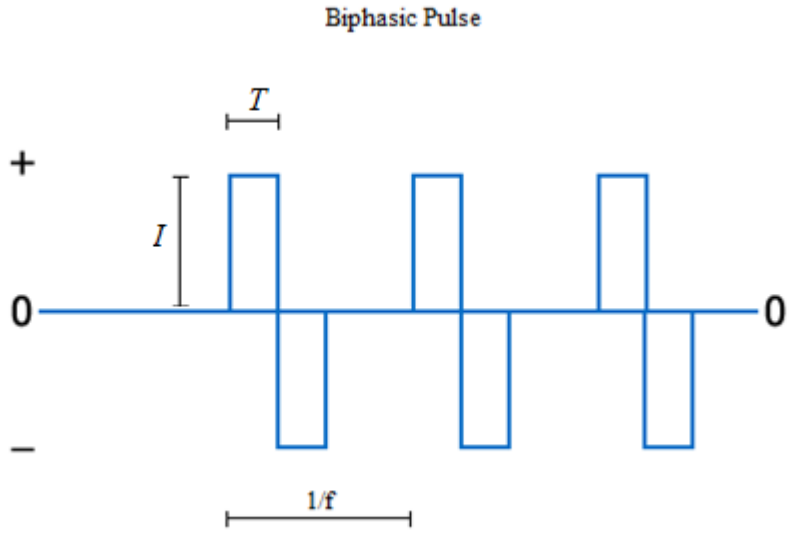

Fig. 4-6. Constant current biphasic stimulation waveform.

Mathematically, this waveform could be written as:

$$i(t) = I[u(t) - 2u(t-T) + u(t-2T)]$$

where $u(t)$ is the Heaviside function, I is the current amplitude, and T is the pulse width. The Laplace transform of this waveform is:

$$I(s) = \frac{I}{s}(1 - 2e^{-sT} + e^{-2sT})$$

Using this waveform, the electric potential for the double layer model is defined as:

$$V_{DL}(s) = \left[R_m + \frac{2Z_f}{(1 + C_{dl}Z_f s)}\right]\left[\frac{I}{s}(1 - 2e^{-sT} + e^{-s2T})\right]$$

With the inverse Laplace transform, the analytical expression of the resulting electric potential is obtained in the time domain:

$$v_{DL}(t) = I\left\{u(t)\left[R_m + 2Z_f\left(1 - e^{-\frac{t}{C_{dl}Z_f}}\right)\right] - 2u(t-T)\left[R_m + 2Z_f\left(1 - e^{-\frac{(t-T)}{C_{dl}Z_f}}\right)\right] + u(t-2T)\left[R_m + 2Z_f\left(1 - e^{-\frac{(t-2T)}{C_{dl}Z_f}}\right)\right]\right\}$$

In the following, we will use this waveform (stimulation artefact) to estimate biophysical parameters, typically the electrical conductivity that is a key parameter. For illustration, we present in Fig. 4-7, a representative stimulation artifact for values of C_{dl} = 0.7 µF, Z_f = 1.5 kΩ, R_m = 1 kΩ and I = 0.2 mA.

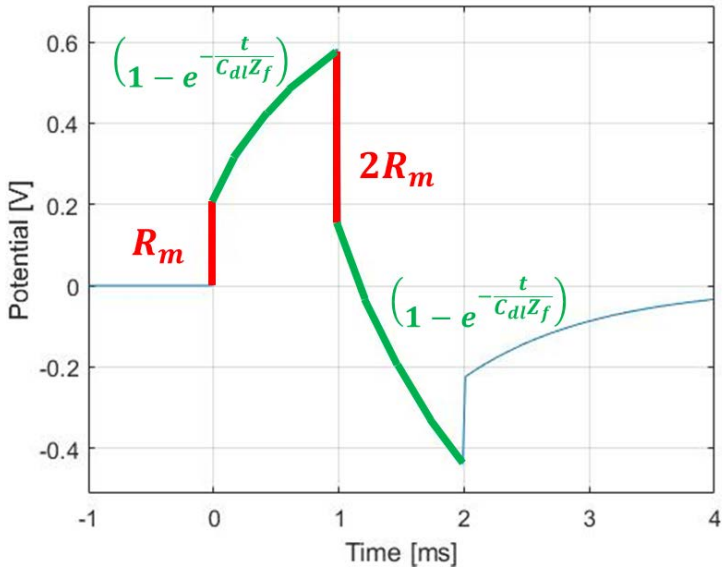

Fig. 4-7. Simulated Electric potential induced in brain tissue in response to a single biphasic stimulation pulse of intensity 0.2 mA. This waveform was generated for C_{dl} = 0.7 µF, Z_f = 1.5 kΩ, and R_m = 1 kΩ.

Importantly, waveform discontinuities are related to the medium resistance, while the exponential part of the waveform is related to electrode polarization. The Fourier transform of the waveform is equivalent to evaluating the Laplace transform at the imaginary axis $s = j\omega = j2\pi f$ (if its region of convergence contains the imaginary axis). Therefore, the corresponding Fourier transform is:

$$V_{DL}(f) = \left[R_m + \frac{2Z_f}{(1 + C_{dl}Z_f j2\pi f)}\right]\left[\frac{I}{j2\pi f}(1 - 2e^{-j2\pi fT} + e^{-j4\pi fT})\right]$$

The Fourier transform of the biphasic constant current pulse is illustrated in Fig. 4-8.

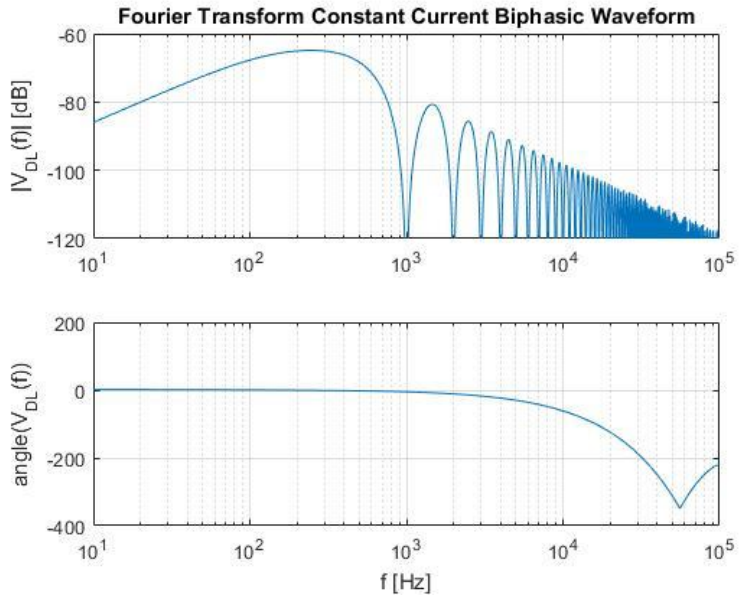

Fig. 4-8. Fourier transform of the biphasic constant current stimulating waveform.

As observed in figure 4.8, the main lobe is found within the 1 kHz band, while the side lobes are at least 14 dB below the main lobe, showing that most of the signal energy is located within the 1 kHz band. This result justifies the use of the quasi-static approximations. We next study the stimulation response signal waveform in the CPE model. The electric potential in the Laplace domain is expressed as:

$$V_{CPE}(s) = [R_m + \frac{2}{As^{\alpha}}]\left[\frac{I}{s}(1 - 2e^{-sT} + e^{-s2T})\right]$$

Applying the inverse Laplace transform, we obtain the electric potential expression:

$$v_{CPE}(t) = I\left\{u(t)\left[R_m + \frac{2t^{\alpha}}{A\Gamma(\alpha+1)}\right] - 2u(t-T)\left[R_m + \frac{2(t-T)^{\alpha}}{A\Gamma(\alpha+1)}\right] + u(t-2T)\left[R_m + \frac{2(t-2T)^{\alpha}}{A\Gamma(\alpha+1)}\right]\right\}$$

where $\Gamma(\cdot)$ is the gamma function. A comparison between the double layer model and the constant phase element model is shown in Fig. 4-9. The values used for the CPE model were: $\alpha = 0.81$, $A = 4.1\ \mu F/s^{(1-\alpha)}cm^2$ and conductivity $\sigma = 0.1\ S/m$.

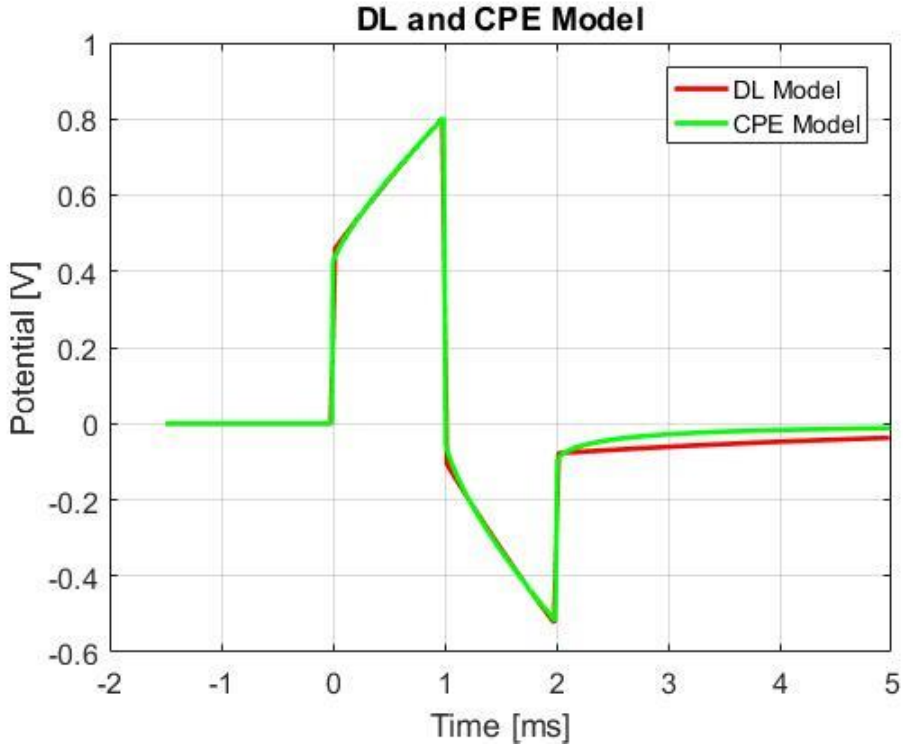

Fig. 4-9. Double layer and constant phase element model comparison.

Both DL and CPE models reproduce the time course of the electric potential for both positive and negative phases. Considering the *in-vivo* medium, an assumption of the model is that the amplitude of the stimulation artifact at the level of the tissue is considerably higher than the level of background activity. Indeed, the background electric potential generally varies between 10 µV and 1 mV. During the electrical stimulation measurement, electric potential ranges from several 100 mV to several volts. Considering this assumption, the contribution of sources from neuronal activity were neglected in the Laplace equation.

4.1.1 Derivation of the model for other waveforms

The most common waveform used during clinical stimulation is the biphasic pulse. Since the chronaxie time for neural stimulation depends on the stimulation waveform, exploring other waveforms could also be interesting for studying tissue properties (Cantrell and Troy, 2008; Foutz and McIntyre, 2010; Sahin and Tie, 2007).

Zeta biphasic pulse

The shape of the stimulating pulse may induce electrolytic damage to tissue, especially if it is a monopolar waveform. So, for clinical applications, waveforms must respect one major constraint: to be charged balanced. The zeta biphasic pulse as shown in Fig. 4-10.(a) is an appropriate candidate as suggested in (Millar and Barnett, 1997). This waveform will be tested in the saline solutions (see Section 5. Results) for analyzing its potential for estimating conductivity and electrode-electrolyte parameters.

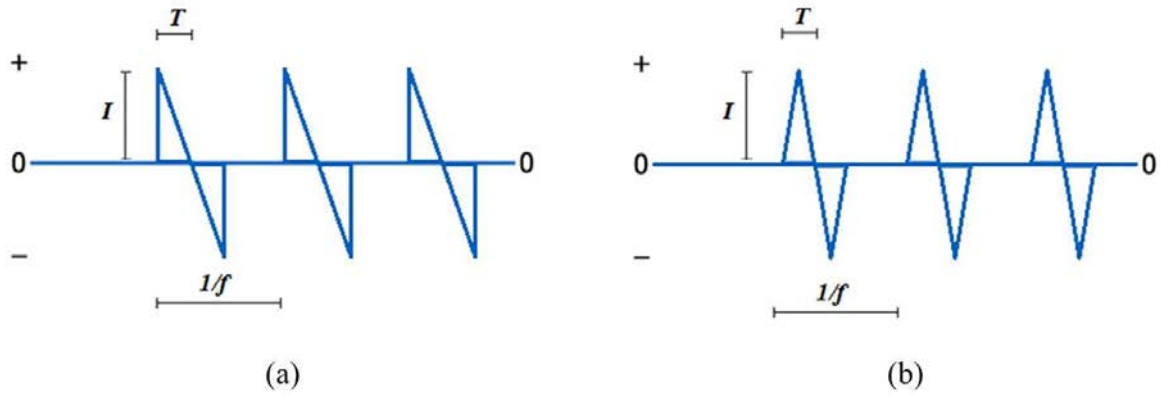

Fig. 4-10. (a) Zeta biphasic pulse stimulation waveform (b) Triangular biphasic stimulation waveform.

The zeta biphasic waveform starts with a discontinuity and then linearly declines until reaching negative amplitude, and writes as:

$$i(t) = [u(t) - u(t - 2T)][I - \frac{I}{T}t]$$

Therefore, the electric potential in the Laplace domain is:

$$V(s) = \left[R_m + \frac{2Z_f}{(1 + C_{dl}Z_f s)}\right]\left[I\frac{sT - 1}{s^2 T}(1 - e^{-s2T}) + \frac{2I}{s}e^{-s2T}\right]$$

Finally, with the inverse Laplace transform, the time domain expression for the zeta stimulation is:

$$v(t) = I\left\{u(t)\left[(R_m + 2Z_f)\left(1 - \frac{t}{T}\right) + \frac{2C_{dl}{Z_f}^2}{T}\left(1 - e^{-\frac{t}{C_{dl}Z_f}}\right) - 2Z_f e^{-\frac{t}{C_{dl}Z_f}}\right]\right.$$
$$\left. - u(t - 2T)\left[(R_m + 2Z_f)\left(1 - \frac{(t-2T)}{T}\right) + \frac{2C_{dl}{Z_f}^2}{T}\left(1 - e^{-\frac{(t-2T)}{C_{dl}Z_f}}\right) - 2Z_f e^{-\frac{(t-2T)}{C_{dl}Z_f}}\right]\right\}$$

The zeta waveform using the double layer parameters, $C_{dl} = 1.5\mu F$ and $Z_f = 10M\Omega$ and conductivity $\sigma = 0.1\ S/m$ is shown in Fig. 4-11.

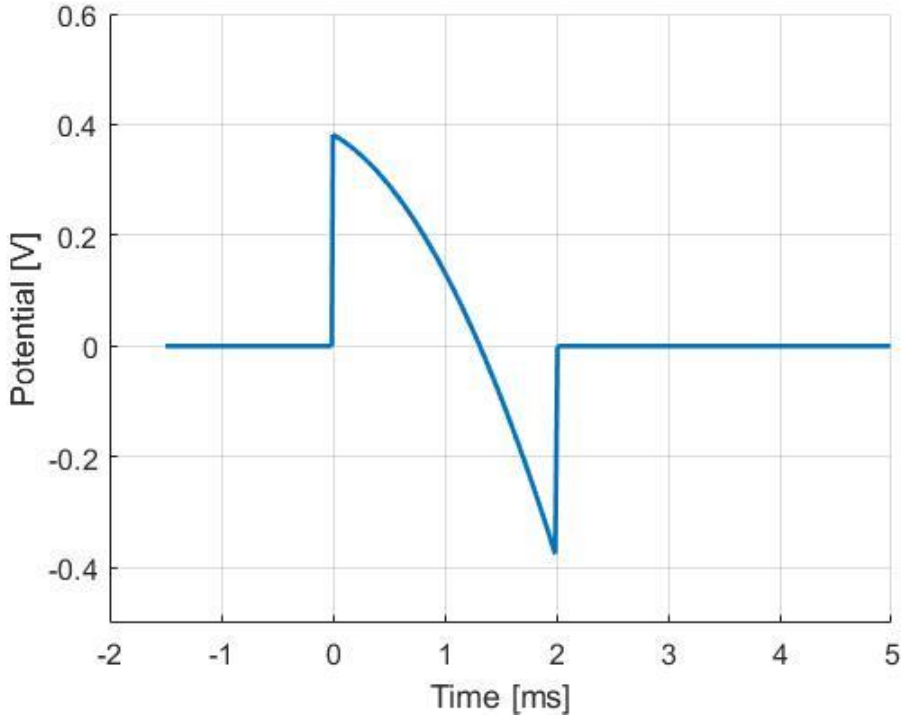

Fig. 4-11. Double layer model for zeta waveform.

Triangle biphasic pulse

Another possible waveform (instead of stimulating with an abrupt discontinuity, as is the case with the zeta biphasic pulse), is to use a triangle biphasic pulse as shown in Fig. 4-10.(b). This waveform has a slower dynamic that may be interesting for brain stimulation (Foutz and McIntyre, 2010).

$$i(t) = 2I\left\{u(t)\frac{t}{T} - \frac{2}{T}u\left(t-\frac{T}{2}\right)\left[t-\frac{T}{2}\right] + \frac{2}{T}u\left(t-\frac{3T}{2}\right)\left[t-\frac{3T}{2}\right] - \frac{1}{T}u(t-2T)[t-2T]\right\}$$

Solving the circuit with this waveform, we get:

$$\begin{aligned} v(t) = I\Bigg\{ & u(t)\left[(R_m+2Z_f)\tfrac{t}{T} + \tfrac{2C_{dl}{Z_f}^2}{T}\left(1-e^{-\frac{t}{C_{dl}Z_f}}\right)\right] \\ & - 2u\left(t-\frac{T}{2}\right)\left[(R_m+2Z_f)\left(\tfrac{(t-T/2)}{T}\right) - 2C_{dl}{Z_f}^2\left(1-e^{-\frac{(t-T)}{C_{dl}Z_f}}\right)\right] \\ & + 2u\left(t-\frac{3T}{2}\right)\left[(R_m+2Z_f)\left(\tfrac{\left(t-\frac{3T}{2}\right)}{T}\right) + \tfrac{2C_{dl}{Z_f}^2}{T}\left(1-e^{-\frac{\left(t-\frac{3T}{2}\right)}{C_{dl}Z_f}}\right)\right] \\ & - u(t-2T)\left[(R_m+2Z_f)\tfrac{(t-2T)}{T} + \tfrac{2C_{dl}{Z_f}^2}{T}\left(1-e^{-\frac{(t-T)}{C_{dl}Z_f}}\right) - 2Z_f e^{-\frac{(t-T)}{C_{dl}Z_f}}\right]\Bigg\} \end{aligned}$$

The resulting triangular waveform using the double layer parameters, $C_{dl} = 1.5\mu F$ and $Z_f = 10M\Omega$ and conductivity $\sigma = 0.1\ S/m$ is shown in Fig. 4-12.

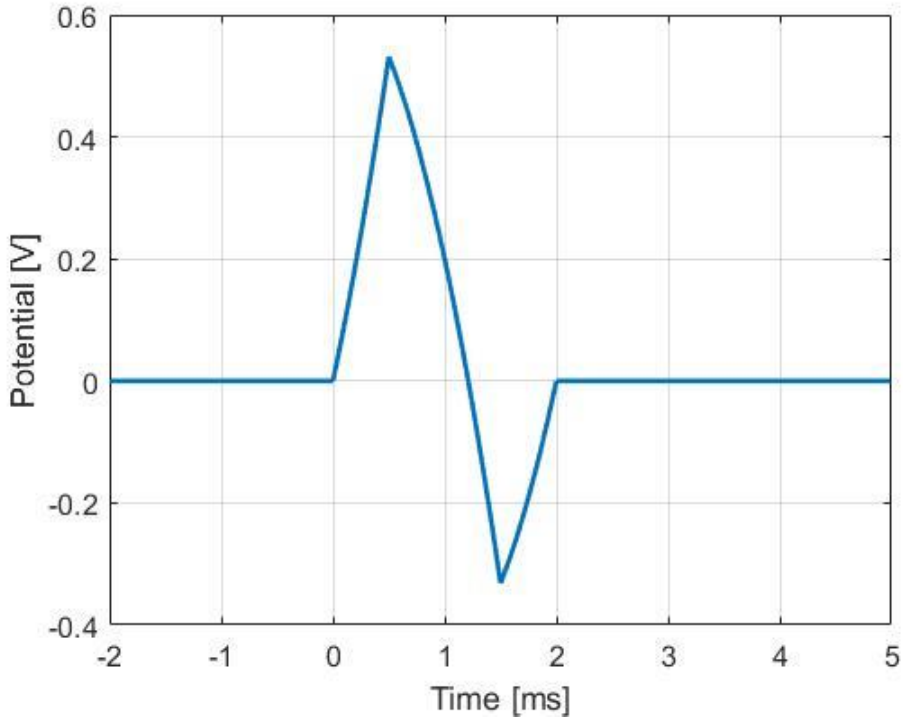

Fig. 4-12. Double layer model for a triangular waveform.

This waveform was studied in DBS for optimization of battery life, which is a real challenge for implanted stimulators (Foutz and McIntyre, 2010).

4.2.2 Limitations of the model

Our model has the advantage of taking into account the electrode/electrolyte interface for estimating conductivity. To our knowledge, this has never reported in the literature. Indeed, in most studies, conductivity is estimated at higher frequencies where the impact of electrode polarization is less important. Still, our approach has some limitations. The first is that the model was developed using the quasi-static approximation, typically used for low frequencies (< 1 kHz) such as the frequency range in EEG (Bossetti et al., 2008; Plonsey and Heppner, 1967). The stimulation artifact, as depicted before, has most of its energy below this frequency. However, there is still some energy in the side lobes at higher frequencies, which means that some dielectric effects could eventually be measured. The second limitation of this model is that, in the following days after implantation, the encapsulation tissue response to an unknown body (the electrode), also referred to as the gliosis process, challenges the estimation of conductivity.

Dielectric properties of tissue model

Brain tissue can be modeled as a medium with its associated conductivity and permittivity. Conductivity is related to resistance, and permittivity is related to the capacitance. Using spatially lumped circuit elements to describe a spatially distributed environment is an approximation and a limitation of the model. Nevertheless, this model can still provide some insight into the physical phenomena occurring during stimulation, evaluating mean values of the spatially distributed environment. Therefore, we can model the capacitive and resistive characteristic of tissues with an electric circuit (e.g. tissue resistance R_m parallel to the tissue capacitance C_m) as shown in Fig. 4-13.

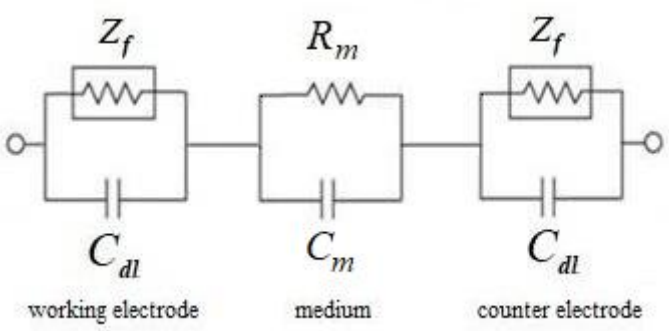

Fig. 4-13. Electric circuit model, with C_m accounting for the tissue capacitance.

Adopting this model, the Laplace expression for the electric potential is:

$$V_m(s) = \left[\frac{2Z_f}{(1 + C_{dl}Z_f s)} + \frac{R_m}{(1 + C_m R_m s)}\right] I(s)$$

Hence, the time domain electric potential using a biphasic constant current pulse $i(t) = I\big[u(t) - 2u(t-T)\big]$ is:

$$v_m(t) = I\left\{u(t)\left[2Z_f\left(1 - e^{-\frac{t}{C_{dl}Z_f}}\right) + R_m\left(1 - e^{-\frac{t}{C_m R_m}}\right)\right] - 2u(t-T)\left[2Z_f\left(1 - e^{-\frac{(t-T)}{C_{dl}Z_f}}\right) + R_m\left(1 - e^{-\frac{(t-T)}{C_m R_m}}\right)\right]\right\}$$

This expression features two exponential functions, with two different time constants, $\tau_1 = C_{dl}Z_f$ modeling the electrode/electrolyte interface and $\tau_2 = C_m R_m$ modeling the tissue.

Gliosis and encapsulation tissue

As aforementioned, within the days following electrodes implantation, an encapsulation tissue starts forming around the electrode, which increases impedance locally. The model proposed for the encapsulation tissue is shown in Fig. 4-14 (Lempka et al., 2009).

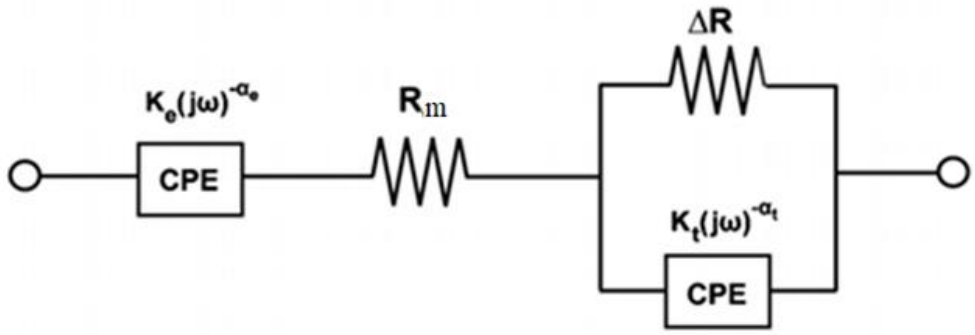

Fig. 4-14. Encapsulation tissue model, as proposed in Section 2, Chapter 2.3.2.

The first CPE is used to model the electrode-electrolyte interface, R_m accounts for the tissue resistance, and the ΔR parallel to CPE represents the encapsulation tissue. Using the Laplace transform, we obtain an analytical expression for the response to stimulation by a biphasic pulse:

$$v(t) = I\left\{u(t)\left[R_m + \frac{2K_e t^{\alpha_e}}{\Gamma(\alpha_e+1)} + 2K_t t^{\alpha_t} E_{\alpha_t,\alpha_t+1}\left(-\frac{K_t}{\Delta R} t^{\alpha_t}\right)\right] - 2u(t-T)\left[R_m + \frac{2K_e (t-T)^{\alpha_e}}{\Gamma(\alpha_e+1)} + 2K_t (t-T)^{\alpha_t} E_{\alpha_t,\alpha_t+1}\left(-\frac{K_t}{\Delta R}(t-T)^{\alpha_t}\right)\right]\right\}$$

where $E_{\alpha,\beta}(\cdot)$ is the Mittag-Leffler function (Kexue and Jigen, 2011; Liang et al., 2015) defined as:

$$E_{\alpha,\beta}(z) = \sum_{k=0}^{\infty} \frac{z^k}{\Gamma(\alpha k + \beta)}$$

On the one hand, this model is more accurate, since it accounts for the gliosis formed the days following implantation. On the other hand, one drawback is that each time that a new component is added to the model, it becomes increasingly challenging to proceed to an accurate estimation of model parameters. Therefore, a compromise between model complexity and parameters estimation must be made to account for the major physical phenomena while relying on reliable approximations.

4.2.3 **Bioimpedance calculation**

Bioimpedance is a commonly used method to study the biophysical parameters of tissue due to its simplicity. Impedance is the ratio between voltage and current, therefore, by definition, bioimpedance is the measured root mean square (rms) electric potential V_{rms}, divided by the I_{rms} root mean squared current:

$$Z_{bio} = \frac{V_{rms}}{I_{rms}} = \frac{\sqrt{\frac{1}{T}\int_{t_0}^{t_0+T} v^2(t)dt}}{\sqrt{\frac{1}{T}\int_{t_0}^{t_0+T} i^2(t)dt}}$$

Bioimpedance measurements are normally performed using sinusoidal waveforms. In this case, the values are easily related to the maximum amplitude of the waveform:

$$Z_{bio} = \frac{V_{rms}}{I_{rms}} = \frac{V_{max}/\sqrt{2}}{I_{max}/\sqrt{2}} = \frac{V_{max}}{I_{max}}$$

As mentioned in Section 2, Chapter 2.5.3, bioimpedance is used as a simple technique to measure biophysical properties of tissue. In this thesis, bioimpedance results are presented, to illustrate the tissue impedance evolution the days after implantation, as a way to quantify the evolution of the encapsulation tissue between patients.

The method to calculate bioimpedance from a biphasic pulse is slightly different than the sinusoidal case. The biphasic constant current bioimpedance is however more challenging to compute than for sinusoidal waveforms. The I_{rms} and V_{rms}, are calculated during a whole period $T_{stim} = {}^{1}/_{f}$ as shown in Fig. 4-15.

$$I_{rms} = \sqrt{\frac{1}{T_{stim}} \int_{t_0}^{t_0+T_{stim}} i^2(t)dt} = \sqrt{\frac{1}{T_{stim}} \int_{0}^{2T} 2I^2 dt} = 2I\sqrt{Tf}$$

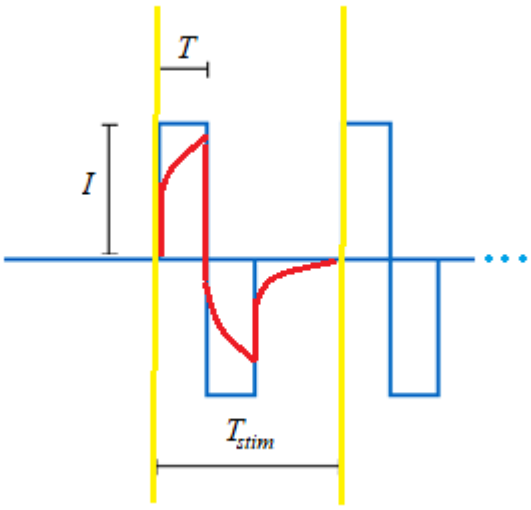

Fig. 4-15. Biphasic constant current stimulation waveform (blue) and recorded artifact (red) during one period.

The value V_{rms} is derived with the observation:

$$V_{rms} = \sqrt{\frac{1}{T_{stim}} \int_{t_0}^{t_0+T_{stim}} {v_{obs}}^2(t)dt}$$

Importantly, bioimpedance does not include the phase information, since only the amplitude is taken into account.

4.3 *Model validation methodology: in vitro, in vivo and in clinico*

In the following, we detail the methodology we proposed to experimentally validate the model we developed. Model validation is made at three different levels, from *in vitro* (saline solutions calibrated in electrical conductivity), *in vivo* (rodents) and *in clinico* (drug-refractory epileptic patients).

4.3.1 *Methodological choices for experimental validation*

Regarding the model validation based on human data, it is worth noting that typical SEEG/EEG systems use sampling frequencies between 512 and 2048 Hz. These frequencies are certainly sufficient to record physiological brain activity, but are too low compared to the stimulation artifact time (which is sub-ms). In order to compare the actual human brain tissue response to that simulated with the model, the sampling frequency must be dramatically increased.

Furthermore, clinical SEEG acquisition systems are typically designed for the acquisition of electrophysiological for signals up to ~100 µV. Since stimulation artifacts (depending on the stimulation current) are on the order of ~1 V, standard SEEG hardware is not an appropriate technical solution to record stimulation-evoked responses. Given these limitations of standard SEEG acquisition systems, we investigated the possibility of an alternative technical solution.

Fig. 4-16. Biopac MP36, acquisition systems (Biopac, CA, USA).

After reviewing various commercially available electrophysiological acquisition systems, we identified the Biopac acquisition system (Biopac MP36, Biopac, CA, USA) as an adequate solution as shown in Fig. 4-16. This system enables the acquisition of signals at a fairly high sampling rate (up to 100 kHz), offering the possibility to record the brain tissue response to brief biphasic pulses with unprecedented detail. The Biopac has 4 available input channels and has isolated human-safe (DC coupled) input amplifiers. The MP36 satisfies the medical safety test standards affiliated with IEC60601-1, and is designated as Class I type BF medical equipment. It also satisfies the medical electromagnetic compatibility (EMC) test standards affiliated with IEC60601-1-1-2 and is CE marked. Therefore, this device was appropriate not only appropriate for *in vitro/in vivo* experiments, but also for human use. Consequently, the Biopac system was chosen, and was used in parallel to the EEG/SEEG acquisition system.

We defined a common stimulation protocol for all modalities, which was: Biphasic constant current pulses of $I = 0.2\,mA$, $T = 1\,ms$ (per phase), with a frequency $f = 5\,Hz$ during $T_{train} = 5s$. The intensity value used was the lowest available on the clinical stimulator, in order to avoid input saturation. This protocol was repeated at least twice. Once the train of pulses was fully delivered for different brain regions, the signal processing was done in Matlab (The Mathworks, USA).

4.3.2 *Parameter estimation*

A commonly used estimator is the minimum mean squared error estimator (MMSE), based on the error between the estimated parameter and the actual parameter value as the basis for optimality. MMSE estimators are chosen in practice for their simplicity over optimal Bayesian estimators (Kay, 1993). We consider β the parameters vector, $v_{obs}(t)$ the observation and $v(t;\beta)$ our model. The error function is defined as:

$$f(t;\beta) = v(t;\beta) - v_{obs}(t)$$

The minimum mean squared error estimator is:

$$\widehat{\beta} = \min_{\beta} E(f(t;\beta)^2)$$

In the case where the model is linearly proportional to the parameters, $v(t;\beta) = H\,\beta$, the estimator is straightforward:

$$\widehat{\beta} = (H^T H)^{-1} H^T v_{obs}$$

For the model defined in the last chapter, the observation is modeled by a function that is a nonlinear combination of model parameters $\beta = [R_m; C_{dl}; Z_f]$. In general, the squared error function is defined as:

$$J(\beta) = \sum f(t;\beta)^2$$

The estimated parameters are those that minimize $J(\beta)$ with lower and upper bounds for the parameters. The MATLAB function used for solving this problem is *lsqnonlin*, which solves the nonlinear least-squares problem of the form:

$$\min_{\beta} \|f(t;\beta)\|_2^2$$

with lower and upper bounds on the components of β. This function uses trust region as an optimization algorithm, that is a modification of Newton's method (Sorensen, 1982). The best-fit parameters are often assumed to be the ones that minimize the sum of squared residuals. The *lsqnonlin* function returns the non-linear minimum squared residual (NLMS Residual) that is the squared 2-norm of the residual at the minimized parameters solution. This value is portrays a goodness of fit, and will be used to illustrate the quality of the estimation.

The parameters Z_f, R_m and C_{dl} were fitted to experimental data. Regarding the fitting procedure, we used a nonlinear approximation to estimate model parameters. To achieve this estimation, we searched for mean range values of Z_f, C_{dl} available in the literature. For C_{dl}, we found a range for the capacitance per unit of area between 10 and 20 µF/cm2 (Merrill et al., 2005). Other studies consider mean values between 20-40 µF/cm^2 with maximum values reaching 60 µF/cm^2 (Łukaszewski, 2016). Given the electrode geometry used in our experimentation, we found a total surface of 0.0503 cm^2, which gives in values of double layer capacitance between 0.5-3 µF. Lower and upper bound for R_m were used, given that the conductivities we are studying for brain tissue conductivities are between 0.05 and 0.4 S/m (Koessler et al., 2017; Latikka et al., 2001).

One critical point is the possibility that our function to optimize has multiple local minima, which can be studied using the Hessian matrix of $J(\beta)$ (of second partial derivatives) that should be positive semidefinite in the interior of our set of parameters (Nocedal and Wright, 1999). As an example, we decided to use a calibrated waveform from saline solutions recordings at $0.2\,S/m$, and then to compute the error function $f(t;\beta)$. We computed the logarithm of the summed squared error for different conductivities as shown in Fig. 4-17. Interestingly, the function is convex in the region of interest, and has only one local minimum with a conductivity value of $0.2\,\mathrm{S/m}$ consistent with the value to be estimated.

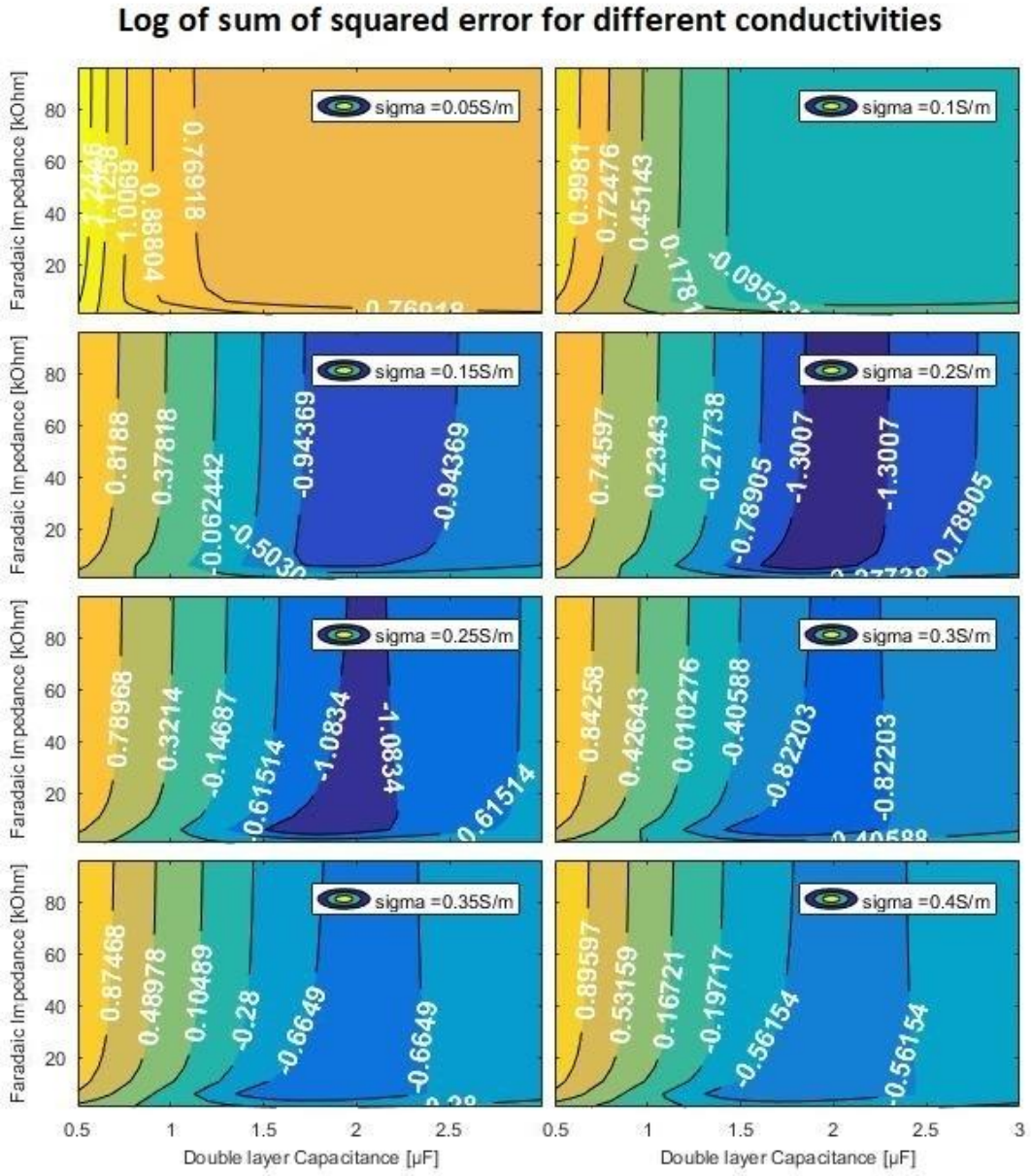

Fig. 4-17. Logarithm of sum of squared error for different parameter conductivities.

4.3.3 *Saline solutions calibration*

The first experimental signals used for validation were obtained from saline solutions, which have the advantage of providing a ground truth (defined conductivity). It should be noted that the electrode/electrolyte parameters could not be calibrated, and only an order of magnitude can be known. The production of these calibrated solutions was made using the following steps. First, we need to express conductivity as a function of the concentration of sodium chloride that was added to distilled water. Distilled water does indeed conduct electricity, and the conductivity depends on the level of purity (e.g.: pure water, ultra-pure water). Considering the ISO 3696:1987 norm, the maximum contaminant (ions) conductivity level in purified water at 25 °C is 0.5 mS/m (https://www.iso.org/standard/9169.html). This value is several orders of magnitude lower than the values used during experimentation, so distilled water conductivity, due to contaminant ions are neglected. When sodium chloride is placed in water, there are strong forces of attraction between the water molecules and the ions of sodium and chlorine. Water molecules are highly polar; the positive or hydrogen end of the water molecule tends to attach itself to the negative chlorine ion, while the negative or oxygen end of the water molecule tends to attach itself to the positive sodium ion as shown in Fig. 4-18, which changes the electrical properties of the solution (Grimnes, 2014).

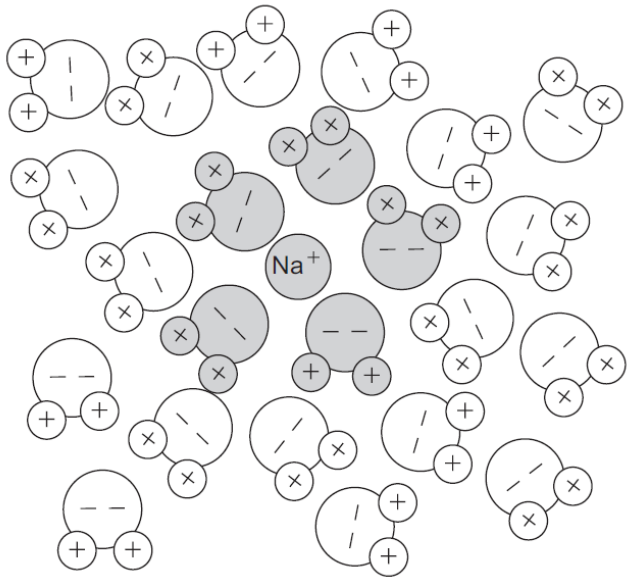

Fig. 4-18. Sodium hydrated by water, giving the property of conducting electricity. Positive and negative ions are free to migrate (Adapted from (Grimnes, 2014)).

The molar conductivity is defined as:

$$\Lambda = \frac{\sigma}{c}$$

where Λ is the molar conductivity, σ is the conductivity, and c is the electrolyte concentration. The Debye-Hückel-Onsager law states that, for strong electrolytes at low concentrations:

$$\Lambda = \Lambda^{\infty} - \mathrm{K}\sqrt{\mathrm{c}}$$

where Λ^{∞} is the molar conductivity at an infinite dilution given by Kohlrausch's law (Atkins et al., 2018). For a NaCl solution:

$$\Lambda^{\infty} = 126.45\,\frac{S\times cm^2}{mol}$$

K is a constant that depends on quantities such as temperature, ionic charges, dielectric constant and viscosity of the solvent. For NaCl at $25°\mathrm{C}$, this constant is equal to:

$$K \cong 60.2\,\frac{\mathrm{S\times cm^2}}{\mathrm{mol}\times\sqrt{\mathrm{M}}}$$

In our experimentation, we used $0.05\mathrm{g}$ of NaCl dissolved in $100\,\mathrm{ml}$ of H_2O, which gives a concentration $\mathrm{c} = 0.0086\,\mathrm{M}$. Hence, the molar conductivity of NaCl is:

$$\Lambda_{NaCl} = 126.45\,\frac{S\times cm^2}{mol} - 60.2\,\frac{S\times cm^2}{mol\times\sqrt{M}} \times \sqrt{0.0086\,M} = 120.88\frac{S\times cm^2}{mol}$$

Resulting in an electrical a conductivity of:

$$\sigma = c \times \Lambda_{NaCl} \cong 0.10\,\frac{S}{m}$$

This value is in agreement with the values found in the Chemistry and Physics Handbook (Rumble, 2017). In order to validate the electrode/electrolyte model, a clinical electrode (DIXI Microtechniques, Besançon, France) was placed into a solution with different calibrated electrical conductivities (4 solutions with electrical conductivity values of 0.10, 0.20, 0.39, and 0.57 S/m, respectively). We used a clinical-grade stimulator (S12X, Grass Technologies, Natus Neurology Inc., USA) to deliver biphasic, charge-balanced pulse electrical stimulation as shown in Fig. 4-19.

Fig. 4-19. Grass Technologies S12X Cortical stimulator system (Natus Neurology Inc.,USA). Constant-current biphasic stimulator.

We used an intensity $I = 0.2\ mA$ stimulating current (the lowest available on this stimulator, to avoid input saturation as aforementioned) and a pulse length of $T = 1\ ms$ per phase (total pulse length of 2 ms). A Biopac acquisition system was used to record the electric potential induced in the solution during stimulation. For values higher than 0.6 S/m, errors due to electrode polarization become significant, so this method is limited to values lower than 0.6 S/m.

4.3.4 *Ex vivo rat brain*

We performed post-mortem conductivity measurement in the brain of *N=2* adults 3 month-old Sprague-Dawley rats euthanized using a CO_2 gradient in accordance with the European Communities Council Directive of 24 November 1986 (86/609/EEC). The skull surface was immediately removed post-mortem and a human intracranial SEEG electrode (ref D08-15AM) was implanted vertically in the rat brain to deliver local, pulsed biphasic stimulation. Stimulation was performed within a few minutes post-mortem in order to avoid post-anoxic tissue degeneration. Stimulation parameters were $I = 0.2\ mA$ for current intensity, and $T = 1\ ms$ per phase for the pulse length. Both hemispheres were stimulated. As in the case of our calibrated saline solutions, a Biopac acquisition system was used to record the induced electric potential.

4.3.5 *In clinico experiment in drug-refractory epileptic patients*

Stimulation data was recorded from $N = 7$ epileptic patients undergoing SEEG in the context of pre-surgical evaluation at La Timone Hospital, Marseille. The seven patients/legal representatives gave informed consent for data acquisition, which involved electrical stimulation intensity that was

significantly lower than that typically used during clinical stimulation sessions in SEEG (i.e., $0.2\ mA$ vs 1-4 mA). Let us mention that this intensity value of $0.2\ mA$ was chosen to avoid input saturation and to minimize stimulation-induced neuronal changes in brain tissue. Visual inspection of the recorded signals confirmed that, at this level of stimulation, no epileptiform discharges were observed in any patient. The material used was a cortical neurostimulator (Inomed, Medizintechnik GmbH, Emmendignen, Germany, Art. No. 504 196), for direct cortical and subcortical stimulation, with a current range of $0.2 - 25\ mA$, pulse duration from to $50\ \mu s - 2\ ms$. The cortical stimulator was connected to a digital switching matrix (Natus Europe GmbH, Robert-Koch-Str. 1, Planegg, Germany). The material configuration is shown in Fig. 4-20. In this configuration, the Biopac system was connected in parallel (very high input impedance). A custom touchproof– DB9 was designed and built in-house to connect the Biopac to the multiplexer.

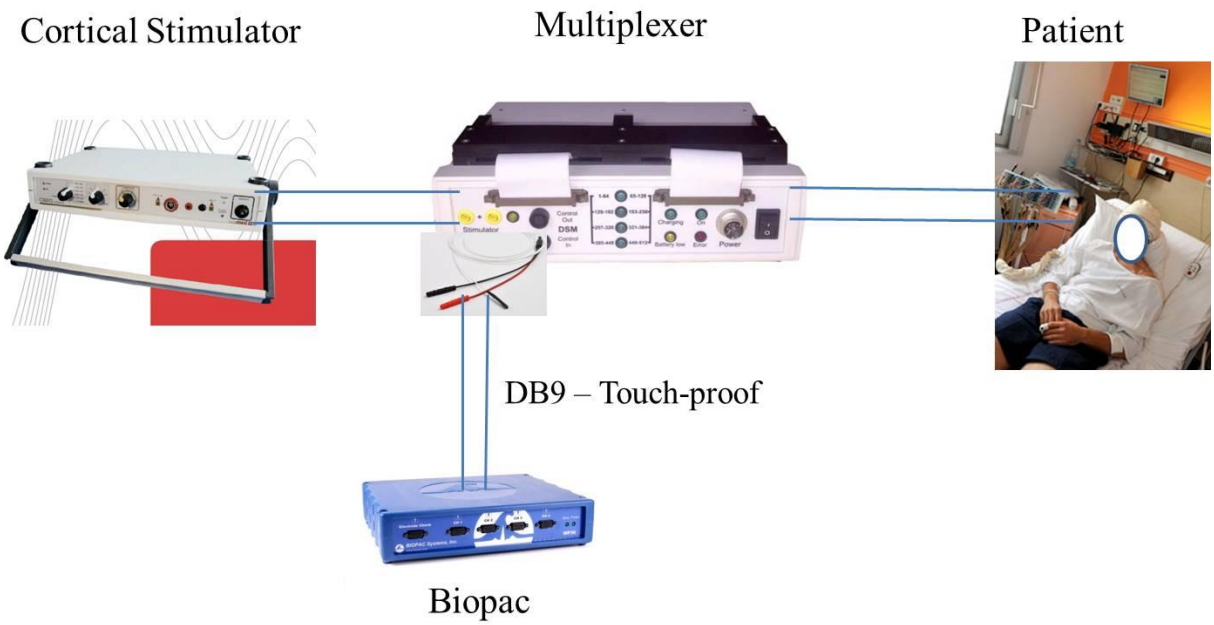

(a)

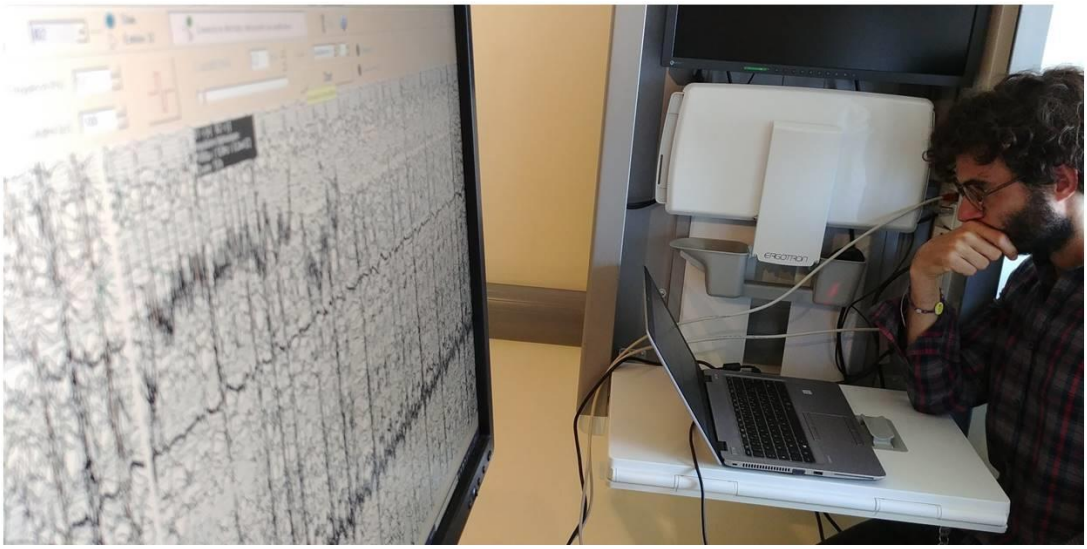

(b)

Fig. 4-20. Configuration setup for recording *in-clinico signals*. (a) Schematic diagram showing the stimulation/sampling system used for the recording signals in patients with intracranial electrodes . (b) A picture that was taken at the La Timone hospital (Marseille) when I participated to the data acquisition. The monitor (left) shows SEEG signals recorded during the low-intensity stimulation protocol we elaborated to test our conductivity-estimation method in human.

The digital switching matrix (multiplexer) was used for connecting the electrodes to the EEG amplifier and in parallel to the cortical stimulator. The connection diagram is depicted in Fig. 4-21. It must be noted that there is a 500 Ω resistance between the cortical stimulator and the patient. This resistance must be taken into account in the estimation.

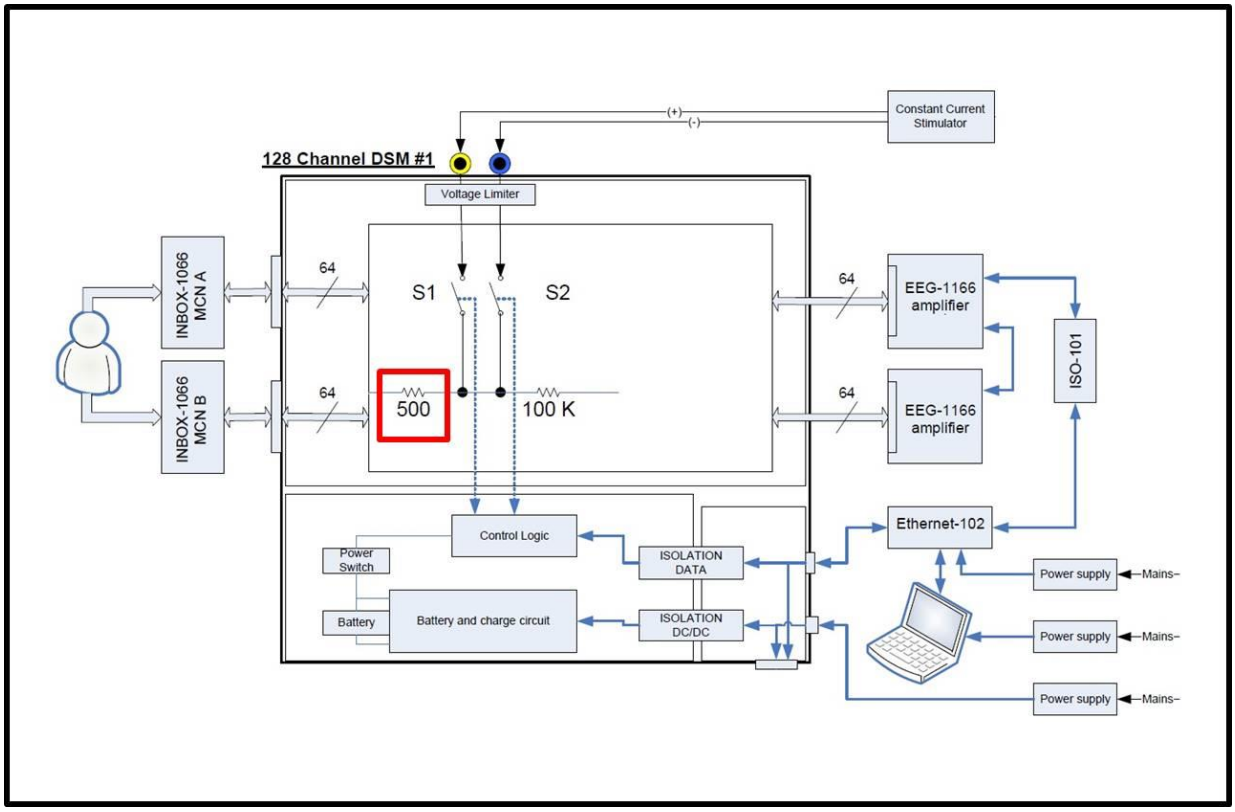

Fig. 4-21. Digital switching matrix internal circuit diagram (Natus Europe GmbH, Planegg, Germany). A 500 Ω resistance is present between the constant current stimulator and the patient.

The patients were stimulated between 1 and 9 days after implantation. The stimulation day after implantation is shown in Tab. 4.1.

STIMULATED PATIENTS – DAY OF TESTING POST-SEEG SURGERY

Patient	Day after implantation	Number of stimulated regions
PAT 1	1	**7**
PAT 2	8	**8**
PAT 3	9	**24**
PAT 4	3	**36**
PAT 5	7	**18**
PAT 6	5	**23**
PAT 7	8	**29**

Tab. 4.1. Stimulation day after implantation for the different patients tested.

SEEG and Electrophysiological recordings

Electrophysiological recordings featured epileptic markers that are routinely used by neurologists to determine if an electrode contact is in the grey or white matter (amplitude and rhythms) and also if

the region is epileptic or healthy (epileptic markers). The selection of stimulated regions was done based on the visual inspection of SEEG data in addition to neuroimaging data (pre-implantation MRI and post-implantation CT). Patients were stimulated between 1 and 9 days after implantation (see Tab. 4.1). The epileptic markers chosen for qualitative evaluation of the region were pre-ictal activity (spikes occurring just before seizure), and fast-onset activity, as shown in Fig. 4-22.

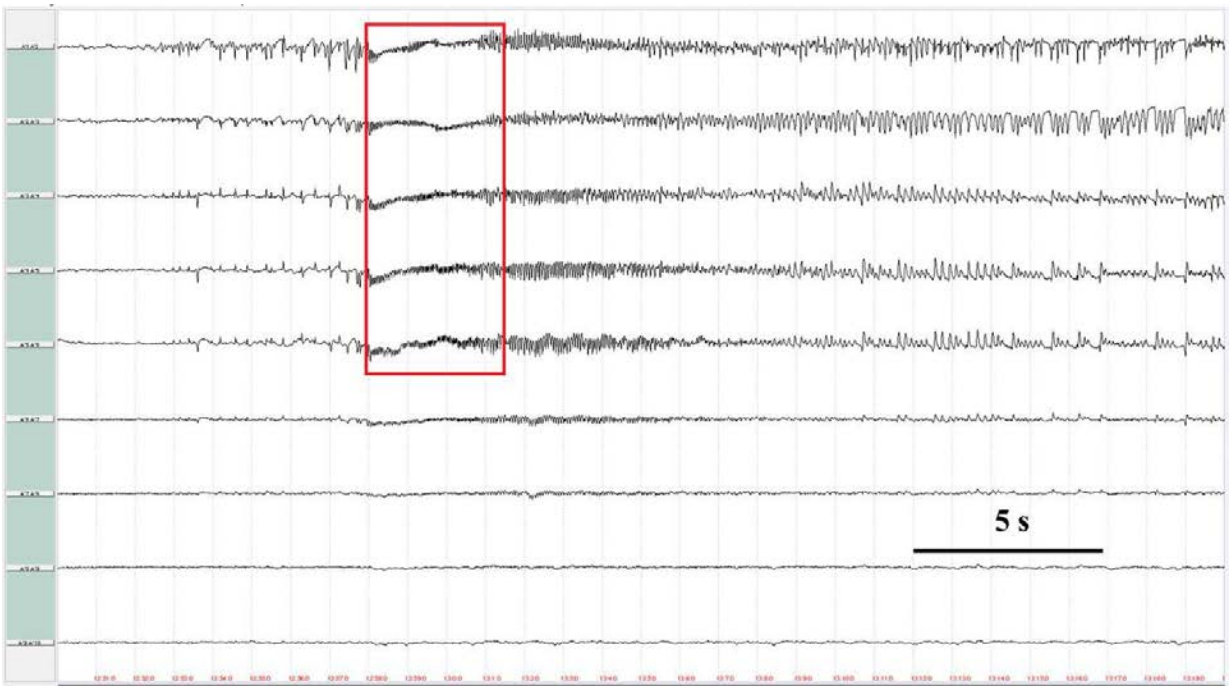

Fig. 4-22. Fast-onset activity occurring at the beginning of a seizure. This electrophysiological marker has long been considered as a hallmark of epileptic regions. This provides a way to assess potential conductivity differences between epileptic and healthy tissue.

During the seizure, sustained rhythmic spikes are observed in some contacts, as shown in Fig. 4-23.

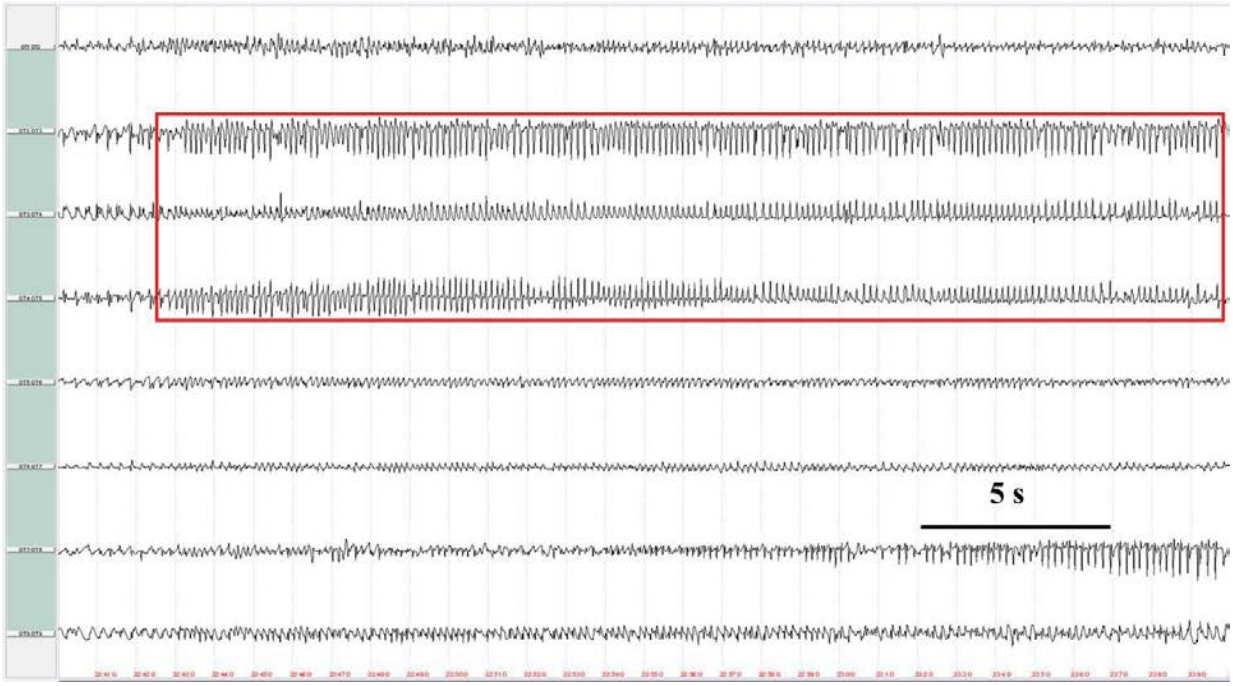

Fig. 4-23. Sustained rhythmic spikes during a seizure, also referred to as ictal activity.

Finally, post-ictal slow waves are also found in some electrodes contacts after seizures as shown in Fig. 4-24.

Fig. 4-24. Slow waves after seizure.

Epileptogenicity index

Brain regions generating seizures can be visually identified from SEEG signals when onset high-frequency oscillations (ictal HFOs) are observed. A quantitative way of measuring the epileptogenicity of brain structures, using intracranial electrodes, is the epileptogenicity index (EI) (Bartolomei et al.,

2008) which was also computed for subsequent analysis of potential correlation with conductivity values estimated from the model proposed in this thesis.

In brief, the Epileptogenicity Index (EI) is a normalized quantity (ranging from 0 to 1) computed from bipolar SEEG signals. It was developed in collaboration between the Rennes and Marseille Epilepsy units (Bartolomei et al., 2008). The basic idea of the EI is to combine, in a single index, i) the propensity of a considered brain structure to generate a rapid discharge and ii) the delay of involvement of this structure with respect to seizure onset. It was designed to provide a normalized value (in the range [0, 1]) which reflects the normal (EI=0, the structure is not involved in the seizure process) or epileptogenic (EI=1, the structure generates a rapid discharge early in the seizure process) nature of brain regions explored by SEEG.

Technically, the EI is estimated using a two-stage procedure. First, for given brain structure S_i, the signal energy ratio ER between high (β and γ) and low (α and θ frequency bands) over a sliding window. Second, a change-point detection algorithm (Basseville and Nikiforov, 1993) is used to automatically determine the time instant N_{di} when ER abruptly increases. A high value of EI_i corresponds to a case where structure S_i generates a rapid discharge (high ER value) and is early involved in the seizure process (N_{di} close to N_0). In contrast, a late involvement of structure S_i and/or slower ictal activity leads to lower EI_i value.

5 Results

Results obtained with the developed models and experiments are presented in this chapter. First of all, the results for the electric potential model are introduced and compared to Comsol Multiphysics (considered as the gold standard) for validation. We then present the results for calibrated saline solutions and *ex-vivo* rat experimentation. The main results, *in-clinico* signals and estimation are introduced, with the analysis of potential conductivity differences between healthy and epileptic region correlations and the evolution of the encapsulation tissue the days following implantation.

5.1 *Electric potential analytical model and Comsol*

The electric potential distribution of a typical SEEG electrode computed using the analytical model is presented in Fig. 5-1 (a). In order to evaluate the accuracy of the electric potential obtained with our model, we computed a numerical solution (FEM) to the PDEs (Maxwell equations) using Comsol Multiphysics (Comsol, Stockholm, Sweden). Since Comsol Multiphysics provides a "gold standard" estimation of the electric field distribution induced by the two electrode contacts, we used it to validate our cylindrical electric model. The electric field distribution computed using Comsol Multiphysics is presented in Fig. 5-1 (b).

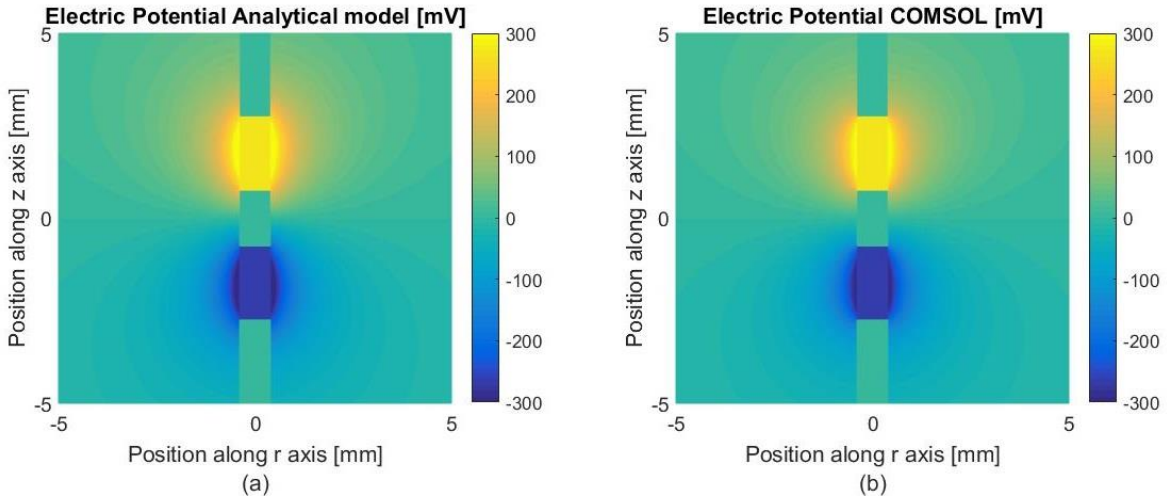

Fig. 5-1. Electric potential distribution of an SEEG electrode. (a) Computed with the cylindrical model (b) computed using Comsol multiphysiscs. The electric potential distribution appears qualitatively in agreement with the analytical model.

As depicted, both model and numerical solutions are in qualitative agreement. This result was confirmed by the difference map (Fig. 5-2) showing a high similarity between the electric field distributions as computed from the proposed analytical model and from the numerical simulation performed using Comsol. The difference between these two field distributions was calculated as follows:

$$e(r,z)_{[\%]} = \frac{\left(V_{analytic}(r,z) - V_{Comsol}(r,z)\right)}{\max(V_{Comsol})} \times 100$$

where $V_{analytic}$ is the analytic function and V_{Comsol} is the dependent variable for the numerical solution. The difference between both models is the highest at the electrode's contact, with values lower than 20%.

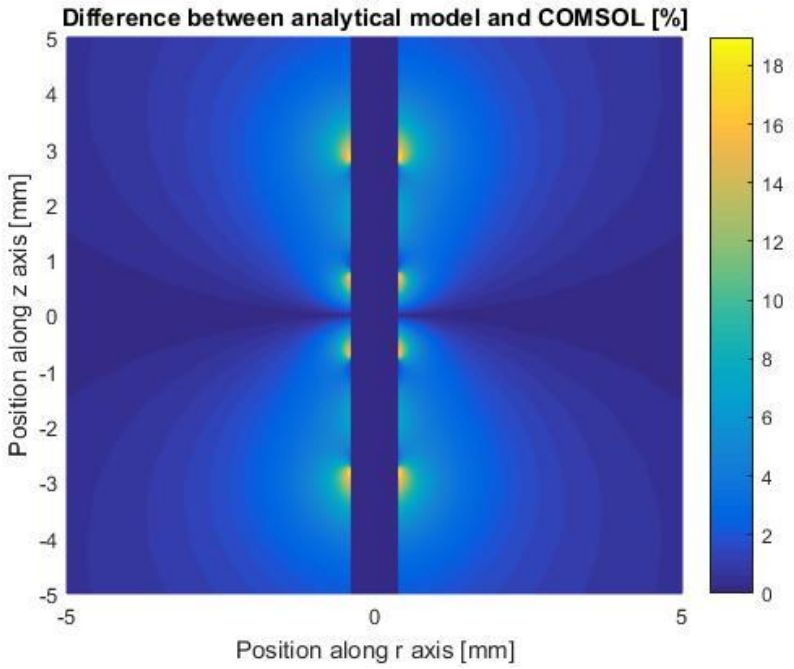

Fig. 5-2. Difference map of the electric potential distribution. The difference between the electric calculation from the cylindrical model and from Comsol Multiphysics is presented as a percentage. Model errors are the highest close to electrode contacts.

Interestingly, at a distance of 1 mm from the electrode, the error between the two estimations remains on average less than 5%, while being considerably faster to compute, confirming the advantage of the presented analytical model as compared to FEM-based methods. This high level of quantitative agreement confirms that model assumptions are reasonable.

5.2 *Saline solution experimentation*

Saline solutions were prepared for testing the stimulation waveform and estimating the parameters using the calibrated solutions as ground truth. This experiment also enables checking the acquisition system that would be used for the *ex-vivo* and *in-clinico* experimentation. Conductivity was calibrated using a precise volume of water along with the precise amount of salt measured with a high-precision scale (precision of 100 µg). Four different solutions within the same range of conductivity values than human brain tissue (0.1-0.6 S/m) were used. The recorded time course of the electric potential during a stimulation pulse depends on electrical conductivity, as can be seen in Fig. 5-3.

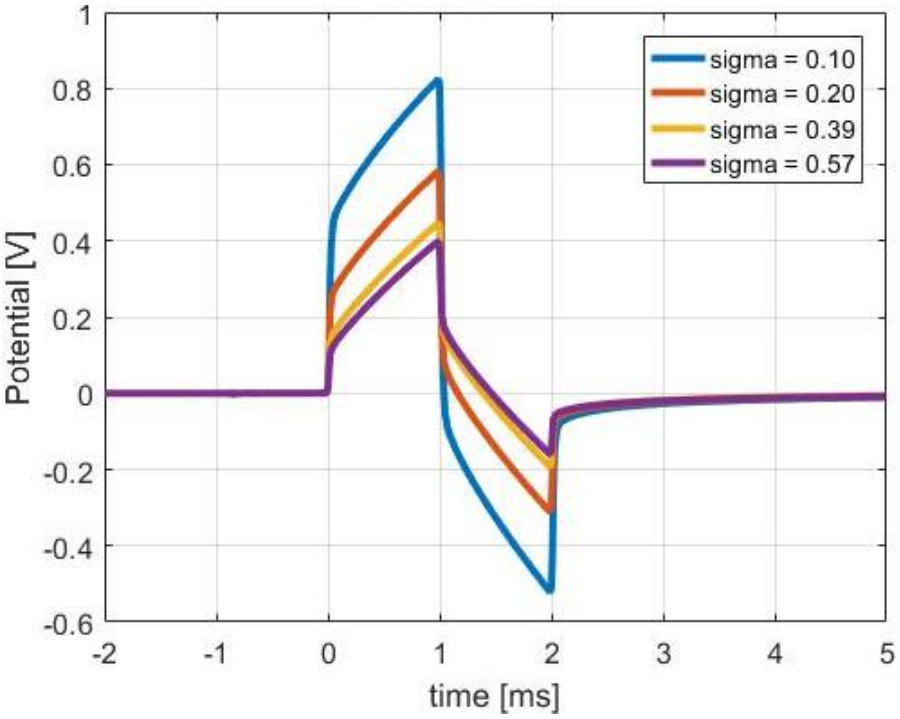

Fig. 5-3. Time course of the induced electric potential in each saline solution following a biphasic, charge-balanced pulsed stimulation at 0.2 mA, 1 ms per phase. Increasing conductivity decreases the amplitude of the electric potential time course.

As detailed in Section 4, waveform discontinuities convey information on electrical conductivity. Since conductivity is inversely proportional to medium resistance, the medium resistance decreases when conductivity increases. The double layer (DL) model and the constant phase element (CPE) model results are presented hereafter. For each solution, the model was used to estimate conductivity and electrode-electrolyte parameters (capacitance of the double layer and faradaic impedance) using the aforementioned estimation/optimization procedure. The agreement between the DL and CPE models on the one hand, and with experimental recordings in saline solutions on the other hand, is compared in Fig. 5-4.

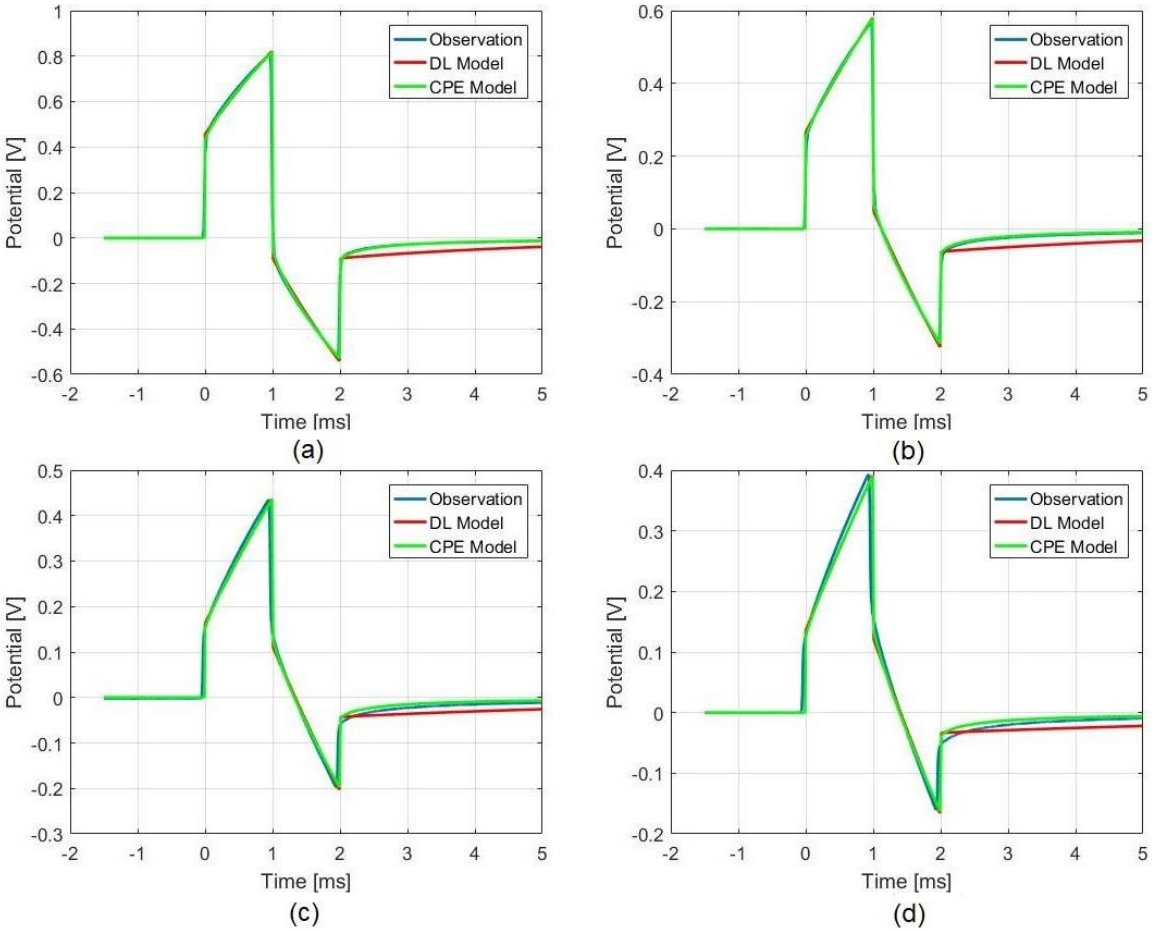

Fig. 5-4. Agreement of the double layer and CPE models with recorded signals in saline solutions. Superimposed time course of simulated (double layer model, red; and CPE model, green) and experimentally recorded (blue) electric potentials for four different conductivity values: (a) 0.10 S/m, (b) 0.20 S/m, (c) 0.39 S/m, and (d) 0.57 S/m.

Both DL and CPE models reproduce accurately the time course of the experimentally recorded potential for both positive and negative phases. One difference is that, in the discharging phase, the CPE model performs better than the DL model. We therefore estimated unknown parameters for the DL, based on the experimental recordings, which are presented in Tab. 5.1. Notably, electrical conductivity was computed from the estimated electrical resistance value (Tab. 5.1). On average, the DL-based estimation of electrical conductivity was within 10% of the ground truth value. The CPE model was presented, since it is frequently used in the literature for modeling metal electrodes interfaces. Importantly, this model effectively had a non-linear minimum squared residual (NLMS Residual) that was lower than the DL model. However, the CPE model is less intuitive, given that it is not common to use pseudo-capacitance in electric circuits. Therefore, in the remainder of this thesis, only DL model estimations will be presented.

Resistance (Ω)	Double layer capacitance (μF)	Faradaic impedance (Ω)	**Conductivity (S/m)**
	*Calibrated Solution (**σ = 0.10**)*		
2079.5 ± 20.9	1.209 ± 0.040	1652.6 ± 92.1	**0.110 ± 0.001**
	*Calibrated Solution (**σ = 0.20**)*		
1161.2 ± 15.3	1.344 ± 0.033	1676.1 ± 83.6	**0.217 ± 0.003**
	*Calibrated Solution (**σ = 0.39**)*		
720.2 ± 10.1	1.449 ± 0.032	1623.4 ± 66.1	**0.392 ± 0.007**
	*Calibrated Solution (**σ = 0.57**)*		
552.9 ± 8.4	1.435 ± 0.036	1486.9 ± 47.5	**0.563 ± 0.014**

Tab. 5.1. Parameter estimation using the double layer model. Estimations were performed from the experimental recordings carried out in each of the four calibrated saline solutions and the ex-vivo rat brain.

Zeta and triangle waveforms

Historically, physicians and researchers primarily used biphasic constant current rectangular pulses. Recent studies suggest that non-rectangular waveforms may have certain advantages over traditional rectangular waveforms (Foutz and McIntyre, 2010). In Section 4, we modeled the zeta and triangle waveform as an attempt to perform parameter estimations using other waveforms. These waveforms were tested in the saline calibrated solutions (solution calibrated at $\sigma = 0.1\ S/m$). The observation and estimated DL model signal waveform are shown in Fig. 5-5.

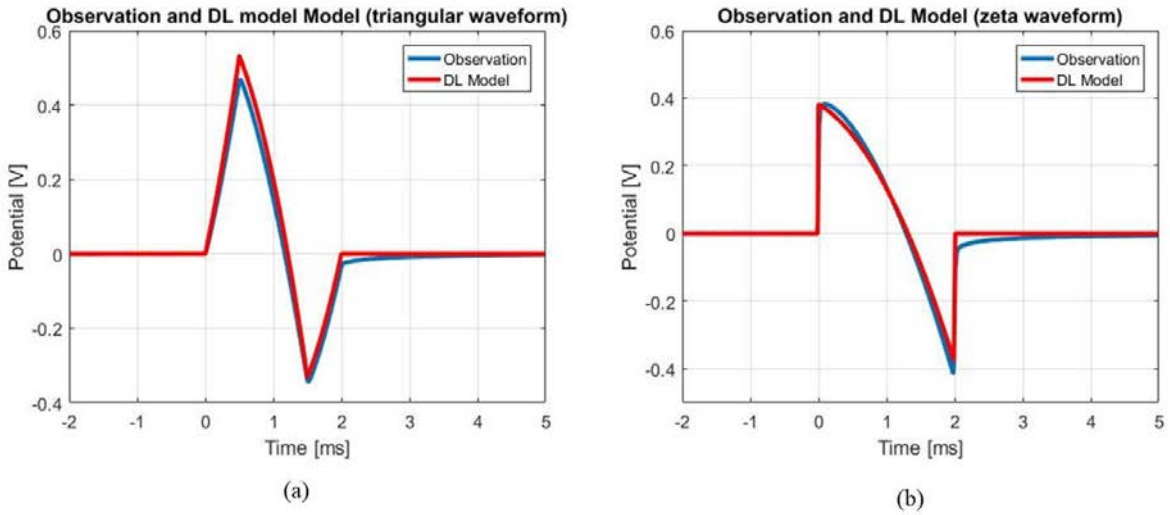

Fig. 5-5. Observation (saline calibrated solution of σ = 0.1 S/m) and double layer model for (a) Triangular waveform and (b) zeta waveform.

The parameters estimation for triangle and zeta biphasic waveforms is shown in Tab. 5.2. The estimated values using the different waveforms are equivalent. Furthermore, conductivity estimation

PARAMETERS ESTIMATION TRIANGLE AND ZETA BIPHASIC PULSE

*Calibrated Solution (σ = **0.10 S/m**)*

Resistance (Ω)	Double layer capacitance (μF)	Faradaic impedance (MΩ)	**Conductivity (S/m)**
		Zeta waveform	
2011.7 ± 20.1	1.5167 ± 0.043	9.9639 ± 0.013	**0.115 ± 0.0013**
		Triangle waveform	
2084.6 ± 4.7	1.4998 ± 0.051	9.9889 ± 0.013	**0.111 ± 0.0004**

Tab. 5.2. Parameter estimation using the double layer model. Estimations were performed from the experimental recordings carried out in the calibrated solution, using zeta and triangular biphasic waveforms.

was consistent with the value of the calibrated solution. Nevertheless, the values of the electrode/electrolyte interface are not the same as the ones shown in Tab. 5.1. This might be because a different electrode and solution was used for this experimentation. It is worth noting that these waveforms will inject half of the charges as compared to the typical constant current pulse (for same values of *I*), provided that the charge injected is the area below the waveform.

5.3 *Ex-vivo* rat brain

Ex-vivo experimentation was done in two Sprague-Dawley rats. The signal and the model fit are shown in Fig. 5-6.

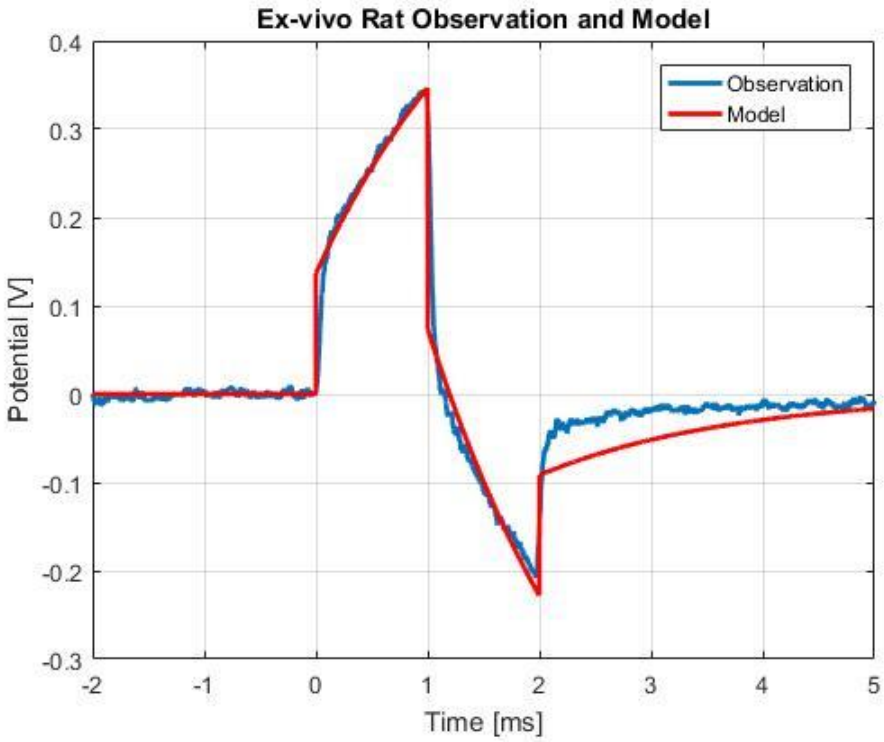

Fig. 5-6. Time course of the induced electric potential in the brain of a Sprague-Dawley rat and DL model.

The experimental and simulated waveforms are in very good qualitative and quantitative agreement. Estimated conductivity values presented in Tab. 5.3. are lower than values reported for grey matter in the literature, possibly because conductivity decreases post-mortem (J. A. Latikka et al., 2001; Schmid et al., 2003). Given that the electrodes were implanted without a precise knowledge of the exact anatomical position of the contacts, it is also possible that electrodes were located in the white matter, accounting for the lower conductivity. Interestingly, we observed a lower conductivity in the left hemisphere than the right hemisphere, possibly due to the fact that hemispheres were recorded one after the other, involving post-mortem changes in the biophysical properties of tissue between recordings.

Resistance (Ω)	Double layer capacitance (μF)	Faradaic impedance (Ω)	**Conductivity (S/m)**
	Right Rat Brain Hemisphere		
1255.1 ± 61.5	0.546 ± 0.046	1631.2 ± 145.2	**0.119 ± 0.006**
	Left Rat Brain Hemisphere		
1825.7 ± 39.4	0.522 ± 0.024	1598.0 ± 77.2	**0.080 ± 0.002**

Tab. 5.3. Parameter estimation using the double layer model. Estimations were performed from the experimental recording carried out in the *ex-vivo* rat brain.

5.4 *In-clinico* acquisitions in drug-refractory epileptic patients

As mentioned previously, SEEG data was collected from a total of $N = 7$ epileptic patients admitted for pre-surgical evaluation at the University Hospital of La Timone, Marseille (service of Pr. F. Bartolomei). Electrical stimulation was delivered to several brain regions considered healthy or epileptogenic, on the basis of electrophysiological markers of epileptiform activity.

5.4.1 *Detailed analysis*

The results for the first patient stimulated are presented below. This patient is presented to illustrate qualitatively the agreement between the recorded signals and the model. This patient (male, age 7 years old) was stimulated the day immediately after electrode implantation. The stimulation signal waveform and reconstructed model waveform are illustrated in Fig. 5-7.(a).

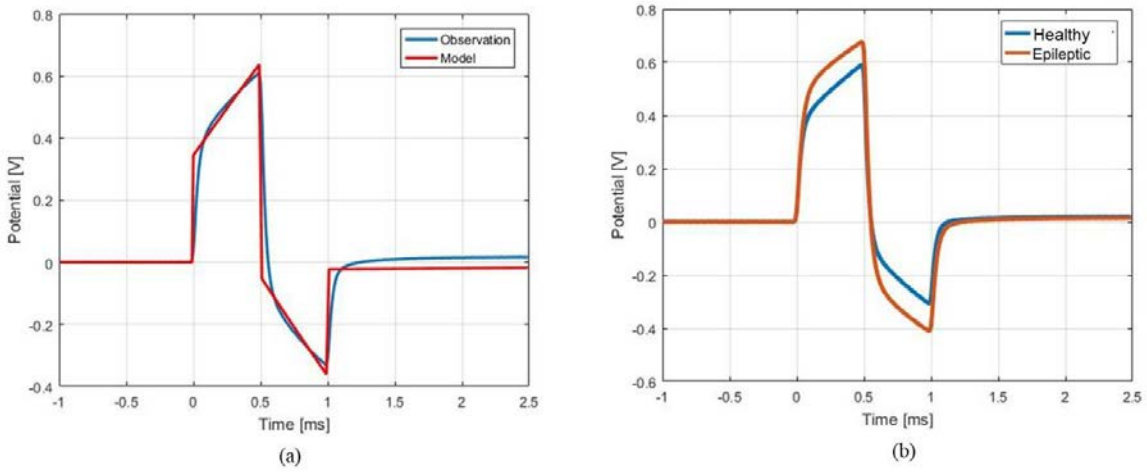

Fig. 5-7. (a) Signal waveform and DL model for the first stimulated patient. (b) Two different electrodes signal waveforms illustrating the amplitude difference.

It is observed that the model is not as good qualitatively as compared to the calibrated solutions. Waveform discontinuities are less pronounced that in the calibrated solutions, suggesting that tissue capacitive effects may be present. Two different stimulated regions are shown in Fig. 5-7 (b), one from TP3-TP4 (epileptogenic) and A9-10 (healthy grey matter). The amplitude difference in the recorded response to constant current stimulation is related to their different conductivity. The difference between signals recorded at the A9-10 and TP3-TP4 contacts reveal that TP3-TP4 has a higher medium resistance than A9-10, hence a smaller conductivity. Estimated conductivity values for the different regions are shown in Tab. 5.4.

An example of patient data is shown in Fig. 5-8, where seven electrode contacts (labeled A4-5, A9-10, CR4-5, B'3-4, TP1-2, B1-2 and TP3-4, referring to each pair of contacts) from different regions are highlighted. Estimated values of conductivity are presented for each electrode along with corresponding electrophysiological recorded signals.

PARAMETER ESTIMATIONS FOR EACH STIMULATED BRAIN REGION

Electrode	Resistance (Ω)	Double layer capacitance (μF)	Faradaic impedance (kΩ)	**Conductivity (S/m)**
A4-5	686.3 ± 27.4	0.647 ± 0.011	1.526 ± 0.049	**0.315 ± 0.013**
A9-10	694.2 ± 29.2	0.742 ± 0.017	1.867 ± 0.117	**0.311 ± 0.014**
CR4-5	1120.1 ± 46.3	0.598 ± 0.009	1.824 ± 0.054	**0.193 ± 0.008**
B'3-4	1066.4 ± 43.6	0.631 ± 0.015	1.410 ± 0.046	**0.202 ± 0.009**
T'1-2	1014.3 ± 35.9	0.728 ± 0.018	1.247 ± 0.046	**0.213 ± 0.008**
B1-2	1007.8 ± 31.6	0.551 ± 0.006	2.027 ± 0.054	**0.214 ± 0.007**
T'3-4	1075.4 ± 42.7	0.689 ± 0.019	1.263 ± 0.056	**0.201 ± 0.008**

Tab. 5.4. DL model parameter estimation for the seven stimulated brain region.

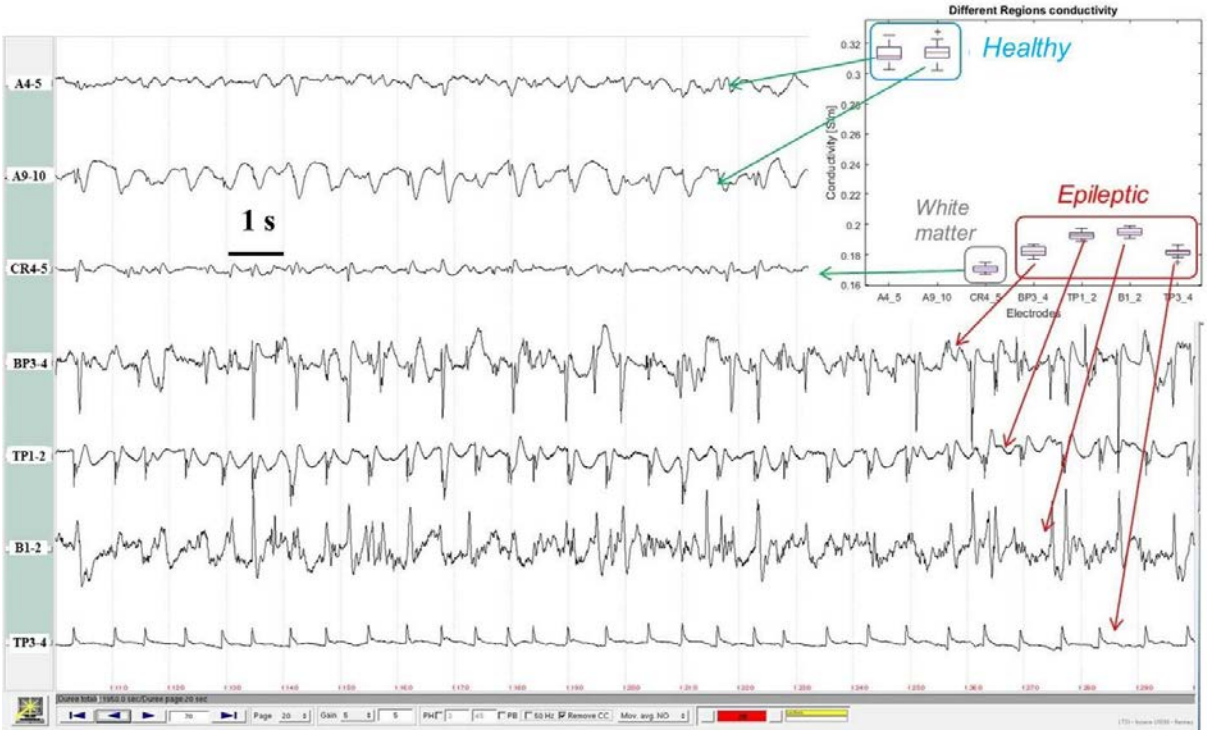

Fig. 5-8. Electrophysiological activity of an epileptic patient recorded in healthy and epileptic regions, with comparison of estimated conductivity.

For A4-5 and A9-10, normal electrophysiological activity characteristic of grey matter was observed, and estimated conductivity values were 0.32 S/m. The signal recorded from the CR4-5 electrode contact had a low-amplitude electrophysiological activity, typically seen in white matter, with an estimated conductivity value of 0.17 S/m. Electrode contacts B'3-4, TP1-2, B1-2 and TP3-4 displayed epileptic activity, with spikes and high frequency oscillations. Interestingly, for these electrodes, lower conductivity was estimated as compared to A4-5 and A9-10, which were electrodes located in healthy brain tissue. Estimated values of DL capacitance and faradaic impedance were between 0.55-0.75 μF and 1.2-2.1 kΩ, respectively, and did not depend on the epileptogenicity of recorded brain regions. Since the electrode-electrolyte interface depends on factors such as local ions redistribution and charge transfer, there is no reason *a priori* that epileptogenic regions have significant differences in the values of Z_f and C_{dl} as compared to healthy regions.

Stimulation of all contacts along one electrode

For one patient, we stimulated the entire length of the electrode (all contacts along this electrode). This electrode was situated in a region where pathological activity and healthy activity were present. The most intern electrodes were located in the parahippocampus gyrus (electrodes OT1-4), followed by a junction and white matter (electrodes OT4-7), then the occipito-temporal sulcus (electrodes OT7-10), another junction (electrodes OT10-12), and finally the inferior temporal gyrus (electrodes OT12-13). The onset of a seizure is shown for the electrodes OT1-12, along with the conductivity (Fig. 5-9) for these electrodes.

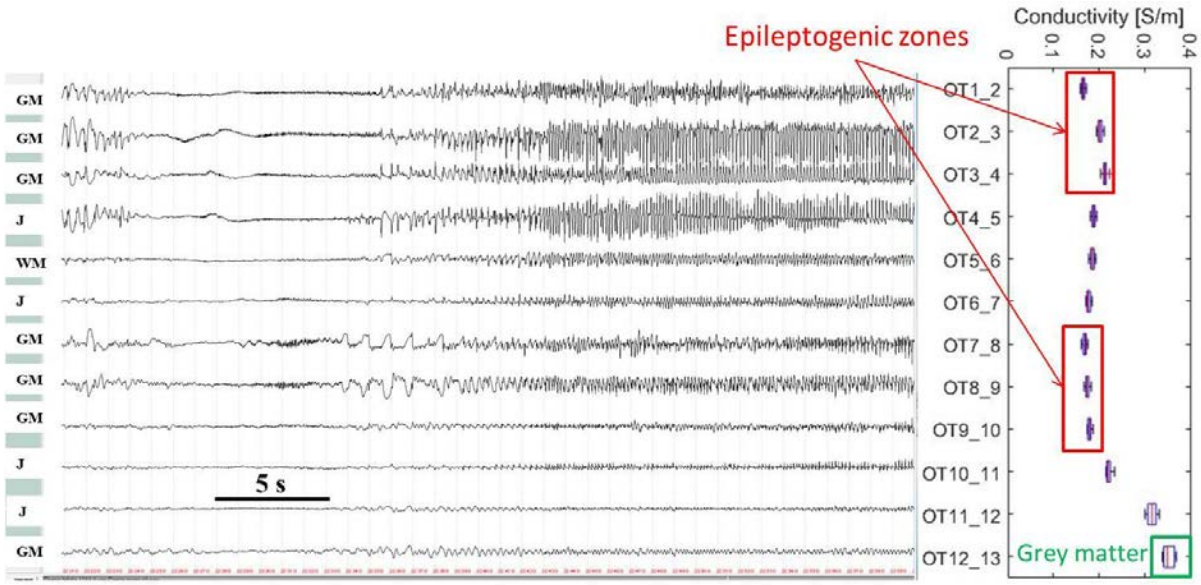

Fig. 5-9. Epileptic seizure recorded in each contact of one whole electrode and estimated conductivity values.

Fast-onset and sustained rhythmic spikes are observed in the para-hippocampus gyrus (OT1-4) and in the occipito-temporal sulcus (OT7-10), electrodes in the junction and in the white matter are not considered to have significant activity and finally the contact in the inferior temporal gyrus (OT12-13) has physiological activity. Interestingly, it is observed that the electrodes in the para-hippocampus gyrus occipito-temporal sulcus grey matter has lower conductivity that the electrode in the inferior temporal gyrus.

Furthermore, we present in Tab. 5.5 the normalized epileptogenicity index (see in section 4.3 for definition). Higher values of epileptogenicity index (EI) means that the tissue is more epileptogenic. Interestingly, for grey matter, EI values are inversely correlated to conductivity.

WHOLE ELECTRODE ANALYSIS

Contact	Localization	GM/WM/J	Normalized EI	Epileptogenicity Classification	**Conductivity (S/m)**
OT1-2	Para-hippocampus gyrus	GM	1	EZ	**0.164**
OT2-3	Para-hippocampus gyrus	GM	1	EZ	**0.201**
OT3-4	Para-hippocampus gyrus	GM	1	EZ	**0.212**
OT4-5		J	0.85	NEZ	**0.187**
OT5-6		WM	0.6	NEZ	**0.184**
OT6-7		J	0.55	NEZ	**0.176**
OT7-8	Occipito-temporal sulcus	GM	1	EZ	**0.167**
OT8-9	Occipito-temporal sulcus	GM	1	EZ	**0.173**
OT9-10	Occipito-temporal sulcus	GM	0.3	EZ	**0.178**
OT10-11		J	0.1	NEZ	**0.220**
OT11-12		J	0.1	NEZ	**0.314**
OT12-13	Inferior temporal gyrus	GM	0	NEZ	**0.351**

Tab. 5.5. Localization, classification, EI and conductivity of one patient entire electrode.

5.4.2 *Post-implantation encapsulation tissue*

As shown in Section 2, Chapter 2.3.2, when a foreign body is introduced in brain tissue, an encapsulation tissue that starts developing during the days following implantation. Since stimulation sessions did not occur at a fixed day (depending on the neurologist and patient availability), it was not possible to have stimulations that were completely consistent in terms of post-surgery testing timing. This resulted in stimulation waveforms that varied from patient to patient, as shown in Fig. 5-10.

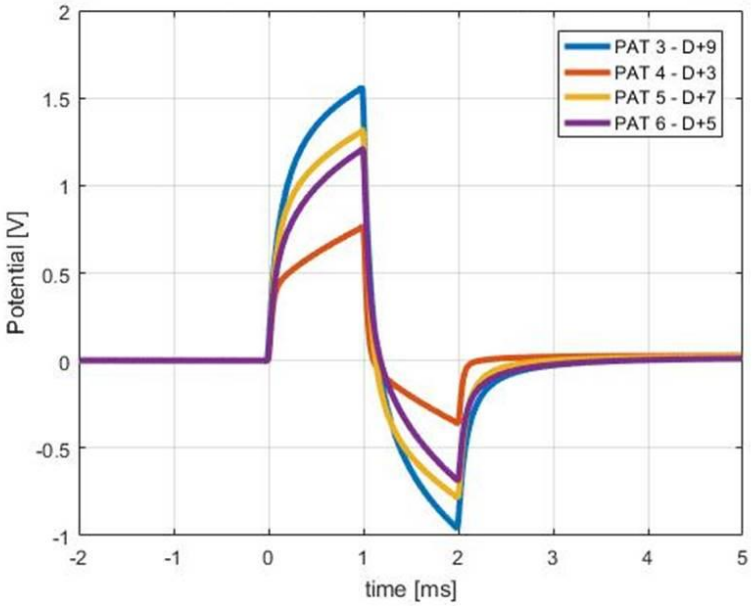

Fig. 5-10. Recorded stimulation waveforms for 4 different patients. Patients were stimulated different days after implantation (D+X, where X is the number of days between surgery and stimulation).

Stimulation waveforms increase in amplitude during the days following implantation, which translated into higher impedance. The encapsulation tissue then adds up to the total medium resistance, which biased the estimation. Waveforms are qualitatively different, as can be seen within patients stimulated over 3 days post-surgery, where slower dynamics and higher amplitude probably due to effects of the encapsulation tissue. These differences will result in higher bioimpedance as shown in Fig. 5-11(a), and induce errors in the model, as shown in Fig. 5-11.(b).

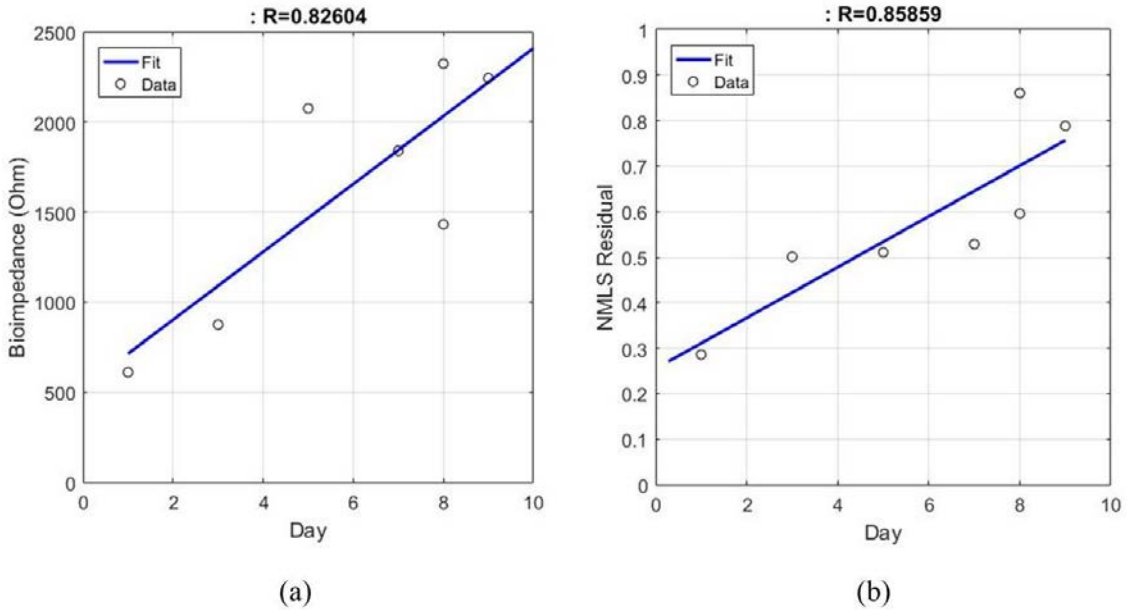

Fig. 5-11. (a) Mean value of the bioimpedance as a function of the post-implantation day. It is observed that the value of bioimpedance increases the days following implantation. (b) Non-linear mean square residual for different patients. The residual increases as a function of the post-implantation day.

As illustrated, when conductivity estimation is performed several days after implantation, higher values of impedances are expected which will cause a decrease in conductivities, as shown in. Fig. 5-12.

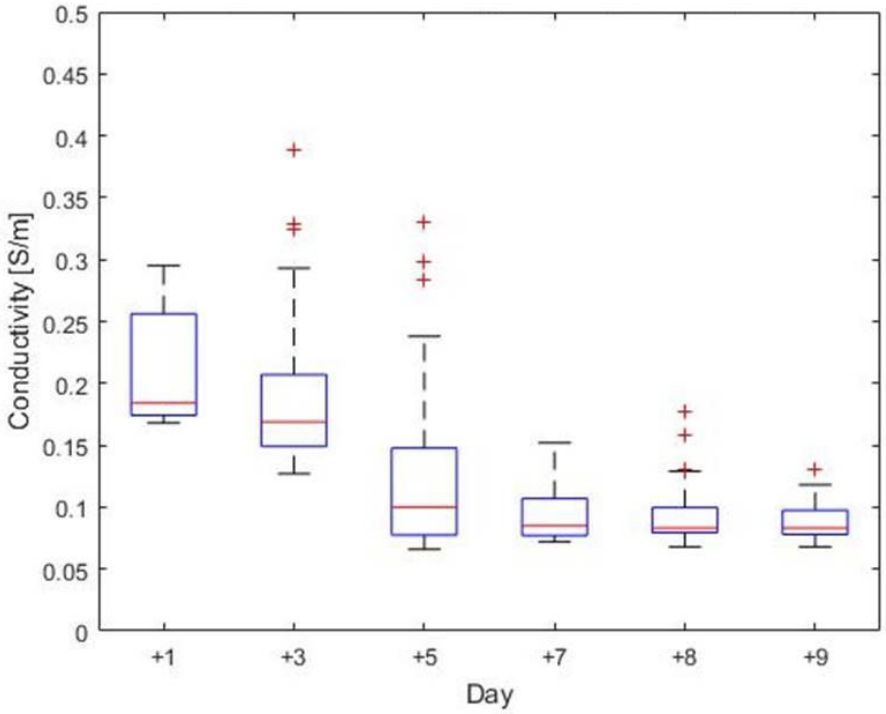

Fig. 5-12. Conductivity estimation as a function of the day after implantation, emphasizing how the estimated conductivity decreases during the days after implantation.

These values make it difficult to compare the results between different patients. Nevertheless, in the results analysis, the biased values of conductivity will be compared between patients in the group analysis. A possible future prospect could be the use of encapsulation tissue impedance values as a function of the post-surgery number of days, and adapt them to the model.

Encapsulation tissue model

As described in the section 4 (Gliosis and encapsulation tissue), an option to understand the stimulation artifact during the days following implantation is modeling this encapsulation tissue. Considering the model proposed by (Lempka et al., 2009), the encapsulation tissue model was implemented as shown in Fig. 5-13 and Fig. 5-14. This model fits well the stimulation artifact, especially those that are stimulated more than 3 days after implantation. It must be noted that this method has more parameters (6 parameters) than the DL (3 parameters), which means a higher computational cost and a more difficult optimization problem for parameter identification.

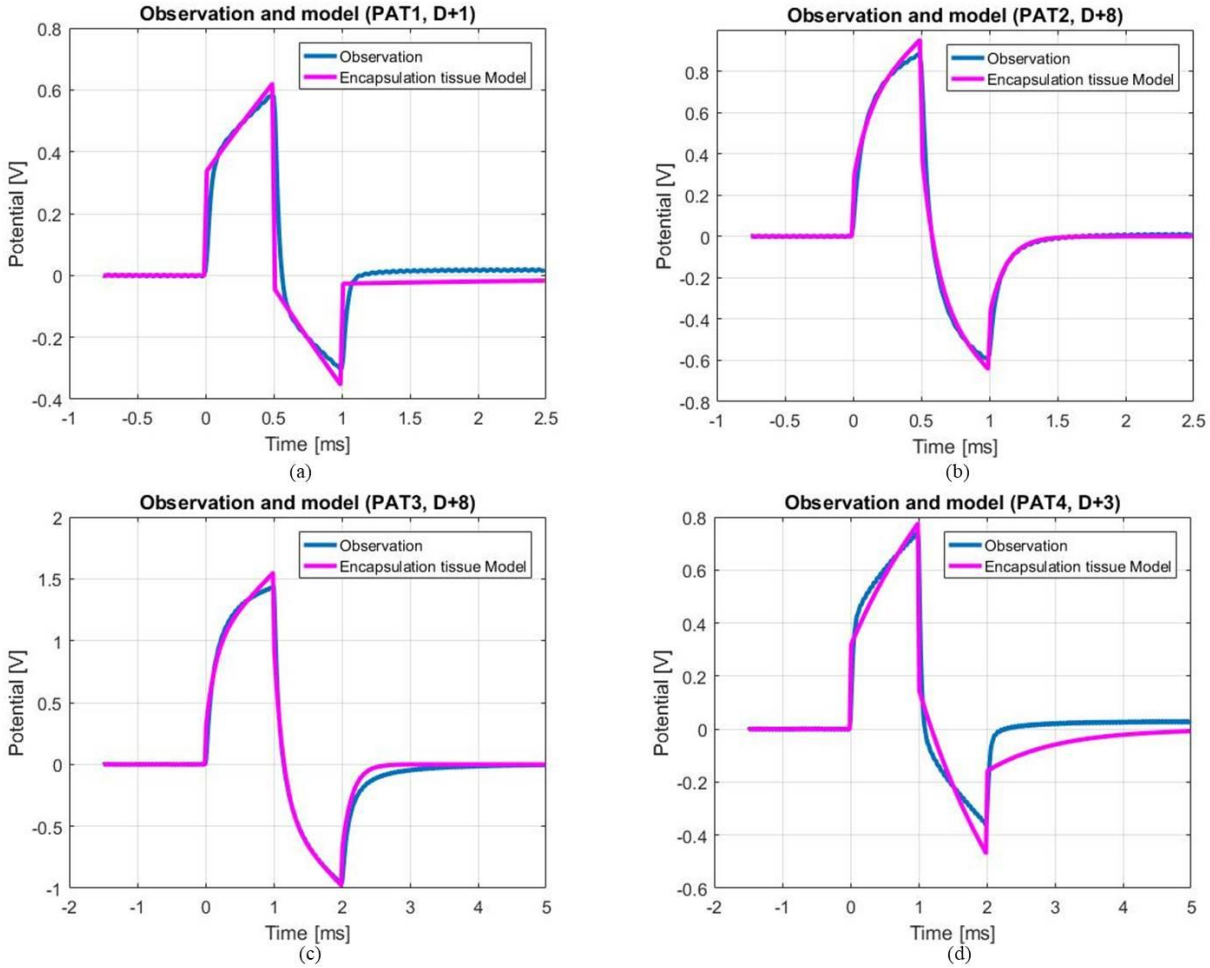

Fig. 5-13. Encapsulation tissue circuit model as described in section 4, Gliosis and encapsulation tissue (violet) compared to the patient observation (blue) for: (a) Patient 1 (PAT1), (b) Patient 2 (PAT2), (c) Patient 3 (PAT3) and (d) Patient 4 (PAT4)

These results open a new possibility for analyzing the gliosis process during the days following implantation, and possibly to find differences between regions that have different types of gliosis.

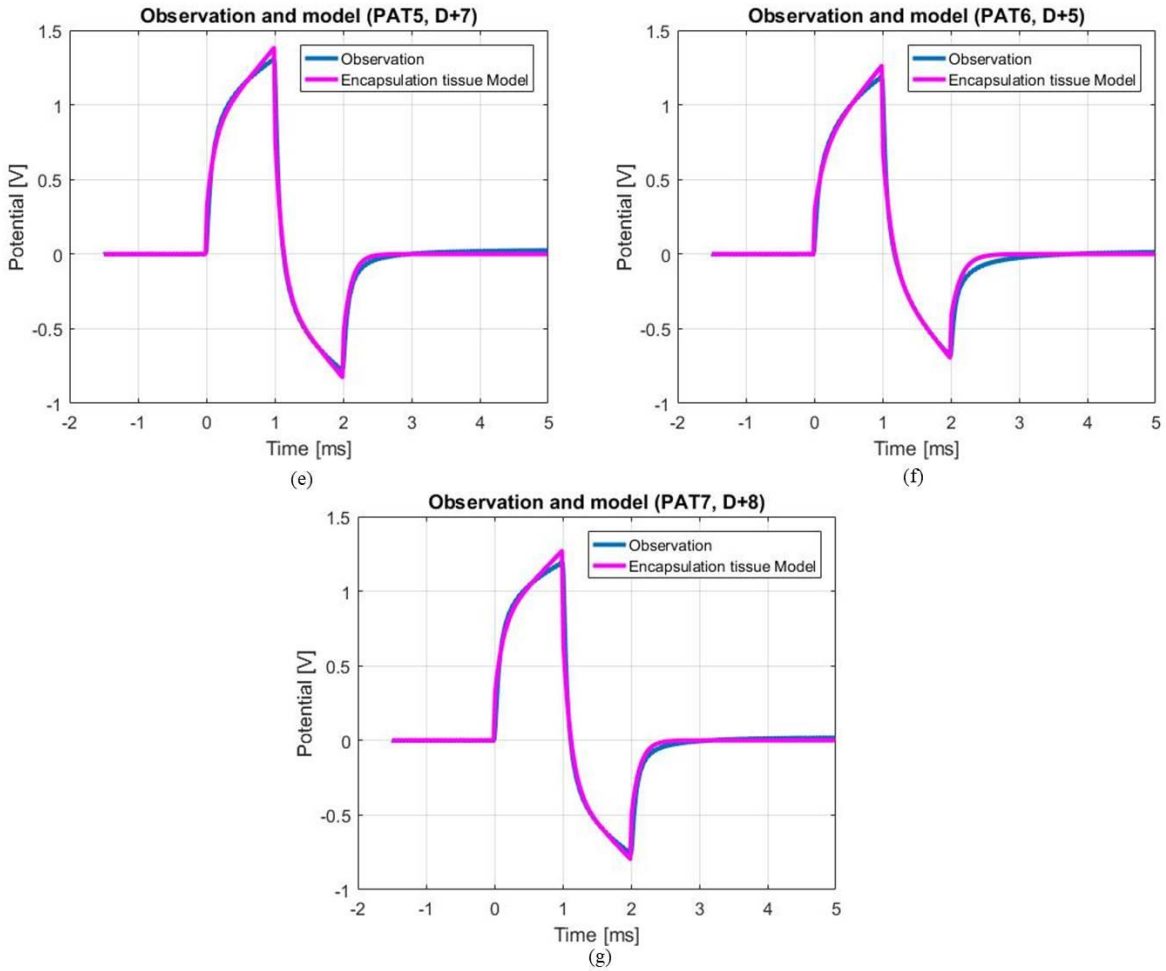

Fig. 5-14. Encapsulation tissue circuit model as described in section 4, Gliosis and encapsulation tissue (violet) compared to the patient observation (blue) for (e) Patient 5 (PAT5), (f) Patient 6 (PAT6) and (g) Patient 7 (PAT7).

5.5 *Statistical analysis*

In the following, results from experimental data are analyzed in the perspective of classifying healthy vs. epileptogenic regions. This is a challenging issue *per se*. As described in Section 2, Chapter 2.2.3 and Section 4, Chapter 4.3.5, there are several electrophysiological patterns (epileptic markers) found in SEEG recordings that characterize epileptic activity. The pathological activities that will be considered for classification are:

- inter-ictal activity (e.g. spikes and spike-wave),
- ictal fast onset,
- sustained rhythmic spikes (during seizures),
- Slow-wave activity (after seizures).

The classification performed was to arrange the electrodes in two groups on the basis of electrophysiological markers. The first group was the electrodes contacts that did not display any

epileptic markers (regions considered healthy, i.e. NEZ). The second was the group of electrode contacts that displayed pathological activity, and are the ones to be considered in the EZ. The propagation zones were not differentiated from the EZ, which will be a perspective for future studies to add the propagation zones to the statistical analysis.

5.5.1 *Single patient-level analysis*

The statistical analysis per patient is divided in two parts: the first two patients are analyzed, and then the last five. This distinction is made since the first two patients were stimulated in fewer regions than the last five, which limits a proper statistical analysis. The reason is that the two first patients were the very first to be stimulated in an experimental setup that was never done before, and consisted in a "proof-of-principle" regarding our method.

Patients 1-2 (PAT 1-2)

PAT 1 was recorded the day following implantation of SEEG electrodes, and seven regions were recorded. From electrophysiological recordings, electrodes, three electrodes were classified in non-epileptogenic zones (NEZ), and four electrodes were in regions generating significant epileptiform activity. PAT 2 was recorded eight days after implantation, and seven regions were stimulated. From SEEG signals, it was evaluated that 4 electrode contacts were in classified as NEZ, while 3 electrode contacts where as EZ, as shown in Fig. 5-15.

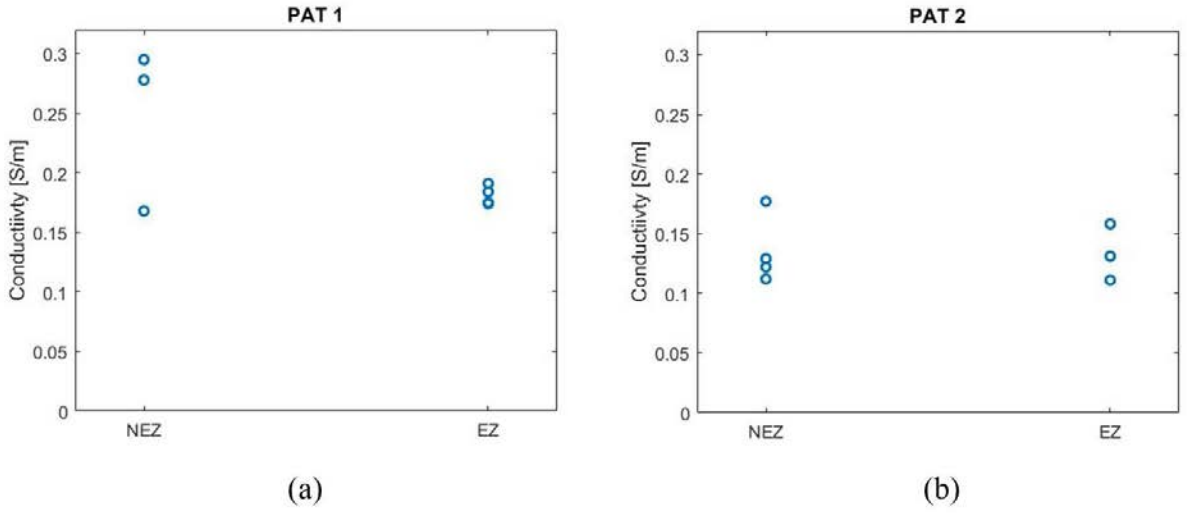

Fig. 5-15. Classification of conductivity using electrophysiological recordings (binary differentiation) (a) Patient 1 (b) Patient 2.

Interestingly, we observe lower values of conductivity for the second patient, which is consistent with the fact that stimulation was delivered eight days after implantation, giving time to the encapsulation tissue to form and locally increase tissue impedance (and therefore, to decrease

conductivity). Given the small number of stimulated regions for the first two patients, no further statistical test was performed at the single patient level.

Patients 3-7 (PAT 3-7)

For patients 3-7, there was a sufficient number of stimulated regions, which gave us the opportunity to perform a statistical analysis. The conductivity computed for each class of electrode contacts (i.e., EZ versus non-EZ) for these patients is shown in Fig. 5-16.

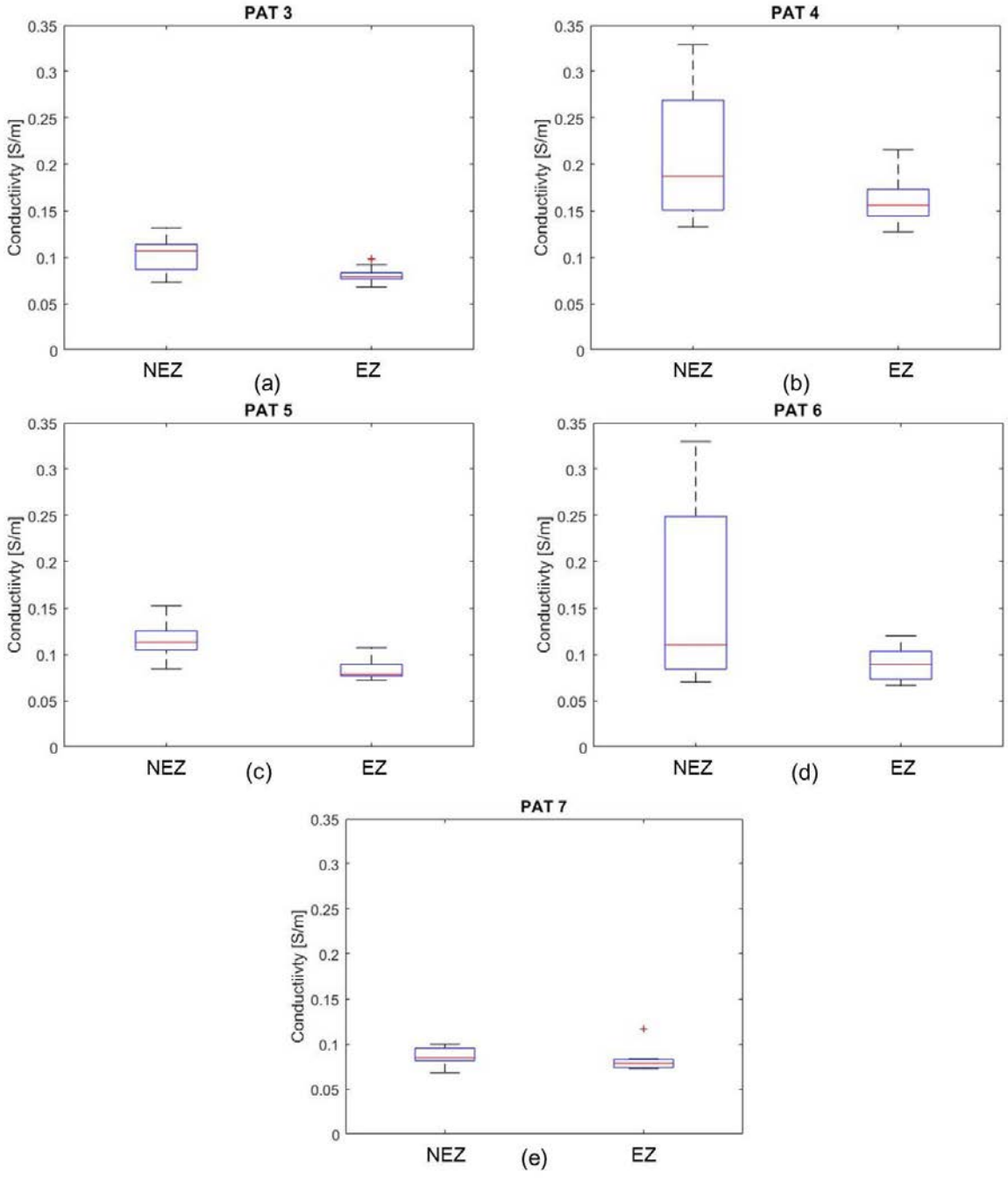

Fig. 5-16. Boxplot of the conductivity as a function of the classification of electrode contacts (EZ versus NEZ) for patients 3-7 using electrophysiological recordings.

NUMBER OF NEZ/EZ AND P-VALUES FOR PATIENT 3-7

Patient ID	Number of stimulated regions	NEZ	EZ	***t*-test *p*-value**
PAT 3	24	9	15	**0,0104**
PAT 4	36	18	18	**0,0041**
PAT 5	18	6	12	**0,0166**
PAT 6	23	13	10	**0,0174**
PAT 7	29	15	14	**0,1428**

Tab. 5.6. Number of NEZ/EZ after classification and *t*-test for patient 3-7.

The difference in electrical conductivity between EZ and NEZ electrode contacts was compared using the parametric Student's *t*-test, which compares two independent samples following a normal distribution. A standard p-value < 0.05 was considered to be statistically significant. The number of stimulated regions, number of NEZ and EZ after classification, along with p-values for the different patients, are shown in Tab. 5.6. For 4 out of 5 patients, conductivity was significantly decreased in EZ regions ($p < 0.05$), which illustrates the consistency and magnitude of this conductivity decrease in epileptogenic tissue, even at the single patient level.

5.5.2 *Group analysis*

A group analysis was performed by pooling together electrode contacts sorted according to their type (epileptogenic zone: EZ versus non-epileptogenic zone: NEZ), along with the estimated electrical conductivity. The total number of NEZ stimulated regions was 68, and EZ stimulated regions was 76. It must be noted that, for an unbiased comparison, the post-surgery delay before testing should be rigorously identical between patients, which is not the case here.

The estimated conductivity values for the different patients were combined, and the mean and the standard error of the mean (SEM) for the two groups (NEZ/EZ) were calculated as shown in Fig. 5-17.

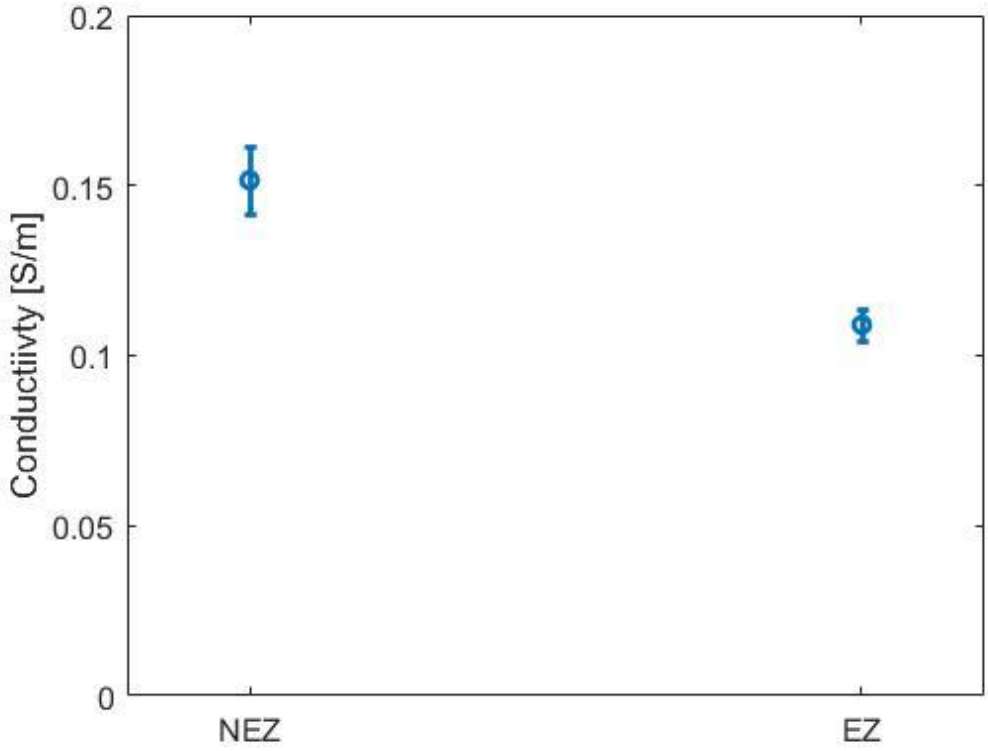

Fig. 5-17. Mean conductivity and standard error of the mean (SEM) for the group analysis (145 stimulated regions, NEZ = 68 and EZ = 76).

Results show a more widespread distribution for conductivity values estimated from NEZ as compared with those obtained in EZ. A higher mean value was also for the NEZ values. By performing a Student *t*-test as previously, we obtained a *p*-value of $p = 0.00017$, confirming that the conductivity decrease in epileptogenic regions is statistically significant.

5.5.3 *Parameters sensitivity analysis*

System inputs (model parameters) uncertainties raise questions regarding their effect over the outputs (signal waveform). Quantifying the effects of changes in parameters values onto the output is of key importance. This is generally achieved using sensitivity analysis and uncertainty analysis. A sensitivity analysis quantifies the incertitude of the output of a system as a function of the inputs, using sensitivity indices that are a measure of the influence of the input on the outputs. There are different methods to perform a sensitivity analysis, and the choice depends on different factors. The two main groups are called *local* and *global* sensitivity methods. *Local* sensitivity focuses on parameters in a small region of parameter space. In this thesis, g*lobal* sensitivity analysis approach will be used, provided that it enables exploring wide regions of input parameters. The most popular family of global sensitivity is the variance-based approach, which aims to identify statistically the part of variability in the output that corresponds to the input. Nevertheless, these methods are considered to be

computationally costly (M. Sobol, 1990; Saltelli, 2008). The first order sensitivity index S_i measures the main effect of the input variable on the output and is defined as:

$$S_i = \frac{Var[\mathbb{E}(Y|X_i)]}{Var[\mathbb{E}(Y)]}$$

where Y is the output and X_i one of the parameters. The second order sensitivity index S_{ij} measures the interaction effect of two inputs together on the output and is defined as:

$$S_{ij} = \frac{Var\left[\mathbb{E}\left(Y\middle|X_i, X_j\right)\right] - Var[\mathbb{E}(Y|X_i)] - Var\left[\mathbb{E}\left(Y\middle|X_j\right)\right]}{Var[\mathbb{E}(Y)]}, \forall\, i \neq j$$

The high dimensional model representation (HDMR) method is a set of tools to calculate variance based sensitivity indices very efficiently (Li et al., 2003; Rabitz et al., 1999). In the following, we use the GUI-HDMR toolbox (a freely available Matlab toolbox with graphical user interface), which computes HDMR for a given model (Ziehn and Tomlin, 2009). The model for the electric potential measured between the electrodes takes the form:

$$v = f(R_m, C_{dl}, Z_f)$$

The medium resistance R_m and brain tissue interface parameters C_{dl}, Z_f are the model inputs that were used to calculate the sensitivity indexes and the systems output v was the electric potential. For computing the sensitivity indices using the toolbox, two files must be created by the user: the first includes the rescaled inputs and the second the corresponding output values. The input values were computed for the expected values of medium resistance and electrode-electrolyte interface, the same range of values as used in the parameters estimation (medium resistance for conductivities between 0.05-0.4 S/m, double layer capacitance for values between 0.5-3 µF and faradaic resistance values 1000-100000 Ω). The output file was created uniformly sampling the electric potential (time-domain) in five points using the corresponding input ranges.

The computed first order sensitivity indexes for the three parameters of our model ($1: R_m$, $2: C_{dl}$ and $3: Z_f$) are the following:

$$S_1 = 0.8774\,; S_2 = 0.0678\,; S_3 = 0.1939$$

It results that R_m is the parameter with the main effect, followed by Z_f and finally C_{dl}. We also calculated the second order sensitivity index:

$$S_{12} = 0.1298\,; S_{13} = 0.2434\,; S_{23} = 0.0106$$

R_m and Z_f are the two inputs that, together, have more pronounced impact on the output. Overall, R_m is the most important model parameter, consistently with the fact that this parameter directly depends on tissue conductivity.

5.6 *Conductivity estimation variability*

It is important to test the possible variability of the estimated conductivity, to observe its limitations when considering a stimulation protocol. In this thesis, we hypothesized that the dielectric properties of tissue did not vary during the time of stimulation (~3 minutes). Changes in neuronal activity may induce variations in the extracellular space and subsequently some changes in tissue conductivity, typically in our case where stimulation is applied for a few minutes. The question is thus to what extent this neuronal activity can modify estimated conductivity values.

To address this issue, we applied a bootstrap method on available recordings consisting of 3 trains of 25 pulses separated by 30 sec to 1 min. From these 75 tissue responses, we randomly selected 25 responses and computed the average conductivity from this reduced sampling. The results as shown in Fig. 5-18 (10 trials, 4 pairs of electrode contacts) indicate that:

1) The estimated conductivity is highly stable when pulse responses are randomized,
2) The variance remains low. The average conductivity values estimated over the 25 responses is identical to that estimated over the 75 responses.

Consequently, these results show that conductivity can be estimated reliably from a limited number of pulses, and that it is independent from the occurrence times of pulses occurring over the ~3-minute recording.

Therefore, and although we cannot rule out the possibility that changes of neuronal activity are induced by low-intensity periodic biphasic stimulation, results suggest that the impact of this stimulation protocol on conductivity estimation is very low.

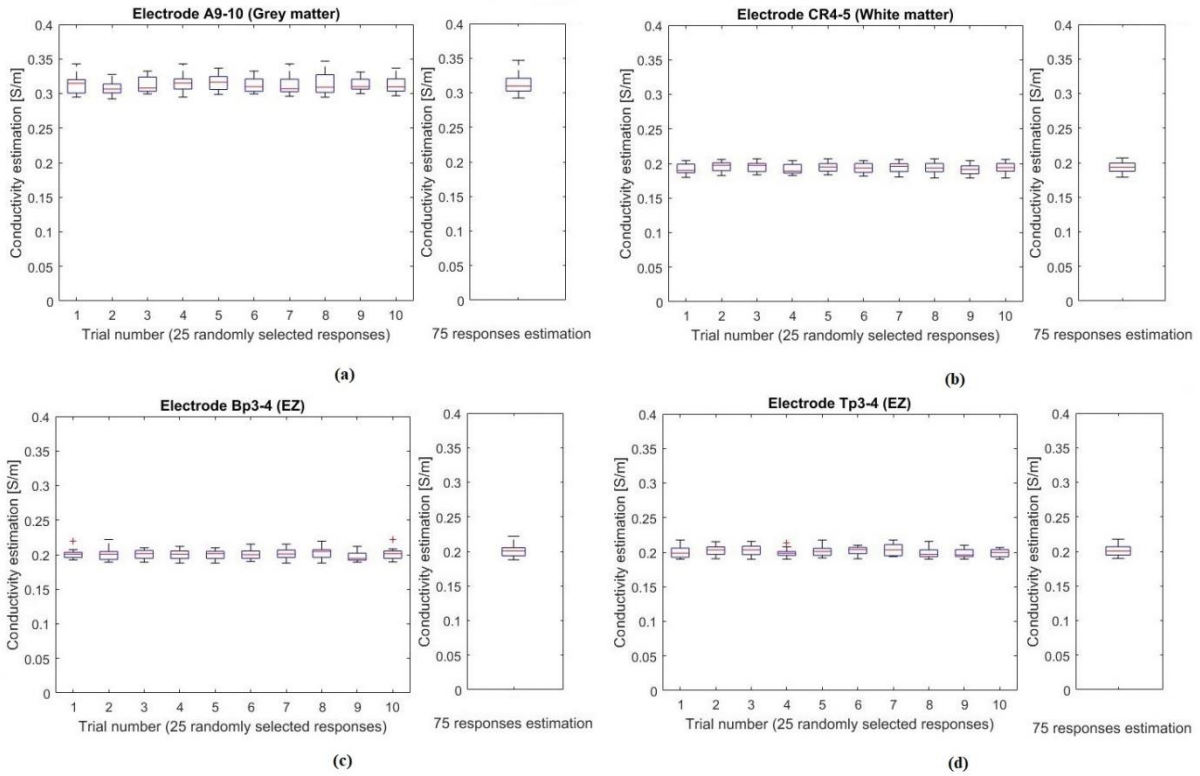

Fig. 5-18. Bootstrap method applied to available recordings. Re-samples were obtained from 25 responses randomly selected in the initial set of 75 responses recorded over a few minutes. (a) Electrode A9-10 is in the grey matter, (b) electrode CR4-5 is in the white matter, (c) electrode Bp3-4 is in the epileptogenic zone (EZ) and (d) electrode Tp3-4 is in the epileptogenic zone.

5.7 *Electrolyte electric potential offset*

During stimulation, electric current implies a flow of ions in the solution. When the stimulation is sufficiently long, the electric properties of the conductive medium will change. Indeed, when a train of charge-balanced biphasic pulses is applied to an electrolyte, an electric potential offset is induced in the electrolyte caused by electron transfer processes (Kumsa et al., 2016). It is suggested that the increase is due to the fact that charge delivered by some electron transfer reactions cannot be recovered and will with time change the properties in the system. This offset was observed in the saline calibrated solution experimentation as observed in Fig. 5-19. (a).

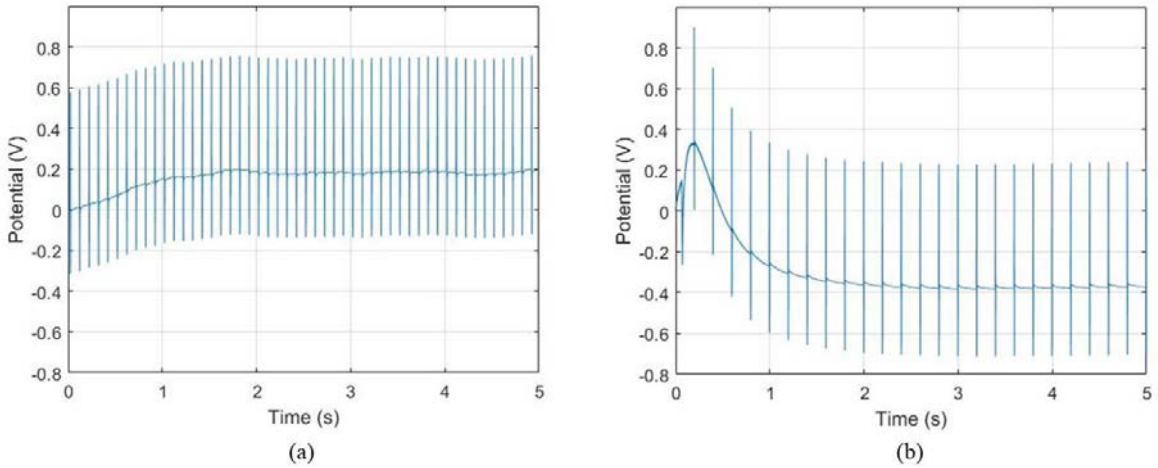

Fig. 5-19. Electrolyte electric potential offset (a) stimulation train in calibrated saline solution (σ=0.1 S/m) and (b) stimulation train in a patient.

It is worth noting that we did not observe this effect during stimulation in patients. Strikingly, in most patients, the offset starts being positive the first two pulses, but then becomes negative after ~0.5 seconds as shown in Fig. 5-19.(b). Interestingly, plotting the offset without the stimulation waveforms for different electrode contacts as shown in Fig. 5-20 (a), it is observed that the final negative value of offset varies between different electrodes. Furthermore, considering two stimulation trains (consecutive, ~30 seconds between trains), the offset between trains are slightly different, a slower response (going negative after ~1s) and values less negative as shown in Fig. 5-20. (b).

At this stage, we do not have a clear explanation of this effect, which could be related to physiological processes. Still, this was not the objective of this thesis and it was not studied in depth. As mentioned in the discussion, it could open a perspective for future work aimed at correlating the potential offset with the epileptogenic property of the underlying tissue.

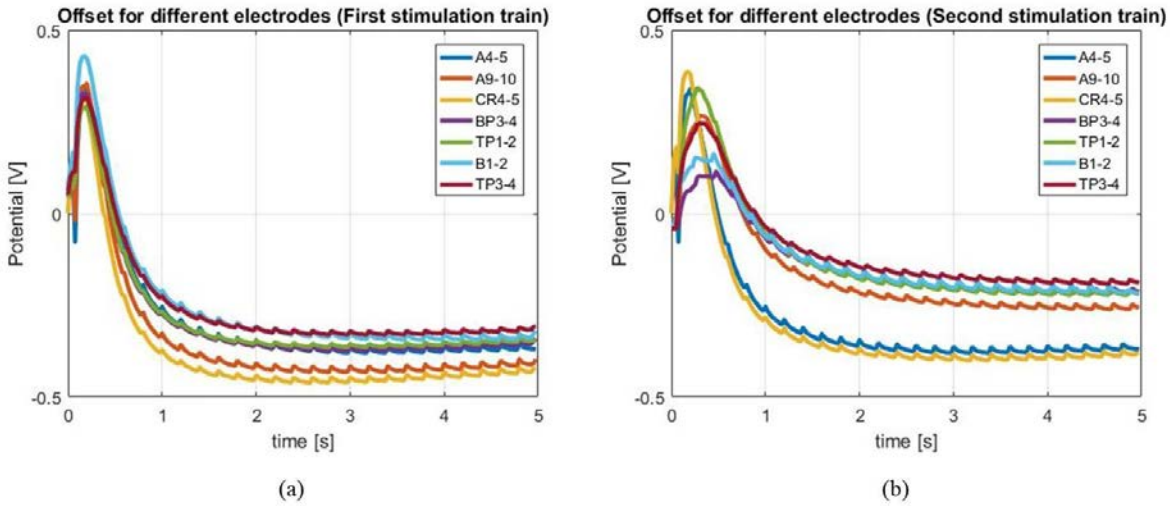

Fig. 5-20. Offset for different electrodes contacts in a patient (a) First stimulation train and (b) second stimulation.

6 Discussion

In the previous chapter, results about conductivity (calibrated solutions and brain tissue) and the correlation between non-epileptogenic and epileptogenic zone were presented. These results showed that: 1) it is possible to estimate the conductivity of a solution using intracranial electrodes and biphasic stimulation, 2) the stimulation artifact can be recorded from patient suffering of drug-resistant epilepsy and that conductivity can be estimated from these stimulation artifacts, and 3) a difference in conductivity between non-epileptogenic and epileptogenic tissue can be established.

An originality of our approach is that we demonstrate that the characteristics of the stimulation artifact (typically discarded since deemed as not exploitable), can be used to gain further knowledge of the biophysical properties of brain tissue. Considering the stimulation artifact, an analytical model of the electric potential generated by the intracranial electrodes was derived, which is original since, in most cases, numerical methods are used to model electric fields or potentials. Moreover, we coupled this electric potential model with an electrode-electrolyte interface model, which is not frequently used, even if it is important for low-frequency conductivity estimation.

The biophysical model was tested using 1) saline solutions calibrated for electrical conductivity, 2) rat brain tissue, and 3) intracerebral data recorded in epileptic patients during pre-surgical evaluation. Each step of validation was used as a possibility to systematically validate the method.

It should be noted that the patient stimulation waveform has to be sampled at a higher sampling frequency and higher input range than those used in clinical SEEG sampling systems. This was a major problem during this thesis, provided that an appropriate sampling system must be placed in parallel to the stimulator, which induces experimental challenges for acquiring the data.

6.1 Conductivity estimation

As reviewed in the state of the art (Section 2), the electrical properties of biological tissue can be analyzed using impedance techniques. However, these approaches do not account for the electrode geometry, and therefore values of impedance cannot be compared between different electrodes. In this thesis, the choice of focusing on conductivity instead of impedance provides more insights into tissue electrical properties.

Tissue anisotropy is an important issue when studying conductivity, and our hypothesis of an isotropic tissue is an approximation. Considering a tissue with a 3-D conductivity tensor would be more rigorous. That being said, supposing tissue as isotropic is an assumption widely used in bio-electromagnetism methods (i.e.: EEG inverse problems) and in our specific study dealing with epilepsy, we focused mainly on the cerebral cortex where anisotropy is much less pronounced (De Lucia et al., 2007). Nevertheless, let us mention that analyzing the influence of anisotropic tissue conductivity on the electric field distribution could be investigated using numerical solutions (i.e. COMSOL Multiphysics), and this approach would be associated with a significantly higher computational cost.

One major limitation of existing invasive measures of brain tissue conductivity is the lack of account for the biophysical processes occurring at the electrode-brain tissue interface and for interaction mechanisms between the electric field and the brain tissue itself (S. Gabriel et al., 1996). As emphasized by our results, notably regarding the impact of the electrode-electrolyte interface on the simulated response, such mechanisms have to be considered to provide accurate estimates of low-frequency conductivity.

Brain tissue conductivity for biomedical applications has been previously mainly investigated using *in-vivo* scalp EEG (Baysal and Haueisen, 2004; Gonalves et al., 2003), freshly excised *ex-vivo* samples (Akhtari et al., 2006; S. Gabriel et al., 1996), *in-vivo* animal intracranial studies (Logothetis et al., 2007) and *in-vivo* human intracranial studies (Koessler et al., 2017; Latikka et al., 2001). Results are not consistent between these studies, possibly due to the differences related to post-mortem changes in tissue, problems related to EEG scalp inverse/forward problems, changes in temperature, or electrode polarization and stimulating frequency. Our method provides conductivity estimates that are in the range of 0.3 S/m and 0.1 S/m for *in vivo* (grey matter) and post-mortem experiments, respectively, which are close to those reported in the literature (Koessler et al., 2017; Latikka et al., 2001;

Logothetis et al., 2007). It is worth noting that these results could be obtained using our new model accounting for the electrode-tissue interface for low-frequency stimulation.

Regarding the contribution of sources of cellular activity to conductivity estimates, they indeed contribute to the recorded response. We neglected this contribution since, under our stimulation conditions, the stimulation artifact is on the order of ~1 V for a background activity that is typically in the order of magnitude of ~100 μVs. Therefore, we made the assumption that background activity is negligible and hence those sources were not considered in our model.

Previous work has shown that carefully designed low-intensity stimulation can specifically activate GABAergic interneurons and not pyramidal cells (Wendling et al., 2016), which might cause changes in the extracellular space and tissue conductivity over time. In order to account for this possible bias, we performed conductivity estimations using randomly resampled segments of data (see Section 5.4). The estimated conductivity was highly stable when pulse responses were randomized. Therefore, it could be assumed that the stimulation does not changes the conductivity over the 3 minutes during which the tissue is stimulated and supports further the interest for the method developed in this thesis. Furthermore, we can conclude that only a very limited number of pulses need to be delivered to provide reliable conductivity estimation, making possible whole-brain conductivity estimates during SEEG session in a very short time.

It has been shown that the cerebrospinal fluid (CSF) has a higher conductivity than brain tissue (S. Gabriel et al., 1996). This can be problematic given that some electrodes could overestimate the conductivity if an excess of CSF is around the electrode. It could be interesting to do a manual inspection of the MRI for each patient, to observe if the electrodes contacts were located within or crossing the border of CSF-filled spaces such as ventricles of surgical cavities. This may explain unexpected conductivity values.

6.2 Relationship between electrical conductivity and pathophysiological processes

Conductivity has increasingly attracted attention for analyzing tissue properties and as discussed in previous sections, it has been studied in different medical fields such as oncology and muscular diseases. In a typical clinical setting in epilepsy surgery units, electrical conductivity is not measured during SEEG recordings since the first focus of invasive stimulation sessions is to map epileptogenic networks based on the analysis of after-discharges elicited by stimulation such as cortico-cortical evoked potentials (Prime et al., 2017). An advantage of our approach is the use of stimulation parameters compatible with standard clinical stimulations performed during presurgical evaluation. Therefore, this opens the possibility to assess, at the same time, electrophysiological data and tissue conductivity.

The results shown in Section 5 illustrate a significant difference in terms of electrical conductivity between healthy and epileptogenic tissues. Two previous studies attempted to identify differences between epileptic tissue, one using DTI and the other using intracranial electrodes. The DTI study measured the electrical conductivities of freshly excised cortex in 21 epilepsy surgery patients (Akhtari et al., 2006), and conductivity varied between patients from 0.066 to 0.156 S/m. Interestingly, focal cortical dysplasia tissue had increased conductivity as compared to epileptogenic tissue without focal cortical dysplasia, leading to the conclusion that understanding how pathophysiological processes impact conductivity could provide supplementary information in epileptic patients candidate to surgery. It must be noted that these results compared the focal cortical dysplasia (a malformation of the cortex) and epileptogenic zones of excised cortex samples. Healthy tissue was not used in the comparison. Nevertheless, the estimated values of epileptogenic tissue found in this study are similar to those presented in this thesis.

In the study based on intracranial recordings (Koessler et al., 2017), conductivity measurements were performed in 15 epileptic patients using a radiofrequency current generator injecting a high frequency sinusoidal waveform, leading to conductivity values of 0.26 S/m for gray matter, and 0.17 S/m for white matter. This study concluded that conductivity was slightly higher than in the EZ (0.29 S/m) than in the GM (0.26 S/m). A possible explanation for the difference between these results and the one presented in this thesis is that the stimulation frequency used to calculate the impedance is high (50 kHz), which is beyond the quasi-static approach. Indeed, differences in the results could come from tissue capacitive effects that cannot be neglected at these frequencies.

Another interesting study (Ridley et al., 2017), used sodium MRI to measure the total sodium concentration surrounding the SEEG electrodes. In this study, 10 drug-refractory epileptic patients candidates for surgery were studied using a new MRI technique (Madelin and Regatte, 2013), that uses sodium instead of hydrogen to create the image. Using this technique, the authors found a 1) chronic sodium concentration augmentation in epileptogenic zones, and 2) acute diminution of sodium concentration during seizures. These results show that possible ionic alterations (hence conductivity alterations) could reflect on potential clinically relevant division of pathological cortex.

6.3 Future prospects and extensions of this work

The influence of tissue heterogeneity is an interesting aspect that was not investigated in this thesis, since we used the isotropy hypothesis to develop an analytical framework. It has indeed been reported that heterogeneous tissue could alter the electric field spatial distribution by up to 10 %, depending on the anatomic region where the electrode were placed (Aström et al., 2012). Such errors are especially important in regions surrounded by multiple fibers such as the subthalamic area. Another possible extension of this work would be to consider the tissue as a heterogeneous medium, notably at the border between grey matter and white matter. In this case, the border of the white/grey matter would

be considered as a medium with two different conductivities (bi-conductivity medium), which could eventually help to determine the white/grey matter junctions using intracranial electrodes.

Another interesting development would be to study the evolution of electrode-tissue interface parameters during the days following SEEG electrode implantation (Grill and Mortimer, 1994; Polikov et al., 2005; Riistama and Lekkala, 2006), possibly reflecting CSF infiltration post-surgery but also gliosis forming around the electrode (Lempka et al., 2009; Yousif et al., 2008). We presented in this thesis a model of encapsulating tissue, which could be used to measure the impedance of the encapsulation tissue, and improve the estimation of conductivity even of the presence of this tissue. It would be possible to study the evolution of the electrode-electrolyte interface over several days within the same patients, which would involve a slightly more time-consuming follow-up but could provide a better view on the evolution of the electrode-tissue interaction.

Furthermore, another possible direction would be to link specifically changes in brain tissue conductivity with pathophysiological mechanisms. For example, since electrical conductivity is proportional to ions mobility in tissue, we could establish links between changes in ionic concentration regulation, electrical conductivity and pathophysiological processes (Cone, 1970; Emin et al., 2015). Exploring further the potential difference in electrical conductivity between healthy and epileptogenic tissue would lead, if confirmed, to insights into pathophysiological processes underlying this difference (Emin et al., 2015; Kadala et al., 2015; Raimondo et al., 2015). Investigating the potential role of changes in ionic concentration regulation within the extracellular medium on the electrical conductivity with biophysical modeling would be an appropriate direction to verify this possibility. Further analyzing the different regions, differentiating the propagation zones from the epileptogenic zones and their correlation with conductivity is another perspective of this work.

7 Conclusion

We have proposed a novel method to estimate the biophysical properties of the brain tissue, and more specifically electrical conductivity. In this model-based approach, we account for the electric potential and field induced by the stimulation electrode, and also for the electrode-electrolyte interface characteristics, to accurately describe the brain tissue response to pulse stimulation. From this fitting of the recorded response, the model provides access to biophysically relevant parameters, notably the electrical conductivity which can be further used for diagnosis.

The proposed method was validated using in *in vitro* and *ex vivo* settings. We obtained excellent matching results for saline solutions and good results for the *ex-vivo* data (small difference between right and left hemisphere). In addition, clinically-relevant results were obtained from intracerebral data recorded in epileptic patients. The main advantages of this model-based method are its accuracy, low computational cost, and compatibility with stimulation hardware and parameters routinely used in clinics, making it immediately applicable.

In this thesis, it was found a conductivity decrease of brain tissue conductivity for epileptic patients ($N = 7$). This tendency must be validated with a larger sample of patients, to confirm this. Electrical conductivity estimation could lead to the development of novel markers of "abnormal brain tissue" which can complement the analysis of SEEG intracerebral recordings classically performed prior to

surgery. For improving the statistical comparison between different groups, it would be more appropriate to stimulate all patients the same day after electrode implantation (ideally the day after implantation) to reduce the effect of encapsulation tissue.

We also studied the evolution of the stimulation artifact during the days following implantation. In this thesis, a model-based solution for the effect related to the implantation tissue was introduced, but conductivity estimation has not yet been confirmed using this method. This represents a promising future perspective to extend this work. Furthermore, considering tissue as a heterogeneous medium is an aspect that has not been studied in this thesis, and it could be fruitful to introduce a model for heterogeneous medium, to determine grey/white matter junction.

Glossaries

EZ: Epileptogenic zones

NEZ: Non-epileptogenic zone

EEG: Electroencephalography

MEG: Magnetoencephalography

SEEG: Stereotactic electroencephalography

CSF: Cerebrospinal fluid

DTI: Diffusion tensor

MRI: Magnetic resonance imaging

EIT: Electrical impedance tomography

MREIT: Magnetic resonance electrical impedance tomography

LFP: Local field potential

ILAE: International league against epilepsy

IED: Inter-ictal epileptiform discharges

HFO: High frequency oscillations

SOZ: Seizure onset zone

PZ: Propagation zone

IZ: Irritating zone

tDCS: Transcranial direct current stimulation

tACS: Transcranial alternating current stimulation

TMS: Transcranial magnetic stimulation

DL: Double layer

CPE: Constant phase element

WM: White matter

GM: Grey matter

PDE: Partial differential equations

FEM: Finite element method

RMS: Root mean square

MMSE: Minimum mean squared error

NLMS: Non-linear minimum squared residual

EI: Epileptogenicity index

HDMR: High dimensional model representation

SEM: Standard error of the mean

List of Figures

Fig. 2-1. Current flow in tissue at low and high frequencies. High frequency is presented with a dotted line, and low frequency with a solid line (adapted from Grimnes, 2014, no permission requested) 7

Fig. 2-2. Anatomical structure of a neuron. The main components of a neuron are dendrites, the cell body (soma), the axon and synapses (adapted from (Grimnes, 2014), no permission requested). 9

Fig. 2-3. Action potential time course. When the firing threshold is exceeded, a rapid depolarization occurs, followed by a repolarization and hyperpolarization phase of the transmembrane potential (Adapted from Plonsey and Barr, 2007)..... 10

Fig. 2-4. EEG inter-ictal epileptiform discharges. Monophasic spike, spike-wave, biphasic spike and poly-spike (Adapted from Bourien, 2003)..... 12

Fig. 2-5. Current-time curve, combination of stimulating current ***I*** and the stimulus duration, that are just sufficient to reach the threshold level (adapted from Plonsey and Barr, 2007, no permission requested). 14

Fig. 2-6. (a) Implanted stereotactic EEG electrodes and (b) postoperative CT of a patient with stereotactic EEG electrodes (courtesy of Dr. A. Biraben)..... 17

Fig. 2-7. Two-contacts seen as a dipole (a) The two dipole source with a constant current *I* and (b) Electric potential generated by a two bipolar electrode modeled by a dipole source..... 18

Fig. 2-8. (a) Ionic distribution at the electrode interface, showing a ion redistribution inducing a double layer. (b)Two-element electrical circuit mode for mechanism of ion redistribution and charge transfer at the electrode interface. 20

Fig. 2-9. The electrode-electrolyte interface and tissue layer impedance equivalent circuit models (adapted from Lempka et al., 2009, no permission requested)..... 23

Fig. 2-10. Charge per phase and charge density for safe stimulation (adapted from (Merrill et al., 2005), no permission requested). 25

Fig. 2-11. Migration of ions in an electrolyte solution..... 26

Fig. 2-12. Basic current-voltage impedance measurement setup. 28

Fig. 2-13. Wheatstone bridge setup..... 28

Fig. 2-14. Permittivity and conductivity of brain tissue (gray matter). Three different experimental arrangements with overlapping frequency coverage are shown from bovine origin (Adapted from (S. Gabriel et al., 1996), no permission requested). 32

Fig. 4-1. Illustration of a cylindrical electrode used clinically. (a) Image of a DIXI medical SEEG electrode, (b) diagram of a 15-contact electrode and (c) electrode geometry with radius $\boldsymbol{R}$, isolation separation $\boldsymbol{l}$ and height $\boldsymbol{h}$. (Adapted from DIXI electrodes datasheet, no permission requested)..... 41

Fig. 4-2.(a) Cylindrical electrode with differential ring, accounting for the electrode geometry and (b) differential ring electric potential contribution, measured in a point $\boldsymbol{P}$, induced by a normal current density $\boldsymbol{J}$..... 44

Fig. 4-3. Comsol Multiphysics FEM solver (a) mesh (b) Electric potential. 47

Fig. 4-4. (a) Graphic representation of the equivalent electric circuit (b) Two-electrode double layer circuit model, where R_m models the medium resistance..... 49

Fig. 4-5. Working and counter electrode modelled as a CPE, and the medium modelled as a resistance. 49

Fig. 4-6. Constant current biphasic stimulation waveform. 50

Fig. 4-7. Simulated Electric potential induced in brain tissue in response to a single biphasic stimulation pulse of intensity 0.2 mA. This waveform was generated for C_{dl} = 0.7 μF, Z_f = 1.5 kΩ, and R_m = 1 kΩ. 51

Fig. 4-8. Fourier transform of the biphasic constant current stimulating waveform. 52

Fig. 4-9. Double layer and constant phase element model comparison. 53

Fig. 4-10. (a) Zeta biphasic pulse stimulation waveform (b) Triangular biphasic stimulation waveform. 54

Fig. 4-11. Double layer model for zeta waveform. 55

Fig. 4-12. Double layer model for a triangular waveform. 56

Fig. 4-13. Electric circuit model, with $\boldsymbol{Cm}$ accounting for the tissue capacitance..... 57

Fig. 4-14. Encapsulation tissue model. 58

Fig. 4-15. Biphasic constant current stimulation waveform (blue) and recorded artifact (red) during one period. 59
Fig. 4-16. Biopac MP36, acquisition systems (Biopac, CA, USA)..... 61
Fig. 4-17. Logarithm of sum of squared error for different parameter conductivities. 63
Fig. 4-18. Sodium hydrated by water, giving the property of conducting electricity. Positive and negative ions are free to migrate (Adapted from (Grimnes, 2014)). 64
Fig. 4-19. Grass Technologies S12X Cortical stimulator system (Natus Neurology Inc.,USA). Constant-current biphasic stimulator..... 66
Fig. 4-20. Configuration setup for recording *in-clinico signals.* (a) Schematic diagram showing the stimulation/sampling system used for the recording signals in patients with intracranial electrodes . (b) A picture that was taken at the La Timone hospital (Marseille) when I participated to the data acquisition. The monitor (left) shows SEEG signals recorded during the low-intensity stimulation protocol we elaborated to test our conductivity-estimation method in human..... 68
Fig. 4-21. Digital switching matrix internal circuit diagram (Natus Europe GmbH, Planegg, Germany). A 500 Ω resistance is present between the constant current stimulator and the patient..... 69
Fig. 4-22. Fast-onset activity occurring at the beginning of a seizure. This electrophysiological marker has long been considered as a hallmark of epileptic regions. This provides a way to assess potential conductivity differences between epileptic and healthy tissue..... 70
Fig. 4-23. Sustained rhythmic spikes during a seizure, also referred to as ictal activity..... 71
Fig. 4-24. Slow waves after seizure. 71
Fig. 5-1. Electric potential distribution of an SEEG electrode. (a) Computed with the cylindrical model (b) computed using Comsol multiphysiscs. The electric potential distribution appears qualitatively in agreement with the analytical model. 74
Fig. 5-2. Difference map of the electric potential distribution. The difference between the electric calculation from the cylindrical model and from Comsol Multiphysics is presented as a percentage. Model errors are the highest close to electrode contacts. 75
Fig. 5-3. Time course of the induced electric potential in each saline solution following a biphasic, charge-balanced pulsed stimulation at 0.2 mA, 1 ms per phase. Increasing conductivity decreases the amplitude of the electric potential time course..... 76
Fig. 5-4. Agreement of the double layer and CPE models with recorded signals in saline solutions. Superimposed time course of simulated (double layer model, red; and CPE model, green) and experimentally recorded (blue) electric potentials for four different conductivity values: (a) 0.10 S/m, (b) 0.20 S/m, (c) 0.39 S/m, and (d) 0.57 S/m. 77
Fig. 5-5. Observation (saline calibrated solution of σ = 0.1 S/m) and double layer model for (a) Triangular waveform and (b) zeta waveform. 78
Fig. 5-6. Time course of the induced electric potential in the brain of a Sprague-Dawley rat and DL model. 80

Fig. 5-7. (a) Signal waveform and DL model for the first stimulated patient. (b) Two different electrodes signal waveforms illustrating the amplitude difference. 81

Fig. 5-8. Electrophysiological activity of an epileptic patient recorded in healthy and epileptic regions, with comparison of estimated conductivity. 83

Fig. 5-9. Epileptic seizure recorded in each contact of one whole electrode and estimated conductivity values. 84

Fig. 5-10. Recorded stimulation waveforms for 4 different patients. Patients were stimulated different days after implantation (D+X, where X is the number of days between surgery and stimulation) 86

Fig. 5-11. (a) Mean value of the bioimpedance as a function of the post-implantation day. It is observed that the value of bioimpedance increases the days following implantation. (b) Non-linear mean square residual for different patients. The residual increases as a function of the post-implantation day. 86

Fig. 5-12. Conductivity estimation as a function of the day after implantation, emphasizing how the estimated conductivity decreases during the days after implantation. 87

Fig. 5-13. Encapsulation tissue circuit model as described in section 4, Gliosis and encapsulation tissue (violet) compared to the patient observation (blue) for: (a) Patient 1 (PAT1), (b) Patient 2 (PAT2), (c) Patient 3 (PAT3) and (d) Patient 4 (PAT4) 88

Fig. 5-14. Encapsulation tissue circuit model as described in section 4, Gliosis and encapsulation tissue (violet) compared to the patient observation (blue) for (e) Patient 5 (PAT5), (f) Patient 6 (PAT6) and (g) Patient 7 (PAT7). 89

Fig. 5-15. Classification of conductivity using electrophysiological recordings (binary differentiation) (a) Patient 1 (b) Patient 2 90

Fig. 5-16. Boxplot of the conductivity as a function of the classification of electrode contacts (EZ versus NEZ) for patients 3-7 using electrophysiological recordings. 91

Fig. 5-17. Mean conductivity and standard error of the mean (SEM) for the group analysis (145 stimulated regions, NEZ = 68 and EZ = 76). 93

Fig. 5-18. Bootstrap method applied to available recordings. Re-samples were obtained from 25 responses randomly selected in the initial set of 75 responses recorded over a few minutes. (a) Electrode A9-10 is in the grey matter, (b) electrode CR4-5 is in the white matter, (c) electrode Bp3-4 is in the epileptogenic zone (EZ) and (d) electrode Tp3-4 is in the epileptogenic zone. 96

Fig. 5-19. Electrolyte electric potential offset (a) stimulation train in calibrated saline solution (σ=0.1 S/m) and (b) stimulation train in a patient. 97

Fig. 5-20. Offset for different electrodes contacts in a patient (a) First stimulation train and (b) second stimulation. 97

List of Tables

Tab. 1.1. Percentage of seizure-free patients on the long-term: overall proportion by type of surgery (adapted from Téllez-Zenteno et al., 2005) 2

Tab. 4.1. Stimulation day after implantation for the different patients tested. 69

Tab. 5.1. Parameter estimation using the double layer model. Estimations were performed from the experimental recordings carried out in each of the four calibrated saline solutions and the ex-vivo rat brain. 78

Tab. 5.2. Parameter estimation using the double layer model. Estimations were performed from the experimental recordings carried out in the calibrated solution, using zeta and triangular biphasic waveforms. 79

Tab. 5.3. Parameter estimation using the double layer model. Estimations were performed from the experimental recording carried out in the *ex-vivo* rat brain. 81

Tab. 5.4. DL model parameter estimation for the seven stimulated brain region. 82

Tab. 5.5. Localization, classification, EI and conductivity of one patient entire electrode. 85

Tab. 5.6. Number of NEZ/EZ after classification and *t*-test for patient 3-7 92

List of Publications

International journal article

Carvallo A., Modolo J., Benquet P., Lagarde S., Bartolomei F., Wendling F. *Biophyical modeling for brain tissue conductivity estimation using sEEG electrodes*. Accepted in IEEE Transactions in Biomedical Engineering, 2018.

International conference

Carvallo A., Modolo J., Benquet P., Wendling F. *A novel method for estimation of brain tissue electrical conductivity: from in silico to in clinico results*. BioEM2018, June 24-28, Portoroz, Slovenia, 2018.

National conference

Carvallo A., Modolo J., Benquet P., Wendling F*, Analytical models of the electric field generated by intracranial stimulation electrodes in humans,* 2016, November. LARC Neurosciences 21th annual meeting.

European Patent

Carvallo A., Modolo J.,Benquet P., Wendling F. *System and method for biophysical parameters estimation of a biological tissue*. European patent, submitted in June 2018. Patent supported by SATT Ouest-Valorisation.

References

Demirci, E., 2012. A method for solving differential equations of fractional order. J. Comput. Appl. Math. 236, 2754–2762. https://doi.org/10.1016/j.cam.2012.01.005

Abascal, J.-F.P.J., Arridge, S.R., Atkinson, D., Horesh, R., Fabrizi, L., De Lucia, M., Horesh, L., Bayford, R.H., Holder, D.S., 2008. Use of anisotropic modelling in electrical impedance tomography; Description of method and preliminary assessment of utility in imaging brain function in the adult human head. NeuroImage 43, 258–268. https://doi.org/10.1016/j.neuroimage.2008.07.023

Akhtari, M., Mandelkern, M., Bui, D., Salamon, N., Vinters, H.V., Mathern, G.W., 2010. Variable Anisotropic Brain Electrical Conductivities in Epileptogenic Foci. Brain Topogr. 23, 292–300. https://doi.org/10.1007/s10548-010-0144-z

Akhtari, M., Salamon, N., Duncan, R., Fried, I., Mathern, G.W., 2006. Electrical Conductivities of the Freshly Excised Cerebral Cortex in Epilepsy Surgery Patients; Correlation with Pathology, Seizure Duration, and Diffusion Tensor Imaging. Brain Topogr. 18, 281–290. https://doi.org/10.1007/s10548-006-0006-x

Aström, M., Lemaire, J.-J., Wårdell, K., 2012. Influence of heterogeneous and anisotropic tissue conductivity on electric field distribution in deep brain stimulation. Med. Biol. Eng. Comput. 50, 23–32. https://doi.org/10.1007/s11517-011-0842-z

Atefi, S.R., Seoane, F., Kamalian, S., Rosenthal, E.S., Lev, M.H., Bonmassar, G., 2016. Intracranial hemorrhage alters scalp potential distribution in bioimpedance cerebral monitoring: Preliminary results from FEM simulation on a realistic head model and human subjects. Med. Phys. 43, 675–686. https://doi.org/10.1118/1.4939256

Atkins, P.W., De Paula, J., Keeler, J., 2018. Atkins' Physical chemistry, Eleventh edition. ed. Oxford University Press, Oxford, United Kingdom ; New York, NY.

Bartolomei, F., Chauvel, P., Wendling, F., 2008. Epileptogenicity of brain structures in human temporal lobe epilepsy: a quantified study from intracerebral EEG. Brain - J. Neurol. 131, 1818–30. https://doi.org/10.1093/brain/awn111

Baumann, S.B., Wozny, D.R., Kelly, S.K., Meno, F.M., 1997. The electrical conductivity of human cerebrospinal fluid at body temperature. IEEE Trans. Biomed. Eng. 44, 220–223. https://doi.org/10.1109/10.554770

Baysal, U., Haueisen, J., 2004. Use of a priori information in estimating tissue resistivities--application to human data in vivo. Physiol. Meas. 25, 737–748.

Beaulieu, C., 2002. The basis of anisotropic water diffusion in the nervous system - a technical review. NMR Biomed. 15, 435–455. https://doi.org/10.1002/nbm.782

Bédard, C., Kröger, H., Destexhe, A., 2006. Model of low-pass filtering of local field potentials in brain tissue. Phys. Rev. E 73, 051911. https://doi.org/10.1103/PhysRevE.73.051911

Bikson, M., Reato, D., Rahman, A., 2012. Cellular and Network Effects of Transcranial Direct Current Stimulation: Insights from Animal Models and Brain Slice, in: Rossini, P. (Ed.), Transcranial Brain Stimulation. CRC Press, pp. 55–91. https://doi.org/10.1201/b14174-5

Bonnefond, M., Kastner, S., Jensen, O., 2017. Communication between Brain Areas Based on Nested Oscillations. eNeuro 4. https://doi.org/10.1523/ENEURO.0153-16.2017

Bossetti, C.A., Birdno, M.J., Grill, W.M., 2008. Analysis of the quasi-static approximation for calculating potentials generated by neural stimulation. J. Neural Eng. 5, 44. https://doi.org/10.1088/1741-2560/5/1/005

Bourien, J., 2003. Analyse de distributions spatio-temporelles de transitoires dans des signaux vectoriels. Application à la détection-classification d'activités paroxystiques intercritiques dans des observations EEG (phdthesis). Université Rennes 1.

Brousse, T., Bélanger, D., Long, J.W., 2015. To Be or Not To Be Pseudocapacitive? J. Electrochem. Soc. 162, A5185–A5189. https://doi.org/10.1149/2.0201505jes

Brummer, S.B., Turner, M.J., 1975. Electrical stimulation of the nervous system: The principle of safe charge injection with noble metal electrodes. Bioelectrochem. Bioenerg. 2, 13–25. https://doi.org/10.1016/0302-4598(75)80002-X

Buxton, R.B., 2013. The physics of functional magnetic resonance imaging (fMRI). Rep. Prog. Phys. Phys. Soc. G. B. 76, 096601. https://doi.org/10.1088/0034-4885/76/9/096601

Cantrell, D.R., Troy, J.B., 2008. A time domain finite element model of extracellular neural stimulation predicts that non-rectangular stimulus waveforms may offer safety benefits. Presented at the 30th Annual International Conference of the IEEE Engineering in Medicine and Biology Society, EMBS'08.

Cohen, R., Abboud, S., Arad, M., 2015. Monitoring brain damage using bioimpedance technique in a 3D numerical model of the head. Med. Eng. Phys. 37, 453–459. https://doi.org/10.1016/j.medengphy.2015.02.011

Cone, C.D., 1974. The role of the surface electrical transmembrane potential in normal and malignant mitogenesis. Ann. N. Y. Acad. Sci. 238, 420–435.

Cone, C.D., 1970. Variation of the transmembrane potential level as a basic mechanism of mitosis control. Oncology 24, 438–470.

Cossu, M., Cardinale, F., Castana, L., Citterio, A., Francione, S., Tassi, L., Benabid, A.L., Lo Russo, G., 2005. Stereoelectroencephalography in the presurgical evaluation of focal epilepsy: a retrospective analysis of 215 procedures. Neurosurgery 57, 706–718; discussion 706-718.

Crile, G.W., Hosmer, H.R., Rowland, A.F., 1922. The electrical conductivity of animal tissues under normal and pathological conditions. Am. J. Physiol.-Leg. Content 60, 59–106. https://doi.org/10.1152/ajplegacy.1922.60.1.59

Daglar, G., Senol, K., Yakut, Z.I., Yuksek, Y.N., Tutuncu, T., Tez, M., Yesiltepe, C.H., 2016. Effectiveness of breast electrical impedance imaging for clinically suspicious breast lesions. Bratisl. Med. J. 117, 505–510. https://doi.org/10.4149/BLL_2016_098

de Curtis, M., Jefferys, J.G.R., Avoli, M., 2012. Interictal Epileptiform Discharges in Partial Epilepsy: Complex Neurobiological Mechanisms Based on Experimental and Clinical Evidence, in: Noebels, J.L., Avoli, M., Rogawski, M.A., Olsen, R.W., Delgado-Escueta, A.V. (Eds.), Jasper's Basic Mechanisms of the Epilepsies. National Center for Biotechnology Information (US), Bethesda (MD).

De Lucia, M., Parker, G.J.M., Embleton, K., Newton, J.M., Walsh, V., 2007. Diffusion tensor MRI-based estimation of the influence of brain tissue anisotropy on the effects of transcranial

magnetic stimulation. NeuroImage 36, 1159–1170. https://doi.org/10.1016/j.neuroimage.2007.03.062
Destexhe, A., Bedard, C., 2013. Local field potential. Scholarpedia 8, 10713. https://doi.org/10.4249/scholarpedia.10713
Dumbrava, V., Svilainis, L., 2008. Uncertainty analysis of I-V impedance measurement technique. Measurements 41, 9–14.
Dymond, A.M., 1976. Characteristics of the Metal-Tissue Interface of Stimulation Electrodes. IEEE Trans. Biomed. Eng. BME-23, 274–280. https://doi.org/10.1109/TBME.1976.324585
Emin, D., Akhtari, M., Ellingson, B.M., Mathern, G.W., 2015. Ionic charge transport between blockages: Sodium cation conduction in freshly excised bulk brain tissue. AIP Adv. 5, 087133. https://doi.org/10.1063/1.4928652
Engel, J., 1993. Intracerebral recordings: organization of the human epileptogenic region. J. Clin. Neurophysiol. Off. Publ. Am. Electroencephalogr. Soc. 10, 90–98.
Epstein, B.R., Foster, K.R., 1983. Anisotropy in the dielectric properties of skeletal muscle. Med. Biol. Eng. Comput. 21, 51. https://doi.org/10.1007/BF02446406
Esser, S.K., Hill, S.L., Tononi, G., 2005. Modeling the effects of transcranial magnetic stimulation on cortical circuits. J. Neurophysiol. 94, 622–639. https://doi.org/10.1152/jn.01230.2004
Fabrizi, L., Sparkes, M., Horesh, L., Abascal, J.F.P.-J., McEwan, A., Bayford, R.H., Elwes, R., Binnie, C.D., Holder, D.S., 2006. Factors limiting the application of electrical impedance tomography for identification of regional conductivity changes using scalp electrodes during epileptic seizures in humans. Physiol. Meas. 27, S163–S174. https://doi.org/10.1088/0967-3334/27/5/S14
Ferree, T.C., Eriksen, K.J., Tucker, D.M., 2000. Regional head tissue conductivity estimation for improved EEG analysis. IEEE Trans. Biomed. Eng. 47, 1584–1592. https://doi.org/10.1109/10.887939
Fisher, R.S., Scharfman, H.E., deCurtis, M., 2014. How Can We Identify Ictal and Interictal Abnormal Activity? Adv. Exp. Med. Biol. 813, 3–23. https://doi.org/10.1007/978-94-017-8914-1_1
Foutz, T.J., McIntyre, C.C., 2010. Evaluation of novel stimulus waveforms for deep brain stimulation. J. Neural Eng. 7, 066008. https://doi.org/10.1088/1741-2560/7/6/066008
Fujiwara, H., Greiner, H.M., Lee, K.H., Holland-Bouley, K.D., Seo, J.H., Arthur, T., Mangano, F.T., Leach, J.L., Rose, D.F., 2012. Resection of ictal high-frequency oscillations leads to favorable surgical outcome in pediatric epilepsy. Epilepsia 53, 1607–1617. https://doi.org/10.1111/j.1528-1167.2012.03629.x
Gabriel, C., Gabriel, S., Corthout, E., 1996. The dielectric properties of biological tissues: I. Literature survey. Phys. Med. Biol. 41, 2231. https://doi.org/10.1088/0031-9155/41/11/001
Gabriel, S., Lau, R.W., Gabriel, C., 1996. The dielectric properties of biological tissues: II. Measurements in the frequency range 10 Hz to 20 GHz. Phys. Med. Biol. 41, 2251–2269.
Gonalves, S., de Munck, J.C., Verbunt, J.P.A., Heethaar, R.M., Lopes da Silva, F.H., 2003. In vivo measurement of the brain and skull resistivities using an eit-based method and the combined analysis of sef/sep data. IEEE Trans. Biomed. Eng. 50, 1124–1128. https://doi.org/10.1109/TBME.2003.816072
Grant, E.H., 1981. Biological effects of microwaves and radio waves. IEE Proc. - Phys. Sci. Meas. Instrum. Manag. Educ. - Rev. 128, 602–606. https://doi.org/10.1049/ip-a-1.1981.0091
Gray, J.R., 2005. Conductivity Analyzers and Their Application, in: Down, R.D., Lehr, J.H. (Eds.), Environmental Instrumentation and Analysis Handbook. John Wiley & Sons, Inc., Hoboken, NJ, USA, pp. 491–510. https://doi.org/10.1002/0471473332.ch23
Grill, W.M., Mortimer, J.T., 1994. Electrical properties of implant encapsulation tissue. Ann. Biomed. Eng. 22, 23–33. https://doi.org/10.1007/BF02368219
Grimnes, S., 2014. Bioimpedance and bioelectricity basics. Elsevier, Boston, MA.
Grinenko, O., Li, J., Mosher, J.C., Wang, I.Z., Bulacio, J.C., Gonzalez-Martinez, J., Nair, D., Najm, I., Leahy, R.M., Chauvel, P., 2018. A fingerprint of the epileptogenic zone in human epilepsies. Brain 141, 117–131. https://doi.org/10.1093/brain/awx306
Güllmar, D., Haueisen, J., Reichenbach, J.R., 2010. Influence of anisotropic electrical conductivity in white matter tissue on the EEG/MEG forward and inverse solution. A high-resolution whole

head simulation study. NeuroImage 51, 145–163. https://doi.org/10.1016/j.neuroimage.2010.02.014
Gutierrez, D., Nehorai, A., Muravchik, C.H., 2004. Estimating brain conductivities and dipole source signals with EEG arrays. IEEE Trans. Biomed. Eng. 51, 2113–2122. https://doi.org/10.1109/TBME.2004.836507
Haemmerich, D., Schutt, D.J., Wright, A.S., Webster, J.G., Mahvi, D.M., 2009. Electrical conductivity measurement of excised human metastatic liver tumours before and after thermal ablation. Physiol. Meas. 30, 459–466. https://doi.org/10.1088/0967-3334/30/5/003
Huggins, R.A., 2002. Simple method to determine electronic and ionic components of the conductivity in mixed conductors a review. Ionics 8, 300–313. https://doi.org/10.1007/BF02376083
Jan, M.M., Sadler, M., Rahey, S.R., 2001. Lateralized postictal EEG delta predicts the side of seizure surgery in temporal lobe epilepsy. Epilepsia 42, 402–405.
Jeong, W.C., Meng, Z.J., Kim, H.J., Kwon, O.I., Woo, E.J., 2014. Experimental validations of in vivo human musculoskeletal tissue conductivity images using MR-based electrical impedance tomography: In Vivo Conductivity of Human Lower Extremity. Bioelectromagnetics 35, 363–372. https://doi.org/10.1002/bem.21852
Jirsch, J.D., Urrestarazu, E., LeVan, P., Olivier, A., Dubeau, F., Gotman, J., 2006. High-frequency oscillations during human focal seizures. Brain J. Neurol. 129, 1593–1608. https://doi.org/10.1093/brain/awl085
Kaatze, U., 2013. Measuring the dielectric properties of materials. Ninety-year development from low-frequency techniques to broadband spectroscopy and high-frequency imaging. Meas. Sci. Technol. 24, 012005. https://doi.org/10.1088/0957-0233/24/1/012005
Kadala, A., Verdier, D., Morquette, P., Kolta, A., 2015. Ion Homeostasis in Rhythmogenesis: The Interplay Between Neurons and Astroglia. Physiology 30, 371–388. https://doi.org/10.1152/physiol.00023.2014
Katscher, U., Voigt, T., Findeklee, C., 2009. Electrical conductivity imaging using magnetic resonance tomography, in: 2009 Annual International Conference of the IEEE Engineering in Medicine and Biology Society. Presented at the 2009 Annual International Conference of the IEEE Engineering in Medicine and Biology Society, pp. 3162–3164. https://doi.org/10.1109/IEMBS.2009.5334031
Kay, S.M., 1993. Fundamentals of statistical signal processing, Prentice Hall signal processing series. Prentice-Hall PTR, Englewood Cliffs, N.J.
Kexue, L., Jigen, P., 2011. Laplace transform and fractional differential equations. Appl. Math. Lett. 24, 2019–2023. https://doi.org/10.1016/j.aml.2011.05.035
Khalil, S.F., Mohktar, M.S., Ibrahim, F., 2014. The Theory and Fundamentals of Bioimpedance Analysis in Clinical Status Monitoring and Diagnosis of Diseases. Sensors 14, 10895–10928. https://doi.org/10.3390/s140610895
Kilbas, A.A.A., Srivastava, H., Trujillo, J., 2006. Theory and applications Of Fractinal Differential Equations. https://doi.org/10.1016/S0304-0208(06)80001-0
Kim, D.H., Chauhan, M., Kim, M.O., Jeong, W.C., Kim, H.J., Serša, I., Kwon, O.I., Woo, E.J., 2015. Frequency-Dependent Conductivity Contrast for Tissue Characterization Using a Dual-Frequency Range Conductivity Mapping Magnetic Resonance Method. IEEE Trans. Med. Imaging 34, 507–513. https://doi.org/10.1109/TMI.2014.2361689
Kim, H.J., Oh, T.I., Kim, Y.T., Lee, B.I., Woo, E.J., Seo, J.K., Lee, S.Y., Kwon, O., Park, C., Kang, B.T., Park, H.M., 2008. *In vivo* electrical conductivity imaging of a canine brain using a 3 T MREIT system. Physiol. Meas. 29, 1145–1155. https://doi.org/10.1088/0967-3334/29/10/001
Koessler, L., Colnat-Coulbois, S., Cecchin, T., Hofmanis, J., Dmochowski, J.P., Norcia, A.M., Maillard, L.G., 2017. In-vivo measurements of human brain tissue conductivity using focal electrical current injection through intracerebral multicontact electrodes: Human In-Vivo Brain Tissue Conductivity. Hum. Brain Mapp. 38, 974–986. https://doi.org/10.1002/hbm.23431
Kumsa, D.W., Montague, F.W., Hudak, E.M., Mortimer, J.T., 2016. Electron transfer processes occurring on platinum neural stimulating electrodes: pulsing experiments for cathodic-first/charge-balanced/biphasic pulses for$0.566 \leq k \geq 2.3$ in oxygenated and deoxygenated sulfuric acid. J. Neural Eng. 13, 056001. https://doi.org/10.1088/1741-2560/13/5/056001

Kuyucak, S., Chung, S.-H., 1994. Temperature dependence of conductivity in electrolyte solutions and ionic channels of biological membranes. Biophys. Chem. 52, 15–24. https://doi.org/10.1016/0301-4622(94)00034-4

Lafon, B., Henin, S., Huang, Y., Friedman, D., Melloni, L., Thesen, T., Doyle, W., Buzsáki, G., Devinsky, O., Parra, L.C., A Liu, A., 2017. Low frequency transcranial electrical stimulation does not entrain sleep rhythms measured by human intracranial recordings. Nat. Commun. 8, 1199. https://doi.org/10.1038/s41467-017-01045-x

Laitinen, L.V., Johansson, G.G., 1967. Locating human cerebral structures by the impedance method. Confin. Neurol. 29, 197–201.

Latikka, J., Kuurne, T., Eskola, H., 2001. Conductivity of living intracranial tissues. Phys. Med. Biol. 46, 1611–1616.

Latikka, J.A., Hyttinen, J.A., Kuurne, T.A., Eskola, H.J., Malmivuo, J.A., 2001. The conductivity of brain tissues: comparison of results in vivo and in vitro measurements, in: 2001 Conference Proceedings of the 23rd Annual International Conference of the IEEE Engineering in Medicine and Biology Society. Presented at the 2001 Conference Proceedings of the 23rd Annual International Conference of the IEEE Engineering in Medicine and Biology Society, pp. 910–912 vol.1. https://doi.org/10.1109/IEMBS.2001.1019092

Laufer, S., Ivorra, A., Reuter, V.E., Rubinsky, B., Solomon, S.B., 2010. Electrical impedance characterization of normal and cancerous human hepatic tissue. Physiol. Meas. 31, 995–1009. https://doi.org/10.1088/0967-3334/31/7/009

Lempka, S.F., Miocinovic, S., Johnson, M.D., Vitek, J.L., McIntyre, C.C., 2009. *In vivo* impedance spectroscopy of deep brain stimulation electrodes. J. Neural Eng. 6, 046001. https://doi.org/10.1088/1741-2560/6/4/046001

Li, G., Artamonov, M., Rabitz, H., Wang, S., Georgopoulos, P.G., Demiralp, M., 2003. High-dimensional model representations generated from low order terms?lp-RS-HDMR. J. Comput. Chem. 24, 647–656. https://doi.org/10.1002/jcc.10232

Li, J., Jafarpoor, M., Bouxsein, M., Rutkove, S.B., 2015. Distinguishing neuromuscular disorders based on the passive electrical material properties of muscle: Passive Electrical Properties of Muscle. Muscle Nerve 51, 49–55. https://doi.org/10.1002/mus.24270

Liang, S., Wu, R., Chen, L., 2015. Laplace transform of fractional order differential equations. Electron. J. Differ. Equ. 2015.

Lilly, J.C., Hughes, J.R., Alvord, E.C., Galkin, T.W., 1955. Brief, Noninjurious Electric Waveform for Stimulation of the Brain. Science 121, 468–469. https://doi.org/10.1126/science.121.3144.468

Llopis, J., Fernández-biarge, J., Fernández, M.P., 1959. Study of the impedance of a platinum electrode in a redox system. Electrochimica Acta 1, 130–145. https://doi.org/10.1016/0013-4686(59)85002-7

Logothetis, N.K., Kayser, C., Oeltermann, A., 2007. In vivo measurement of cortical impedance spectrum in monkeys: implications for signal propagation. Neuron 55, 809–823. https://doi.org/10.1016/j.neuron.2007.07.027

M. Sobol, I., 1990. Sensitivity Estimates for Nonlinear Mathematical Models. Mat. Model. 2.

Madelin, G., Regatte, R.R., 2013. Biomedical Applications of Sodium MRI In Vivo. J. Magn. Reson. Imaging JMRI 38, 511–529. https://doi.org/10.1002/jmri.24168

Malmivuo, J., Plonsey, R., 1995. Bioelectromagnetism - Principles and Applications of Bioelectric and Biomagnetic Fields. https://doi.org/10.1093/acprof:oso/9780195058239.001.0001

Marsh, E.D., Peltzer, B., Brown, M.W., Wusthoff, C., Storm, P.B., Litt, B., Porter, B.E., 2010. Interictal EEG spikes identify the region of electrographic seizure onset in some, but not all, pediatric epilepsy patients. Epilepsia 51, 592–601. https://doi.org/10.1111/j.1528-1167.2009.02306.x

McCreery, D.B., Agnew, W.F., Yuen, T.G.H., Bullara, L., 1990. Charge density and charge per phase as cofactors in neural injury induced by electrical stimulation. IEEE Trans. Biomed. Eng. 37, 996–1001. https://doi.org/10.1109/10.102812

McCreery, D.B., Agnew, W.F., Yuen, T.G.H., Bullara, L.A., 1992. Damage in peripheral nerve from continuous electrical stimulation: Comparison of two stimulus waveforms. Med. Biol. Eng. Comput. 30, 109–114. https://doi.org/10.1007/BF02446202

Mercier, P., Guénot, M., Duffau, H., Scarabin, J.-M., Kahane, P., 2012. Stereotaxy and epilepsy surgery. J. Libbey Eurotext, Montrouge.
Merrill, D.R., Bikson, M., Jefferys, J.G.R., 2005. Electrical stimulation of excitable tissue: design of efficacious and safe protocols. J. Neurosci. Methods 141, 171–198. https://doi.org/10.1016/j.jneumeth.2004.10.020
Miklavcic, D., Pavselj, N., X. Hart, F., 2006. Electric Properties of Tissues, in: Wiley Encyclopedia of Biomedical Engineering. https://doi.org/10.1002/9780471740360.ebs0403
Millar, J., Barnett, T.G., 1997. The Zeta pulse: a new stimulus waveform for use in electrical stimulation of the nervous system. J. Neurosci. Methods 77, 1–8. https://doi.org/10.1016/S0165-0270(97)00101-5
Miocinovic, S., Lempka, S.F., Russo, G.S., Maks, C.B., Butson, C.R., Sakaie, K.E., Vitek, J.L., McIntyre, C.C., 2009. Experimental and theoretical characterization of the voltage distribution generated by deep brain stimulation. Exp. Neurol. 216, 166–176. https://doi.org/10.1016/j.expneurol.2008.11.024
Mortimer, J.T., Kaufman, D., Roessmann, U., 1980. Intramuscular electrical stimulation: Tissue damage. Ann. Biomed. Eng. 8, 235–244. https://doi.org/10.1007/BF02364479
Mortimer, J.T., Shealy, C.N., Wheeler, C., 1970. Experimental Nondestructive Electrical Stimulation of the Brain and Spinal Cord. J. Neurosurg. 32, 553–559. https://doi.org/10.3171/jns.1970.32.5.0553
Muftuler, L.T., Hamamura, M., Birgul, O., Nalcioglu, O., 2004. Resolution and contrast in magnetic resonance electrical impedance tomography (MREIT) and its application to cancer imaging. Technol. Cancer Res. Treat. 3, 599–609. https://doi.org/10.1177/153303460400300610
Muftuler, L.T., Hamamura, M.J., Birgul, O., Nalcioglu, O., 2006. In vivo MRI electrical impedance tomography (MREIT) of tumors. Technol. Cancer Res. Treat. 5, 381–387.
Munari, C., Hoffmann, D., Francione, S., Kahane, P., Tassi, L., Lo Russo, G., Benabid, A.L., 1994. Stereo-electroencephalography methodology: advantages and limits. Acta Neurol. Scand. Suppl. 152, 56–67, discussion 68-69.
Ngugi, A.K., Bottomley, C., Kleinschmidt, I., Sander, J.W., Newton, C.R., 2010. Estimation of the burden of active and life-time epilepsy: a meta-analytic approach. Epilepsia 51, 883–890. https://doi.org/10.1111/j.1528-1167.2009.02481.x
Nitsche, M.A., Paulus, W., 2009. Noninvasive brain stimulation protocols in the treatment of epilepsy: current state and perspectives. Neurother. J. Am. Soc. Exp. Neurother. 6, 244–250. https://doi.org/10.1016/j.nurt.2009.01.003
Nocedal, J., Wright, S.J., 1999. Numerical optimization, Springer series in operations research. Springer, New York.
Nunez, P.L., 1995. Neocortical Dynamics and Human EEG Rhythms, 1st edition. ed. Oxford University Press, New York, NY.
Nunez, P.L., Srinivasan, R., 2006. Electric fields of the brain: the neurophysics of EEG, 2nd ed. ed. Oxford University Press, Oxford ; New York.
Oh, T.I., Jeong, W.C., McEwan, A., Park, H.M., Kim, H.J., Kwon, O.I., Woo, E.J., 2013. Feasibility of magnetic resonance electrical impedance tomography (MREIT) conductivity imaging to evaluate brain abscess lesion: in vivo canine model. J. Magn. Reson. Imaging JMRI 38, 189–197. https://doi.org/10.1002/jmri.23960
Olivier, A., Boling, W.W., Tanriverdi, T., 2012. Techniques in Epilepsy Surgery: The MNI Approach. Cambridge University Press, Cambridge. https://doi.org/10.1017/CBO9781139021951
Onaral, B., Schwan, H.P., 1982. Linear and nonlinear properties of platinum electrode polarisation. Part 1: frequency dependence at very low frequencies. Med. Biol. Eng. Comput. 20, 299–306. https://doi.org/10.1007/BF02442796
Opitz, A., Falchier, A., Linn, G.S., Milham, M.P., Schroeder, C.E., 2017. Limitations of ex vivo measurements for in vivo neuroscience. Proc. Natl. Acad. Sci. U. S. A. 114, 5243–5246. https://doi.org/10.1073/pnas.1617024114
Pethig, R., Kell, D.B., 1987. The passive electrical properties of biological systems: their significance in physiology, biophysics and biotechnology. Phys. Med. Biol. 32, 933–970.
Peyman, A., Kos, B., Djokić, M., Trotovšek, B., Limbaeck-Stokin, C., Serša, G., Miklavčič, D., 2015. Variation in dielectric properties due to pathological changes in human liver: Dielectric

Properties of Liver Tumors. Bioelectromagnetics 36, 603–612. https://doi.org/10.1002/bem.21939
Plonsey, R., Barr, R.C., 2007. Bioelectricity: a quantitative approach, 3. ed. ed. Springer, New York, NY.
Plonsey, R., Heppner, D.B., 1967. Considerations of quasi-stationarity in electrophysiological systems. Bull. Math. Biophys. 29, 657–664.
Polikov, V.S., Tresco, P.A., Reichert, W.M., 2005. Response of brain tissue to chronically implanted neural electrodes. J. Neurosci. Methods 148, 1–18. https://doi.org/10.1016/j.jneumeth.2005.08.015
Prime, D., Rowlands, D., O'Keefe, S., Dionisio, S., 2017. Considerations in performing and analyzing the responses of cortico-cortical evoked potentials in stereo-EEG. Epilepsia. https://doi.org/10.1111/epi.13939
Pugliatti, M., Beghi, E., Forsgren, L., Ekman, M., Sobocki, P., 2007. Estimating the Cost of Epilepsy in Europe: A Review with Economic Modeling. Epilepsia 48, 2224–2233. https://doi.org/10.1111/j.1528-1167.2007.01251.x
Qiao, G., Duan, W., Chatwin, C., Sinclair, A., Wang, W., 2010. Electrical properties of breast cancer cells from impedance measurement of cell suspensions. J. Phys. Conf. Ser. 224, 012081. https://doi.org/10.1088/1742-6596/224/1/012081
Rabitz, H., Aliş, Ö.F., Shorter, J., Shim, K., 1999. Efficient input—output model representations. Comput. Phys. Commun. 117, 11–20. https://doi.org/10.1016/S0010-4655(98)00152-0
Radiometer analytical, 2008. Conductivité Théorie et Pratique - PDF [WWW Document]. URL http://docplayer.fr/9339133-Conductivite-theorie-et-pratique.html (accessed 6.12.18).
Radman, T., Ramos, R.L., Brumberg, J.C., Bikson, M., 2009. Role of Cortical Cell Type and Morphology in Sub- and Suprathreshold Uniform Electric Field Stimulation. Brain Stimulat. 2, 215–228. https://doi.org/10.1016/j.brs.2009.03.007
Raimondo, J.V., Burman, R.J., Katz, A.A., Akerman, C.J., 2015. Ion dynamics during seizures. Front. Cell. Neurosci. 9. https://doi.org/10.3389/fncel.2015.00419
Ranta, R., Le Cam, S., Tyvaert, L., Louis-Dorr, V., 2017. Assessing human brain impedance using simultaneous surface and intracerebral recordings. Neuroscience 343, 411–422. https://doi.org/10.1016/j.neuroscience.2016.12.013
Ridley, B., Marchi, A., Wirsich, J., Soulier, E., Confort-Gouny, S., Schad, L., Bartolomei, F., Ranjeva, J.-P., Guye, M., Zaaraoui, W., 2017. Brain sodium MRI in human epilepsy: Disturbances of ionic homeostasis reflect the organization of pathological regions. NeuroImage 157, 173–183. https://doi.org/10.1016/j.neuroimage.2017.06.011
Riistama, J., Lekkala, J., 2006. Electrode-electrolyte interface properties in implantation conditions. Conf. Proc. Annu. Int. Conf. IEEE Eng. Med. Biol. Soc. IEEE Eng. Med. Biol. Soc. Annu. Conf. 1, 6021–6024. https://doi.org/10.1109/IEMBS.2006.259712
Robinson, B.W., 1962. Localization of intracerebral electrodes. Exp. Neurol. 6, 201–223. https://doi.org/10.1016/0014-4886(62)90003-1
Rubbieri, G., Mossello, E., Di Bari, M., 2014. Techniques for the diagnosis of sarcopenia. Clin. Cases Miner. Bone Metab. 11, 181–184.
Rumble, J.R. (Ed.), 2017. CRC handbook of chemistry and physics, 98th edition 2017-2018. ed. CRC Press, Taylor & Francis Group, Boca Raton London New York.
Sahin, M., Tie, Y., 2007. Non-rectangular waveforms for neural stimulation with practical electrodes. J. Neural Eng. 4, 227–233. https://doi.org/10.1088/1741-2560/4/3/008
Saltelli, A. (Ed.), 2008. Global sensitivity analysis: the primer. John Wiley, Chichester, England ; Hoboken, NJ.
Schmid, G., Neubauer, G., Mazal, P.R., 2003. Dielectric properties of human brain tissue measured less than 10 h postmortem at frequencies from 800 to 2450 MHz. Bioelectromagnetics 24, 423–430. https://doi.org/10.1002/bem.10123
Schnitzler, A., Gross, J., 2005. Normal and pathological oscillatory communication in the brain. Nat. Rev. Neurosci. 6, 285–296. https://doi.org/10.1038/nrn1650
Schulze-Bonhage, A., Feldwisch-Drentrup, H., Ihle, M., 2011. The role of high-quality EEG databases in the improvement and assessment of seizure prediction methods. Epilepsy Behav. 22, S88–S93. https://doi.org/10.1016/j.yebeh.2011.08.030

Schwan, H.P., Kay, C.F., 1957. The conductivity of living tissues. Ann. N. Y. Acad. Sci. 65, 1007–1013.

Selvitelli, M.F., Walker, L.M., Schomer, D.L., Chang, B.S., 2010. The Relationship of Interictal Epileptiform Discharges to Clinical Epilepsy Severity: A Study of Routine Electroencephalograms and Review of the Literature: J. Clin. Neurophysiol. 27, 87–92. https://doi.org/10.1097/WNP.0b013e3181d64b1e

Seo, J.K., Kwon, O., Woo, E.J., 2005. Magnetic resonance electrical impedance tomography (MREIT): conductivity and current density imaging. J. Phys. Conf. Ser. 12, 140–155. https://doi.org/10.1088/1742-6596/12/1/014

Seoane, F., Reza Atefi, S., Tomner, J., Kostulas, K., Lindecrantz, K., 2015. Electrical Bioimpedance Spectroscopy on Acute Unilateral Stroke Patients: Initial Observations regarding Differences between Sides. BioMed Res. Int. 2015, 613247. https://doi.org/10.1155/2015/613247

Shin, J., Kim, M.J., Lee, J., Nam, Y., Kim, M., Choi, N., Kim, S., Kim, D.-H., 2015. Initial study on in vivo conductivity mapping of breast cancer using MRI: In Vivo Conductivity Mapping of Breast Cancer. J. Magn. Reson. Imaging 42, 371–378. https://doi.org/10.1002/jmri.24803

Silva, F.L. da, Niedermeyer, E., PhD, F.L. da S.M., 2012. Electroencephalography: Basic Principles, Clinical Applications, and Related Fields, Fifth. ed. Lippincott Williams & Wilkins.

Sorensen, D.C., 1982. Newton's Method with a Model Trust Region Modification. SIAM J. Numer. Anal. 19, 409–426. https://doi.org/10.1137/0719026

Sree, V.G., Udayakumar, K., Sundararajan, R., 2011. Electric Field Analysis of Breast Tumor Cells. Int. J. Breast Cancer 2011, 1–8. https://doi.org/10.4061/2011/235926

Talairach, J., Bancaud, J., 1973. Stereotaxic Approach to Epilepsy. Prog. Neurol. Surg. 5, 297–354. https://doi.org/10.1159/000394343

Tecchio, F., Cottone, C., Porcaro, C., Cancelli, A., Di Lazzaro, V., Assenza, G., 2018. Brain Functional Connectivity Changes After Transcranial Direct Current Stimulation in Epileptic Patients. Front. Neural Circuits 12, 44. https://doi.org/10.3389/fncir.2018.00044

Téllez-Zenteno, J.F., Dhar, R., Wiebe, S., 2005. Long-term seizure outcomes following epilepsy surgery: a systematic review and meta-analysis. Brain J. Neurol. 128, 1188–1198. https://doi.org/10.1093/brain/awh449

Tuch, D.S., Wedeen, V.J., Dale, A.M., George, J.S., Belliveau, J.W., 2001. Conductivity tensor mapping of the human brain using diffusion tensor MRI. Proc. Natl. Acad. Sci. 98, 11697–11701. https://doi.org/10.1073/pnas.171473898

Ung, H., Cazares, C., Nanivadekar, A., Kini, L., Wagenaar, J., Becker, D., Krieger, A., Lucas, T., Litt, B., Davis, K.A., 2017. Interictal epileptiform activity outside the seizure onset zone impacts cognition. Brain J. Neurol. 140, 2157–2168. https://doi.org/10.1093/brain/awx143

von Bartheld, C.S., Bahney, J., Herculano-Houzel, S., 2016. The Search for True Numbers of Neurons and Glial Cells in the Human Brain: A Review of 150 Years of Cell Counting. J. Comp. Neurol. 524, 3865–3895. https://doi.org/10.1002/cne.24040

Warsaw University, Department of Chemistry, Pasteura 1, 02-093 Warsaw, Poland, Łukaszewski, M., 2016. Electrochemical Methods of Real Surface Area Determination of Noble Metal Electrodes – an Overview. Int. J. Electrochem. Sci. 4442–4469. https://doi.org/10.20964/2016.06.71

Wendling, F., Gerber, U., Cosandier-Rimele, D., Nica, A., De Montigny, J., Raineteau, O., Kalitzin, S., Lopes da Silva, F., Benquet, P., 2016. Brain (Hyper)Excitability Revealed by Optimal Electrical Stimulation of GABAergic Interneurons. Brain Stimulat. 9, 919–932. https://doi.org/10.1016/j.brs.2016.07.001

Woo, E.J., Kim, H.J., Lee, B.I., Kim, Y.T., Lee, S.Y., 2007. Electrical Conductivity Imaging of Postmortem Canine Brains using Magnetic Resonance Electrical Impedance Tomography. IEEE, pp. 4146–4149. https://doi.org/10.1109/IEMBS.2007.4353249

Woods, A.J., Antal, A., Bikson, M., Boggio, P.S., Brunoni, A.R., Celnik, P., Cohen, L.G., Fregni, F., Herrmann, C.S., Kappenman, E.S., Knotkova, H., Liebetanz, D., Miniussi, C., Miranda, P.C., Paulus, W., Priori, A., Reato, D., Stagg, C., Wenderoth, N., Nitsche, M.A., 2016. A technical guide to tDCS, and related non-invasive brain stimulation tools. Clin. Neurophysiol. 127, 1031–1048. https://doi.org/10.1016/j.clinph.2015.11.012

Worrell, G.A., Gardner, A.B., Stead, S.M., Hu, S., Goerss, S., Cascino, G.J., Meyer, F.B., Marsh, R., Litt, B., 2008. High-frequency oscillations in human temporal lobe: simultaneous microwire and clinical macroelectrode recordings. Brain 131, 928–937. https://doi.org/10.1093/brain/awn006

Yamada, Y., Nishizawa, M., Uchiyama, T., Kasahara, Y., Shindo, M., Miyachi, M., Tanaka, S., 2017. Developing and Validating an Age-Independent Equation Using Multi-Frequency Bioelectrical Impedance Analysis for Estimation of Appendicular Skeletal Muscle Mass and Establishing a Cutoff for Sarcopenia. Int. J. Environ. Res. Public. Health 14, 809. https://doi.org/10.3390/ijerph14070809

Yang, L., Worrell, G.A., Nelson, C., Brinkmann, B., He, B., 2012. Spectral and spatial shifts of post-ictal slow waves in temporal lobe seizures. Brain 135, 3134–3143. https://doi.org/10.1093/brain/aws221

Yousif, N., Bayford, R., Liu, X., 2008. The influence of reactivity of the electrode-brain interface on the crossing electric current in therapeutic deep brain stimulation. Neuroscience 156, 597–606.

Ziehn, T., Tomlin, A.S., 2009. GUI–HDMR – A software tool for global sensitivity analysis of complex models. Environ. Model. Softw. 24, 775–785. https://doi.org/10.1016/j.envsoft.2008.12.002

Zuluaga, M.A., Rodionov, R., Nowell, M., Achhala, S., Zombori, G., Cardoso, M.J., Miserocchi, A., McEvoy, A.W., Duncan, J.S., Ourselin, S., 2014. SEEG Trajectory Planning: Combining Stability, Structure and Scale in Vessel Extraction, in: Golland, P., Hata, N., Barillot, C., Hornegger, J., Howe, R. (Eds.), Medical Image Computing and Computer-Assisted Intervention – MICCAI 2014, Lecture Notes in Computer Science. Springer International Publishing, pp. 651–658.

UNIVERSITE BRETAGNE LOIRE / MATHSTIC

Titre : Modèle biophysique pour la mesure de la conductivité cérébrale et apport diagnostique.

Mots clés : Conductivité électrique, stimulation intracrânien, interface électrode-électrolyte, épilepsie.

Résumé : *Objectif* : Nous avons cherché à fournir une estimation précise de la conductivité électrique des tissus cérébraux humains en clinique, en utilisant une stimulation pulsée locale de faible intensité.

Méthodes : À l'aide de l'approximation quasi-statique des équations de Maxwell, nous avons établi un modèle analytique du champ électrique généré par les électrodes intracérébrales stéréotaxiques-EEG (SEEG). Nous avons couplé ce modèle de champ électrique avec un modèle de l'interface électrode-électrolyte pour fournir une expression analytique explicite de la conductivité du tissu cérébral basée sur la réponse enregistrée du tissu cérébral à la stimulation.

Résultats: Nous avons validé notre modèle biophysique en utilisant i) des solutions salines calibrées en conductivité électrique, ii) des tissus cérébraux de rat, et iii) des données électrophysiologiques enregistrées en clinique chez sept patients épileptiques au cours de la SEEG. Nous avons trouvé une possible correlation entre la conducitivé et le caractere epileptique du tissu.

Conclusion: Cette nouvelle méthode basée sur un modèle offre une estimation rapide et fiable de la conductivité électrique des tissus cérébraux en tenant compte des contributions de l'interface électrode-électrolyte.

Signification: Cette méthode surpasse les mesures standard de bioimpédance. L'application pour le diagnostic est envisagée puisque les valeurs de conductivité diffèrent fortement lorsqu'elles sont estimées dans le tissu cérébral sain versus hyperexcitable.

Title: Biophysical model for measurement of brain tissue conductivity and diagnostic applications.

Keywords: Electrical conductivity, intracranial electrodes, electrode-electrolyte interface, epilepsy.

Abstract: *Objective*: We aimed at providing an accurate estimation of human brain tissue electrical conductivity in clinico, using local, low-intensity pulsed stimulation.

Methods: Using the quasi-static approximation of Maxwell equations, we derived an analytical model of the electric field generated by intracerebral stereotactic-EEG (SEEG) electrodes. We coupled this electric field model with a model of the electrode-electrolyte interface to provide an explicit, analytical expression of brain tissue conductivity based on the recorded brain tissue response to pulse stimulation.

Results: We validated our biophysical model using: i) saline solutions calibrated in electrical conductivity, ii) rat brain tissue, and iii) electrophysiological data recorded in clinico from two epileptic patients during SEEG.

Conclusion: This new model-based method offers a fast and reliable estimation of brain tissue electrical conductivity by accounting for contributions from the electrode-electrolyte interface.

Significance: This method outperforms standard bioimpedance measurements since it provides absolute (as opposed to relative) changes in brain tissue conductivity. Application for diagnosis is envisioned since conductivity values strongly differ when estimated in the healthy vs. hyperexcitable brain tissue.